

**SEISMIC PERFORMANCE ASSESSMENT OF A POST
TENSIONED BOX GIRDER VIADUCT**

EMİR ARSLANBOĞAN

**IŞIK UNIVERSITY
JANUARY, 2022**

SEISMIC PERFORMANCE ASSESSMENT OF OF A POST
TENSIONED BOX GIRDER VIADUCT

EMİR ARSLANBOĞAN
B.S., Civil Engineering, ISIK UNIVERSITY, 2018

Submitted to the Graduate School of Science and Engineering
in partial fulfillment of the requirements for the degree of
Master of Science
in
Civil Engineering

IŞIK UNIVERSITY
JANUARY, 2022

IŞIK UNIVERSITY
GRADUATE SCHOOL OF SCIENCE AND ENGINEERING
MASTER OF SCIENCE IN CIVIL ENGINEERING

SEISMIC PERFORMANCE ASSESSMENT OF A POST TENSIONED BOX
GIRDER VIADUCT

EMIR ARSLANBOĞAN

APPROVED BY:

Asst. Prof. Önder UMUT Işık University
(Thesis Supervisor)

Assoc.Prof. Dr. Ferit Çakır Gebze Technical University

Asst.Prof. Bora AKŞAR Işık University

APPROVAL DATE : 31.01.2022 .

SEISMIC PERFORMANCE ASSESSMENT OF A POST TENSIONED BOX GIRDER VIADUCT

ABSTRACT

In the 1999 Marmara earthquakes (Kocaeli and Düzce earthquakes), some of the existing bridges and viaducts were completely or partially destroyed and the earthquake performance of the existing bridges and viaducts began to be questioned. Evaluating the seismic performance of existing structures is one of the most important preliminary steps before seismic retrofitting of structures, as well as a way to validate the analysis and design specifications.

The subject of this study is the seismic performance evaluation of the Molla Gürani Viaduct, located in front of the Elmalı Dam on the TEM (O-2 highway) in Istanbul, according to the Turkey Bridge Earthquake Code published in 2020 and its annexes. First of all, all kinds of information, documents, projects, reports and test results related to the viaduct were examined, analyzed and tried to be verified. It has been tried to obtain healthy information about the current situation of the viaduct by making visual inspections in the region where the viaduct is located.

The seismic performance assesment of the existing viaduct were made with the Nonlinear Time History Analysis method described in TBEC 2020. The three dimensional model of the viaduct was prepared using the SAP2000 software. The moment-curvature relationship of the sections were determined with the XTRACT section analysis program, using the axial loads obtained from the non-linear static analysis results performed under non-seismic loads.

The cracked section stiffnesses and other section properties were modified before dynamic analyses. Due to the large stirrup spacing in the columns, unconfined concrete properties were used in the moment-curvature analyses. The bending cracked section stiffnesses of each column were calculated separately and included in the model. The nonlinear behavior has been tried to be characterized by the acceptance of

lumped plastic hinges. For each of the pier columns, 2 plastic hinges in both directions are defined in the foundation-column junction area and just below the 1.4 m solid part at the top end of the columns.

The Nonlinear Time History analyses was carried out using 7 earthquake records selected by considering earthquake magnitudes, fault distances, source mechanisms and local ground conditions compatible with DD1 and DD2a earthquake ground motion levels defined in TBEC-2020 Chapter 2. Selected ground motion records are scaled according to TBEC-2020 Section 2.5.

As a result of the existing situation analysis of the viaduct, it has been observed that the deformations occurring in the elastomeric bearings in the longitudinal and transverse directions for the DD-1 Earthquake Ground Motion Level are higher than the values allowed in the TBEC-2020 section 5.4.5.1. The fact that the superstructure is continuous and that it is anchored to the abutment by tie bars eliminates the possibility of falling off the support in the longitudinal direction.

As a result of possible ruptures that may occur because of high deformations in elastomeric bearings, elastomeric bearings may not fulfill their function. In this case, the viaduct superstructure beams are likely to be free in the transverse direction and may pound each others under the effects of earthquakes, despite the 1.50 m gap between them.

In the seismic performance evaluation analyses of the viaduct, it has been determined that the shear keys on the abutments do not have the capacity to meet the earthquake loads. In the observations made in the field, it is seen that macro cracks are formed in the shear keys on the abutments.

Limiting elastomeric bearings deformation and strengthening shear keys before a possible Istanbul earthquake in the Molla Gürani viaduct are among the some of the most important precautions to be taken immediately before an earthquake.

Key words: Earthquake, Post-tensioned, Rectangular Hollow Section, Retrofit.

ARDGERMELİ KUTU KİRİŞLİ BİR VİYADÜĞÜN DEPREM PERFORMANS DEĞERLENDİRMESİ

ÖZET

1999 yılında meydana gelen Marmara depremlerinde(Kocaeli ve Düzce depremleri) mevcut köprü ve viyadüklerin bazıları tamamen veya kısmen yıkılmış ve mevcut köprü ve viyadüklerin deprem performansları sorgulanmaya başlanmıştır. Mevcut yapıların sismik performanslarının değerlendirilmesi, yapıların sismik güçlendirilmesinden önceki en önemli ön adımlardan biridir, ayrıca bu, analiz ve tasarım özelliklerini doğrulamanın bir yoludur.

Bu çalışmanın konusu 2020 yılında yayımlanan Türkiye Köprü Deprem Yönetmeliği ve eklerine göre İstanbulda TEM(O-2 otoyolu) üzerinde, Elmalı Barajı önünde bulunan Molla Gürani Viyadüğü'nün sismik performans değerlendirmesidir. Öncelikle viyadük ile ilgili elde edilebilen her türlü bilgi, belge, proje, rapor ve test sonuçları gözden geçirilip analiz edilerek doğrulanmaya çalışılmıştır. Viyadüğün bulunduğu sahada incelemelerde bulunularak viyadüğün mevcut durumu hakkında gözle muayene yapılarak, sağlıklı bilgiler elde edilmeye çalışılmıştır.

Mevcut viyadüğün sismik performans analizleri TBEC 2020 de anlatılan Zaman Tanım Alanında Doğrusal Olmayan hesap yöntemi ile yapılmıştır. Viyadüğün üç boyutlu hesap modeli SAP2000 programı kullanılarak hazırlanmıştır. Ölü yükler altında yapılan doğrusal olmayan statik analiz sonuçlarından elde edilen eksenel yükler kullanılarak XTRACT kesit analiz programı ile kesitlerin moment-eğrilik ilişkileri belirlenmiştir.

Dinamik analizlere başlanmadan önce çatlamış kesit rijitlikleri ve diğer kesit özelliklerinin modifikasyonu yapılmıştır. Kolonlarda etriye aralıklarının fazla olması nedeniyle moment-eğrilik hesaplarında sargısız beton özellikleri kullanılmıştır. Her bir kolona ait eğilme çatlamış kesit rijitlikleri ayrı ayrı hesaplanarak modele dahil edilmiştir. Orta ayak kolonlarının her birisi için, temel-kolon birleşim bölgesinde ve

kolonların üst uç kısımlarındaki 1.4 m lik dolu kesite sahip kısmın hemen altında her iki yönde 2 şer adet plastik mafsal tanımlanmıştır. Doğrusal olmayan davranış yığılı plastik mafsal kabülü ile karakterize edilmeye çalışılmıştır.

Zaman Tanım Alanında Analizler, TBEC-2020 Bölüm 2 de tanımlanan DD1 ve DD2a deprem yer hareketi düzeyleri ile uyumlu deprem büyüklükleri, fay uzaklıkları, kaynak mekanizmaları ve yerel zemin koşulları dikkate alınarak seçilen 7 adet deprem kaydı kullanılarak yapılmıştır. Yer hareketi kayıtları, TBEC-2020 Bölüm 2.5'e göre ölçeklendirilmiştir.

Viyadüğün mevcut durum analizleri neticesinde DD-1 Deprem Yer Hareket Düzeyi için elastomer mesnetlerde boyuna ve enine doğrultuda meydana gelen deformasyonların yönetmelikte izin verilen değerlerden daha yüksek olduğu görülmüştür. Üstyapının sürekli olması ve çekme çubukları ile kenar ayağa tutturulması boyuna yönde mesnetten düşme (boşa çıkma) ihtimalini ortadan kaldırmaktadır.

Elastomer mesnetlerde yüksek deformasyonlar neticesinde meydana gelebilecek muhtemel yırtılmalar sonucunda elastomer mesnetler işlevini yerine getiremeyebilirler. Bu durumda viyadük üstyapı kirişleri enine yönde serbest kalarak aralarındaki 1.50 m lik boşluğa rağmen deprem etkileri altında birbirlerine çarpmaları muhtemeldir.

Mevcut durum analizlerinde kenar ayaklardaki deprem takozlarının deprem yüklerini karşılayabilecek kapasiteye sahip olmadığı tespit edilmiştir. Sahada yapılan gözlemlerde de kenar ayaklardaki deprem takozlarında makro çatlaklar oluştuğu görülmektedir. Molla Gürani viyadüğünde muhtemel bir İstanbul depremi öncesi elastomer mesnet deformasyonlarının sınırlandırılması, deprem takozlarının güçlendirilmesi deprem öncesi ivedilikle alınması gereken bazı tedbirlerin başında gelmektedir.

Anahtar Kelimeler: Deprem, Ardgerme, Dikdörtgen Kutu Kesit, Güçlendirme

ACKNOWLEDGMENT

This study was carried out under the supervision of Prof. Dr. H.Faruk Karadođan and Asst. Prof. Önder Umut. I gratefully appreciate their guidance, criticism, support, encouragement and friendship throughout this study.

I would like to thank sincerely to Prof. Dr. H. Faruk Karadođan, Prof. Dr. Esin Inan, Prof. Dr. Hilmi Demiray, Prof. Dr. Kutay Orakçal, Prof. Dr. Ismail Karakurt, Prof. Dr. Nazmiye Yahniođlu, Assoc. Prof. Dr. Ahmet Kiriş, Assoc.Prof. Dr. Serkan Sütli, Asst. Prof. Bora Akşar for their warm and instructive attitude.

I would also like to thank M.Sc.Eng. Mustafa Uzyardođan for sharing her knowledge and experience.

TABLE OF CONTENT

APPROVAL PAGE.....	i
ABSTRACT.....	ii
ÖZET.....	iv
ACKNOWLEDGMENT.....	vi
TABLE OF CONTENT.....	vii
LIST OF TABLES.....	x
LIST OF FIGURES.....	xii
LIST OF ABREVIATION.....	xiv
CHAPTER 1.....	1
1. INTRODUCTION.....	1
1.1 Introduction.....	1
1.2 Aims and Scope of the Study.....	3
CHAPTER 2.....	4
2. LITERATURE REVIEW.....	4
2.1 Literature Review.....	4
CHAPTER 3.....	6
3. SITE INSPECTION AND GEOTECHNICAL PROPERTIES.....	6
3.1 Site Inspection.....	6
3.2 Geotechnical Parameters and Soil Properties.....	7
3.2.1 General Geology.....	7
3.2.2 Information obtained from two 10 m borehole logs.....	8
3.2.3 Soil classification according to FEMA 356 Specification.....	10
3.2.4 Equations for calculation of shear wave velocity of soil.....	11
3.2.5 Hooke-Brown Strength Criterion.....	13
3.2.6 Bearing Capacity of Shallow Foundation Prandtl-Caquot Equations.....	14
3.2.7 Bearing Capacity of Pile Foundation.....	15
3.2.8 Williams and Pells Method for Skin Resistance in Weak Rock.....	16
CHAPTER 4.....	21
4. ROUTE AND FEATURES OF THE PROJECT.....	21
4.1 Route and Features of the Project.....	21
4.2 General Information about Molla Gürani(Elmalı) Viaduct.....	22
4.3 Superstructure of Viaducts.....	23
4.4 Typical Pier Sections and Substructure of Viaducts.....	25
4.5 Elastomeric Bearings.....	28
CHAPTER 5.....	34
5. EARTHQUAKE GROUND MOTION.....	34
5.1 Bridge Performance Earthquake Ground Motion Level.....	34
5.1.1 Earthquake Ground Motion Level-1 (DD-1).....	34
5.1.2 Earthquake Ground Motion Level-2 (DD-2).....	34

5.1.3 Earthquake Ground Motion Level-3 (DD-2a)	34
5.1.4 Earthquake Ground Motion Level-4 (DD-3)	35
5.2 Standard Earthquake Ground Motion Spectrums	35
5.2.1 Determination of spectral acceleration coefficients.....	35
5.2.2 Determination of the local soil effect parameters	35
5.2.3 Horizontal Earthquake Design Spectrum.....	36
5.2.4 Horizontal Elastic Design Spectrum of Molla Gürani Viaduct	38
CHAPTER 6	42
6. PERFORMANCE BASED DESIGN AND SEISMIC PERFORMANCE EVALUATION OF BRIDGES.....	42
6.1 Bridge Importance Classes in TBEC-2020.....	42
6.1.2 BIC(KÖS)=1 Important and Special Bridges	42
6.1.3 BIC(KÖS)=2 Normal Bridges	42
6.1.4 BIC(KÖS)=3 Simple(Other) Bridges	43
6.2 Seismic Design Category.....	43
6.3. Bridge Performance Levels And Performance Targets	45
6.3.1 Bridge Performance Levels.....	45
6.3.2 Bridge Performance Targets	46
6.3.3 Near fault effect	47
CHAPTER 7	48
7. MATERIAL PROPERTIES AND WEIGHT OF SUPERSTRUCTURE	48
7.1 Concrete Material	48
7.2 Unconfined and Confined Concrete Models	49
7.3 Steel Material Properties.....	53
7.4 Moment Curvature Relationship.....	54
7.4.1 Generation Moment-Curvature relation for a given beam section	60
7.4.2 Cross Sectional Analysis of column of Molla Gürani Viaduct piers..	64
7.4.3 Bilinearization of Moment-Curvature.....	66
7.4.4 Verification of the Results	68
7.5.1 Weight of Girder Section (Span)	69
7.5.2 Weight of Girder Section (Support).....	69
7.5.3 Total Weight of One Span	69
CHAPTER 8	70
8. SEISMIC PERFORMANCE ASSESSMENT OF THE MOLLA GÜRANİ VIADUCT.....	70
8.1 Seismic Performance Assessment	70
8.2 Modelling of the Viaduct.....	71
8.2.1 Modelling of the Viaduct Superstructure.....	71
8.2.2 Modelling of the Viaduct Piers	71
8.2.3 Modelling of the Abutments	73
8.2.4 Modelling of the Tie Bars and Shear Keys at Abutments	74
8.3 Nonlinear Static Analysis Under Non-Seismic Loads.....	75
8.4 Modal Analysis	76
8.4.1 Verification of Mass Participation	79
8.4.2 Mass and Stifness Damping Proportional Coefficients	79
8.5 Response Spectrum Analysis.....	81
8.6 Nonlinear Time History Analysis	82
8.6.1 Deformation of the Elastomeric Bearings.....	84
8.6.2 Hinge States and Plastic Deformation	86
8.6.3 Tie Bar Deformations	88

8.6.4 Pounding Effect	91
8.6.5. Shear Strength of the Pier Columns.....	92
8.6.6. Shear Strength of Transverse Reinforcement	94
8.6.7. Longitudinal and Transversal Reinforcement Requirement for Columns	99
8.6.8. Shear Force Strength of Transverse Reinforcement	100
CHAPTER 9	104
9. CONCLUSION	104
9.1 Conclusion	104
REFERENCES.....	106
APPENDICES	107
APPENDIX A : EARTHQUAKE RECORDS	107
A1. KERN COUNTY EARHQUAKE	108
A2. HECTOR MINE EARHQUAKE.....	112
A3. LOMA PRIETO EARHQUAKE	116
A4. LANDERS EARHQUAKE	120
A5. KOCAELI EARHQUAKE	124
A6. CHICHI EARHQUAKE	128
A7. CAPE MENDOCINO EARHQUAKE	132
A8. Avarage of DD1 Ground Motion Level Response Spectrums.....	135

LIST OF TABLES

Table 3. 1 Geotechnical parameters of soil, idealized from SK-1.....	8
Table 3. 2 Soil classes in FEMA 356.....	10
Table 3.3 Comparison of Site Classification Systems.....	12
Table 3.4 Mass factor J values corresponding to RQD.....	17
Table 3.5 Safety factors in calculating the pile bearing capacity.....	19
Table 3.6 Young's Modulus and coefficient of horizontal subgrade reaction.....	20
Table 4.1 Top Cross Section Reinforcement Ratio of North Viaduct Pier 3.....	27
Table 4.2 Bottom Cross Section Reinforcement Ratio of North Viaduct Pier 3.....	27
Table 4.3 Foundation Type and Pier(Column Elevations) Heights.....	28
Table 4.4 The dimensions of the elastomeric bearings.....	29
Table 4.5 Symbolic Representation of Bearing Function.....	32
Table 5.1. Short period spectral region local soil effect coefficients.....	36
Table 5.2. Long period spectral region local soil effect coefficients.....	36
Table 5.3 Peak Ground Acceleration and Spectral Acceleration Values.....	40
Table 6.1 Seismic(Earthquake) Design Category(Class) (SDC).....	43
Table 6.2 Analysis and Evaluation Methods in TBEC-2020.....	44
Table 6.3 Bridge Performance Targets for Special and Standard Bridges.....	46
Table. 7.1. Concrete Material Properties According to As-built projects.....	48
Table 7.2 Mechanical Properties of Steel Reinforcement	53
Table 7.3 Reinforcing Steel Stresses and Strains.....	61
Table 7.4 Forces in the section from reinforcing steel and concrete.....	62
Table 7.5 Moment-Curvature Analysis Results of Column of Molla Gürani Piers...	64
Table 8.1 Pier Columns Cracked Section Stiffness Modification Ratios	73
Table 8.2 Gewi Bars 40 mm ST500/600 Material Properties.....	74
Table 8.3. Axial Forces from the Nonlinear Static Analysis Results.....	75
Table 8.4. Modal Analysis Results and Mass - Stiffness Proportional Coefficient....	80

Table 8.5. Elastomeric Bearing Shear deformations (DD1).....	85
Table 8.6. Elastomeric Bearing Shear deformations (DD2a - DD2a 90° Rotated).....	85
Table 8.7. Elastomeric Bearing Shear deformations (DD1 and DD1- 90° Rotated)...	86
Table 8.8. Plastic Hinge Rotation Capacity in Longitudinal Direction.....	87
Table 8.9. Plastic Hinge Rotation Capacity in Transversal Direction.....	87
Table 8.10. Tie Bar Deformations (DD1).....	89
Table 8.11. Tie Bar Deformations (DD2a).....	90
Table 8.12. Tie Bar Deformations (90° Rotated DD1).....	90
Table 8.13. Transversal Deformations of Superstructure (DD1).....	91
Table 8.14. Column Shear Force Capacity in Longitudinal Direction (DD1).....	95
Table 8.15. Column Shear Force Capacity in Transversal Direction (DD1).....	96
Table 8.16. Column Shear Force Capacity in Longitudinal Direction (DD2a).....	97
Table 8.17. Column Shear Force Capacity in Longitudinal Direction (DD2a).....	98
Table 8.18. Shear Forces on Shear Keys (DD1).....	101
Table 8.19. Shear Forces on Shear Keys (90° Rotated DD1).....	101
Table 8.20. Cohesion and Friction Factors.....	102

LIST OF FIGURES

Figure 3.1 Visual Inspection.....	6
Figure 3.2 Viaduct SPT(N)-Depth Graph and Idealized Soil Profile.....	9
Figure 3.3 RocLab Result.....	13
Figure 3.4 The adhesion factor of intact weak rocks (mudstone, shale, sandstone, etc.) from Williams and Pells	16
Figure 3.5 The correction factor β in Williams and Pells method.....	17
Figure 4.1 Location description map.....	21
Figure 4.2 Molla Gürani Viaduct.....	22
Figure 4.3 Box Girder Section at Span.....	23
Figure 4.4 Viaduct Plan and Elevation.....	24
Figure 4.5 Typical Pier Section (North Viaduct Axis 3).....	25
Figure 4.6 Foundation Plan and Typical Sections (North Viaduct Axis 3).....	26
Figure 4.7 General Reinforcement Layout Type I (North Viaduct Axis 3).....	26
Figure 4.8 The detail of top Pier.....	28
Figure 4.9 The detail of elastomeric bearings. (axes 0, 1, 2, 3, 9.).....	29
Figure 4.10 The horizontal stiffness coefficient of Pier 8 elastomeric bearings.....	30
Figure 4.11 The function and configuration plan of the viaduct bearings.....	33
Figure 5.1 Horizontal elastic design spectrum (TBEC-2020).....	37
Figure 5.2 Horizontal elastic design displacement spectrum(TBEC-2020).....	38
Figure 5.3 TBEC 2020 Design Acceleration Response Spectrums.....	41
Figure 5.4 TBEC 2020 Design Displacement Response Spectrums.....	41
Figure 6.1 Distance to nearest fault line.....	47
Figure 7.1 Stress-strain model of concrete.....	49
Figure 7.2 Stress-strain model of reinforcing steel B420C.....	53

Figure 7.3 Moment-Curvature relationship a reinforced concrete cross-section.....	54
Figure 7.4 Moment-Curvature relationship.....	56
Figure 7.5 Types of failures in RC members (related to ductility) (K.Orakcal).....	56
Figure 7.6 Internal Stress Distribution (K.Orakcal).....	57
Figure 7.7 Moment – Curvature relationship for beams (U. Ersoy).....	58
Figure 7.8 Material models.....	59
Figure 7.9 A rectangular beam section.....	60
Figure 7.10 Reinforcing steel and concrete material models.....	61
Figure 7.11 Stresses, Strains and Forces in the section.....	61
Figure 7.12 Linear distribution of σ_c	63
Figure 7.13 Moment – Curvature diagram for a given section.....	63
Figure 7.14 M– ϕ diagrams of Pier Columns in Longitudinal Direction	65
Figure 7.15 M– ϕ diagrams of Pier Columns in Transversal Direction	65
Figure 7.16 Moment–Curvature diagrams of Pier 1 Columns	67
Figure 8.1 Pier Column Discretization.....	71
Figure 8.2 SAP2000 Section Property /Stiffness Modification.....	72
Figure 8.3 Tie bars.....	73
Figure 8.4 1st Vibration Mode of the Viaduct in Transversal Direction.....	76
Figure 8.5 2nd Vibration Mode of the Viaduct in Transversal Direction.....	77
Figure 8.6 3 rd Vibration Mode of the Viaduct in Longitudinal Direction.....	78
Figure 8.7 Rayleigh Proportional Damping.....	79
Figure 8.8 RS Definition – DD1 Earthquake Ground Motion Level	81
Figure 8.9 RS Definition – DD2a Earthquake Ground Motion Level	81
Figure 8.10 NLTH Load Case and Modal Proportional Damping Definition.....	82
Figure 8.11 Nonlinear Time History Analysis – Deformed Shape.....	83
Figure 8.12 Tie Bar Deformation- RNS1166 Kocaeli Earthquake (DD1).....	88
Figure 8.13 Tie Bar Force-Deformation- RNS1166 Kocaeli Earthquake (DD1).....	88
Figure 8.14 Tie Bar Force-Displacement Relation.....	89
Figure 8.15 Molla Gürani Pier Column Shear Capacity Calculation.....	93
Figure 8.16 Single Column Cantilever Bridge Pier.....	94
Figure 8.17 Shear Forces on Shear Key at Abutments.....	100
Figure 8.18 Shear Deformations at Shear Keys of Molla Gürani Viaduct.....	101

LIST OF ABBREVIATION

GNP Gross National Product

RQD Rock Quality Designation

AASHTO American Association of State Highway and Transportation Officials

LFD Load Factor Design

LRFD Load and Resistance Factor Design

KGM General Directorate of Highway

METU Middle East Technical University

ITU Istanbul Technical University

ATC American Technology Council

IO Immediate Occupancy

LS Life Safety

CP Collapse Prevention

FEMA Federal Emergency Management Agency

SAP Structural Analysis Program

SDOF Single Degree of Freedom

TBEC-2020 Turkish Bridge Earthquake Code

CHAPTER 1

1. INTRODUCTION

1.1 Introduction

Earthquakes are among the most dangerous geologic phenomena on our planet, whose time and magnitude remain unpredictable. Although numerous studies have been carried out to predict earthquakes in advance, no such system or method has yet been found. The reduction of the devastating effects of the earthquakes, depend to be effectively prepared for them in every fields.

Turkey is highly vulnerable to natural disasters, particularly earthquakes, great loss of life and property has been experienced in previous earthquakes. In the 1999 Marmara earthquakes, the death toll reached over 17,000 with a direct economic impact estimated at about US\$5 billion, or around 2.5 percent of GNP.

Despite the fact that many scientific and experimental studies have been carried out on the evaluation of the seismic performance of existing residential and commercial buildings until the 1999 Marmara earthquake, studies devoted to the assessment of the seismic performance of existing bridges and viaducts, which are one of the most important parts of the transportation network, were very limited.

Until the 1999 Marmara earthquakes, it can be said that the seismic performance of bridges was much more adequate than the seismic performance of commercial and residential buildings. However, partial structural damage or complete collapse of Bolu viaduct, Mustafa İnan Viaduct, Arifiye and Sakarya bridges after the

Kocaeli and Düzce earthquakes in the Marmara region has led to the questioning of the seismic performance of existing bridges and viaducts in Turkey.

According to recent assessments, the probability of major earthquake affecting Istanbul in the next 30 years 62% -12%, while the likelihood of such devastation in the next decade is 32% - 12%. If a seismic event of the same magnitude as that in 1999 were occur near Istanbul, the human suffering as well as the social economic, and environmental impacts would be dramatically higher than in the Marmara region, as Istanbul is not only the financial, cultural and industrial center of country, but is also a nexus of intercontinental importance and home of about 15 million people. An interruption of Istanbul's social, economic and financial life would be felt for many years to come.(Parsons 2000-2004)

The General Directorate of Highways, taking into account the above-mentioned situations, started to work on the evaluation of the earthquake performance of the existing viaducts and bridges in Istanbul and the preparation of reinforcement projects according to their importance classes, by receiving consultancy services from the Japan Bridge&Structure Institute, Inc.

As in many countries in the world, U.S. (American Association of State Highway and Transportation Officials Standard Specifications for Highway Bridges - AASHTO LFD) , Japanese specifications and European Union, Eurocode specifications are generally used in the design, seismic performance evaluation and the retrofiting of bridges in Turkey.

General Directorate of Highways (KGM) and Middle East Technical University (METU) conducted a project, (Türkiye Köprü Mühendisliğinde Tasarım ve Yapıma İlişkin Teknolojilerin Geliştirilmesi Kılavuzu) based on Load and Resistance Factor Design (LRFD) to update current practice in Turkey.

General Directorate of Highways of Turkey, has launched an effort to develop specifications for the seismic design of highway and railway bridges and other lifeline structures and seismically isolated highway and railway bridges. In this thesis seismic performance assessment of a post tensioned box girder viaduct is studied based on the procedures of seismic isolation bridge design specifications of Turkey, as part of the newly developed Turkish Bridge Design Code(TBEC-2020).

1.2 Aims and Scope of the Study

The aim of this study can be listed as:

- To evaluate seismic performance of the Molla Gürani Viaducts in terms of new Turkey Bridge Earthquake Code (TBEC-2020) and Annexes.
- Explaining the seismic assessment method, nonlinear time history analysis method described in the new bridge earthquake code and guiding its use in later studies.
- To create a preliminary evaluation and analysis work template that can be used in the strengthening of bridges and viaducts that are likely to be made in the future.
- The author of this study chose to work on a real problem that will have likely be strengthened in the near future to measure and test his knowledge and skills in seismic performance assessment and reinforcement. Thus, the author aims to closely follow the rapid technological developments in seismic performance evaluation, seismic retrofit and seismic isolation, to renew his technical intelligence in accordance with today's conditions on newly developed techniques and solution methods, and to increase her skills in seismic performance assessment, retrofit and seismic isolation subject.
- It is aimed to use this study not only as a thesis study, but also as a preliminary report of a research project to be continued in the future on improving the seismic performance of bridges and viaducts, which has the technical competence to be included in the literature.

CHAPTER 2

2. LITERATURE REVIEW

2.1 Literature Review

In Turkey, mostly American Specifications have been used in bridge design and earthquake performance evaluation, and the use of Japanese Specifications has increased in recent years. Although the first written specification on bridge design was prepared by AASHTO in the United State in 1931, the first specification on seismic design could only be prepared by Caltrans in 1973, after the 1971 San Fernando earthquake. This was the first specification in the U.S. which considering dynamic-response characteristics of the structure and to force-reduction factors that account for inelastic behavior. These California seismic design criteria formed the basis of the national seismic provisions published in the 1977 AASHTO Standard Specifications for Highway Bridges.

In 1978, Applied Technology Council (ATC) developed an improved ATC-6 Seismic Design Guidelines for Highway Bridges that would be applicable to all regions in the U.S. FHWA followed this pioneering work by publishing Report No FHWA/RD-83/007, Seismic Retrofitting Guidelines for Highway Bridges[FHWA 1983]. This was the first document to focus on the seismic evaluation and retrofitting of ordinary highway bridges and provided nationally applicable guidelines to the bridge design profession. This work updated two times by FHWA in 1987 and 1995 , by the new knowledge gained from analytical and experimental research, and reconnaissance trips to earthquake-devastated areas. Seismic Retrofitting Manual for Highway Bridges [FHWA, 1995] manual has been revised, updated, an expanded by MCEER as the two

parts, Seismic Retrofitting Manual for Highway Structures: Part 1-Bridges (2006) and Part 2: Retaining Structures, Slopes, Tunnels, Culverts, and Pavements(2004). The working stress specification and limit state specification(LRFD Bridge Design Specifications) are the two national bridge design specifications in the United State at the present time.

Each country is trying to create specifications suitable for its own conditions on earthquake resistant bridge design, seismic performance evaluation and retrofit. The first bridge design guide in our country was prepared by the Middle East Technical University for the General Directorate of Highways with the TUBITAK project numbered 110G093 in March 2014. This guide was based on the Load and Resistance Factor Design (LRFD).

The first Bridge Earthquake Code and Seismic Isolation Bridge Design Specification of Turkey published by The Ministry of Transportation and Infrastructure in 2020 (Official Gazette No.: 31266, 2020). Structural damages at different levels or destruction mechanisms that occur in structures after each new earthquake make it necessary to update and develop seismic design specifications according to newly emerging conditions. It may also take a long time for the new seismic design specifications, which are becoming more and more complex and more comprehensive, to be fully understood and correctly applied by the practitioners or engineers.

The created specifications continue to be updated and developed by use of experiences gained from earthquakes and by using the results of some researches in progress such as dynamic behaviour of soil under the effect of earthquake ground motion, soil liquefaction, soil-structure interaction, pile group effects, etc.

CHAPTER 3

3. SITE INSPECTION AND GEOTECHNICAL PROPERTIES

3.1 Site Inspection

The information obtained from the site inspection at the location of the viaduct to determine the existing condition of the structural elements of the viaduct are as follows:

- The cross section geometric properties of the existing viaduct piers are compatible with the As-built projects.
- Elastomeric bearing have been installed on the viaduct inspected which were only visible on abutments at 0 and 9 axes. Even though elastomeric bearing were found to be in good condition in the visual inspection, the more reliable results must be obtained from a series of lab tests for a making decision to replace them with the new bearings or with different type of bearings. The remaining bearings (on the piers) were not visible without access equipment.



Figure 3.1 Visual Inspection

- At the bearings shelves debris from the construction phase was still evident. In locations with open expansion joints above the bearings, large accumulations of additional debris was observed on the bearing shelf. (Figure 3.1.)
- The dimensions of the elastomeric bearings were in agreement with those given in the As - built projects.

3.2 Geotechnical Parameters and Soil Properties

The information that obtained about the soil properties of the viaduct area and all the information about the engineering properties of the soil obtained by using the empirical equations in the literature are summarized below.

3.2.1 General Geology

The area where the viaduct is built and its immediate surroundings are within the Kartal Formation. Kartal formation, siltstone is rarely sandstone interlayer and is in the form of laminated-thin bedded shales. The clastic limestone layers towards the top of the formation are interbedded with shales. Shales; It has good cleavage properties, generally silt in size, quartz, feldspar, micaceous. There are locally altered zones several meters thick at the top of the outcrops. These altered cuttings; It easily turns into mud when they take in water.

Sandstone layers are generally sharp at the bottom, parallel inside and micro-cross laminated, sometimes convolute laminated. Quartz, feldspar, sericite, muscovite are among the main rock-forming minerals. These minerals are firmly bonded with cement. In addition, chertization, sericitization and clayization are observed in the matrix.

The lower faces of the clastic limestones are sharp and eroded, the interior is graded, parallel flow and rip laminated. These limestones are transitive to shales. Layer thickness varies between 10 cm and 2 m.

3.2.2 Information obtained from two 10 m borehole logs

According to the SK-1 borehole drilling, there is an artificial filling layer of 0.00-0.50 m, 0.50 m thick consisting of blocks, gravel and sand units without engineering value. And between 0.50-10.00 m. dark gray, blackish middle separated, limestone, medium weak units were passed. Groundwater was encountered at 5.00 m.

According to the SK-2 borehole drilling, there is an artificial filling layer of 0.00-4.00 m, 4.00 m thick consisting of blocks, gravel and sand units without engineering value. And between 4.00-12.00 m. dark gray, blackish middle separated, limestone, medium .weak units were passed. Groundwater was encountered at 5.00 m.

The soil profile for the viaduct location was idealized by using the SK-1 drilling and calculations were made on this idealized section. The graphs containing the relevant idealized profile and the geotechnical parameters of these layers are presented in Figure-3.2. Since there is no laboratory test available, the values of natural unit weight of soil were determined using the tables given in the references (7) and (8).

Table 3.1 Geotechnical parameters of soil, idealized from SK-1

Soil Type	Depth (m)	SPT (N)	C_u (kPa)	Point load index (MPa)	Natural Unit weight of soil, γ_n , (kN/m ³)
Infill Soil	0,00-0,50				17
Limestone	0,50-10,00		175	5,04 - 4,97	23

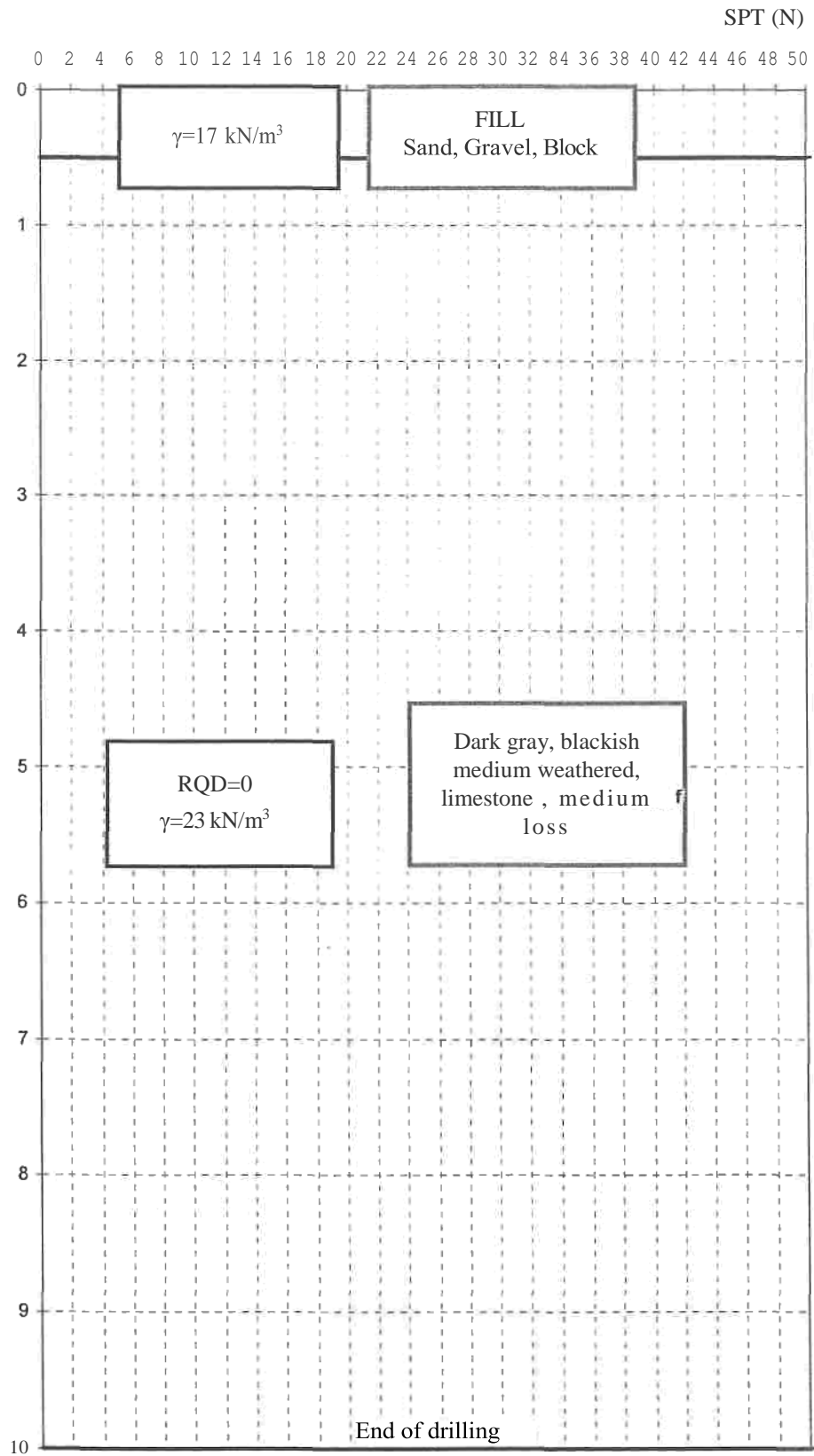


Figure 3.2 Viaduct SPT(N)-Depth Graph and Idealized Soil Profile

3.2.3 Soil classification according to FEMA 356 Specification.

Table 3. 2 Soil classes in FEMA 356

Soil Class	Shear Wave Velocity v_s ,(m/s)	Water Content $w(\%)$	Plasticity Index $PI(\%)$	Undrained Shear Strength c_u (kP)	SPT(N)	Notes
A	*1500					Hard Rock
B	$750 < v_s < 1500$					Rock
C	$360 < v_s < 750$			>96	>50	Very dense soil and soft rock
D	$180 < v_s < 360$			$48 < c_u < 96$	$15 < N < 50$	Stiff Soil
E	•90	>40	•20	•24		Any profile with more than 3 m of soft clay.
F1	Soils vulnerable to potential failure or collapse under seismic loading, such as liquefiable soils, quick and highly-sensitive clays, collapsible weakly-cemented soils					
F2	Peats and/or highly organic clays (H > 3 meter of peat and/or highly organic clay, where H= thickness of soil)					
F3	Very high plasticity clays (H > 7,5 meter with $PI > 75$)					
F4	Very thick soft/medium stiff clays (H > 36 meter).					

The parameters v_s , N , and c_u are, respectively, the average values of the shear wave velocity, Standard Penetration Test (SPT) blow count, and undrained shear strength of the upper 30 meter of soils at the site. These values shall be calculated from Equation (3.1), below:

$$v_s, N, c_u = \frac{\sum_{i=1}^n d_i}{\sum \frac{d_i}{v_{si}}, \frac{d_i}{N_i}, \frac{d_i}{c_{ui}}} \quad \text{Eqn. (3.1)}$$

where :

N_i : SPT blow count in soil layer “ i ”

n : Number of layers of similar soil materials for which data is available

d_i : Depth of layer “i”

- c_u : Undrained shear strength in layer “i”
- v_{si} : Shear wave velocity of the soil in layer “i”

and

$$\sum_{i=1}^n d_i = 30 \text{ m} \quad \text{Eqn. (3.2)}$$

If the shear wave velocity of soil is known soil classification can be made according to that velocity, otherwise according to undrained cohesion for cohesive soils, and according to the number of SPT(N) blow for cohesionless soils. The primary (pressure) wave velocity of soil is obtained from literature as $v_{p,10}=2000$ m/s and $v_{p,05}=1298$ m/s using the following formulation that given by Walls, J. D. et al.(2006), shear wave velocity calculated.

$$v_s = 0.73v_p - 767 \quad \text{Eqn. (3.3)}$$

$$v_s = 0.73 \times 2000 - 767 = 693 \text{ m/s}$$

$$v_{s,0.5} = 0.73 \times 1298 - 767 = 180 \text{ m/s}$$

3.2.4 Equations for calculation of shear wave velocity of soil

- **Sitharam et al.2006**

The regression equation developed between v_s and $(N_1)_{60cs}$ is given by the following equation:

$$v_s = 78[(N_1)_{60cs}]^{0.40} \quad \text{Eqn. (3.4)}$$

Where v_s is the shear velocity in m/s and $(N_1)_{60cs}$ is the corrected SPT “N” value. The regression equation useful for residual soil such as silty and sand silt with small amount of clay content.

$$v_s = 103[(N_1)_{60cs}]^{0.40} \dots\dots\dots \text{Upper Bound (+47 to 17 \% variation) Eqn.(3.5)}$$

$$v_s = 53[(N_1)_{60cs}]^{0.40} \dots\dots\dots \text{Lower Bound (-47 to 17 \% variation) Eqn.(3.6)}$$

- **Boominathan et al. 2006**

The SPT N-values obtained from the field were corrected for various factors:

- a. Overburden pressure
- b. Hammer energy
- c. Bore hole diameter
- d. Rod length
- e. Fines content

Shear wave velocity v_s was estimated from the corrected SPT-N values using the following empirical equations of Japon Road Association(JRA, 1980)

$$v_s = 100N^{1/3} \text{ m/s (For clay)} \quad \text{Eqn.(3.7)}$$

$$v_s = 80N^{1/3} \text{ m/s (For sand)} \quad \text{Eqn.(3.8)}$$

by using Egn. (1.1) average shear wave velocity calculated.

$$v_{s,avg} = \frac{\sum_{i=1}^n d_i}{\sum \frac{d_i}{v_{si}}} = \frac{10}{\frac{0.5}{180} + \frac{9.5}{693}} = 606.56 \text{ m/s}$$

So according to FEMA 356 soil classes table , the class of soil between 0-0.5 m depth is D while the class of second limestone layer between 0.50 - 9.50 m depth is C.

Table 3. 3 Comparison of Site Classification Systems

FEMA 356 NEHRP FEMA 273		BOORE	BOORE Suggested for NEHRP	AASHTO
Site Class	V_{S30} [m/s]	V_{S30} [m/s]	V_{S30} [m/s]	V_{S30} [m/s]
A	> 1500	> 750		
B	750 - 1500	350 - 750	1070	I > 760
C	360 - 750	180 - 360	520	II
D	180 - 360	< 180	250	III
E	< 180			IV < 150
F	N.A.			

3.2.5 Hooke-Brown Strength Criterion.

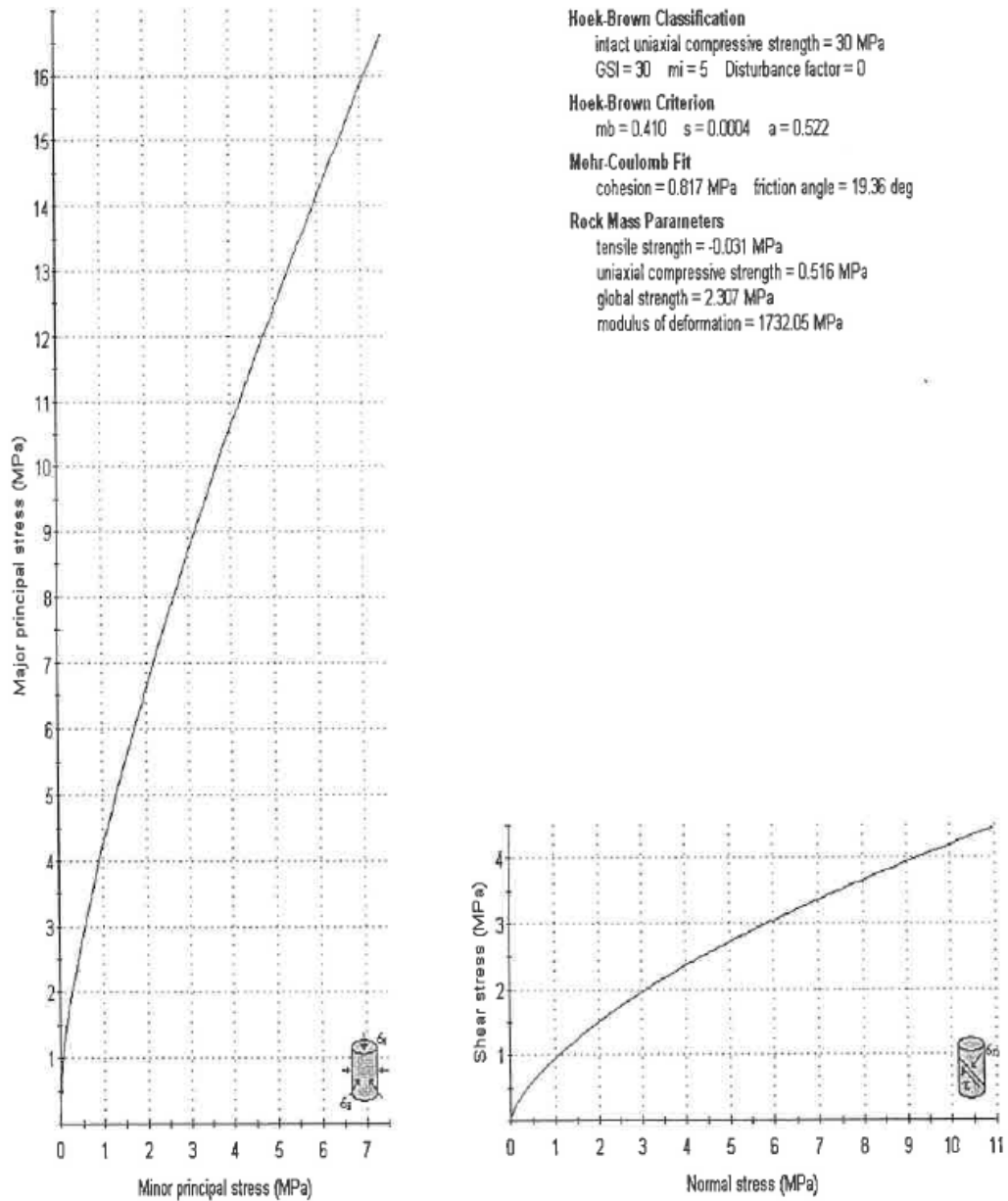


Figure 3. 3 RocLab Result

$$a = \frac{1}{2} + \frac{1}{6} \left(e^{-\frac{GSI - 20}{15} \frac{-20}{3}} \right) = \frac{1}{2} + \frac{1}{6} \left(e^{-\frac{30 - 20}{15} \frac{-20}{3}} \right) = 0.522$$

$$s = \exp\left(\frac{GSI - 100}{9 - 3D}\right) = \exp\left(\frac{30 - 100}{9 - 3 \times 0}\right) = 4.189 \times 10^{-4} \cong 0.0004$$

$$m_b = m_i \exp\left(\frac{GSI - 100}{28 - 14D}\right) = 5 \exp\left(\frac{30 - 100}{28 - 14 \times 0}\right) = 0.410424993 \cong 0.410$$

$$\sigma_c = \sigma_{ci} s^a = 30 \times 0.0004^{0.522} = 0.516 \text{ MPa}$$

$$\sigma_t = s \frac{\sigma_{ci}}{m_b} = 0.0004189 \frac{30}{0.410} = 0.031 \text{ MPa}$$

$$E_m = 1732.05 \text{ MPa} = 1732050 \frac{kN}{m^2}, \quad \phi = 20^\circ, \quad c = 0.817 \text{ MPa}$$

where :

- m_i : Material constant for intact rock in the Hoek-Brown failure criterion
(to be found from triaxial test on rock cores or simply by table values corresponding to rock type)
- m_b : Material constant for broken rock in the Hoek-Brown failure criterion
JP = jointing parameter (Palmstrom, 1995a)
- s : Material constant in the Hoek-Brown failure criterion
- a : Material constant for broken rock in the Hoek-Brown failure criterion
- D : Disturbance factor; the degree of disturbance caused by blast damage and stress relaxation
- GSI : Geological Strength Index
- σ_{ci} : Intact uniaxial compressive strength
- σ_c : Uniaxial compressive strength
- σ_t : Tensile strength
- E_m : Modulus of Deformation
- ϕ : Internal friction angle
- RQD : Rock Quality Designation that is a simple way of classifying the rock in terms of discontinuity intensity.

3.2.6 Bearing Capacity of Shallow Foundation Prandtl-Caquot Equations.

Allowable bearing capacity	: q_a	Depth, Z	: 0 m
Safety Factor	: SF	$\tan \phi$: 0.364
Ultimate bearing capacity	: q_{ult}	Cohesion, c	: 0.817 MPa
Internal friction angle			: 20°

As a result of the analysis made with RocLab, it was determined that there is a soft limestone with very low RQD value and very low strength parameters. Therefore, the factor of safety will be taken as 10.

Safety Factor, SF : 10

$$\alpha = \tan^2 \left(\frac{\pi}{4} + \frac{\phi}{2} \right) e^{(\pi \tan \phi)} = \alpha = \tan^2 \left(\frac{\pi}{4} + \frac{20}{2} \right) e^{(\pi \tan 20)} = 6.3994$$

Effective unit weight of soil : $\gamma=17 \text{ kN/m}^3$

$$q_{ult} = \gamma z_i \alpha + c(\alpha - 1) \cot \phi$$

$$q_{ult} = 17 \times 0 \times 6.3994 + 0.817(5.3994) \cot(20) = 12119 \frac{\text{kN}}{\text{m}^2}$$

$$q_a = \frac{q_{ult}}{SF} = \frac{12119}{10} = 1211.9 \frac{\text{kN}}{\text{m}^2}$$

Modulus of subgrade reaction of soil

$$k_s = 40 SF q_{ult} = 40 \times 10 \times 1211.9 \frac{\text{kN}}{\text{m}^2} = 484760 \frac{\text{kN}}{\text{m}^3}$$

In the calculations and analysis of the structure, modulus of subgrade reaction of soil $k_s = 484760 \text{ kN/m}^3$ is used.

3.2.7 Bearing Capacity of Pile Foundation

The superstructure loads were carried to the pile group with a diameter of 165 cm. The pile lengths are approximately 12 m and the pile heads are driven into the 3-4 m thick cap beam. It is shown in the pile application projects that the piles are socketed at least 8 m into the limestone.

For the values of deformation modulus $E_m = 1732.05 \text{ MPa}$, the unconfined compressive strength of limestone is given between 1.40 - 5.70 MPa from the unit load test results (Appendix D). The average unconfined compressive strength of limestone has taken as $q_{uc} = 3 \text{ MPa}$.

3.2.8 Williams and Pells Method for Skin Resistance in Weak Rock

This method takes into consideration the joints of the rock mass represented by the Rock Quality Designation RQD of that rock. (Williams and Pells,1981)

$$f_{sult} = \alpha \beta q_{uc}$$

where α is an adhesion factor of the intact rock recommended in the graph in Fig. 4.4, and β is a reduction factor that is related to the mass continuity factor j as shown in Fig. 4.5. The mass continuity factor in return, is related to the number of joints in a unit distance or in other words the spacing between the joints and it can be directly estimated from the RQD of the rock, see Table 4.4.

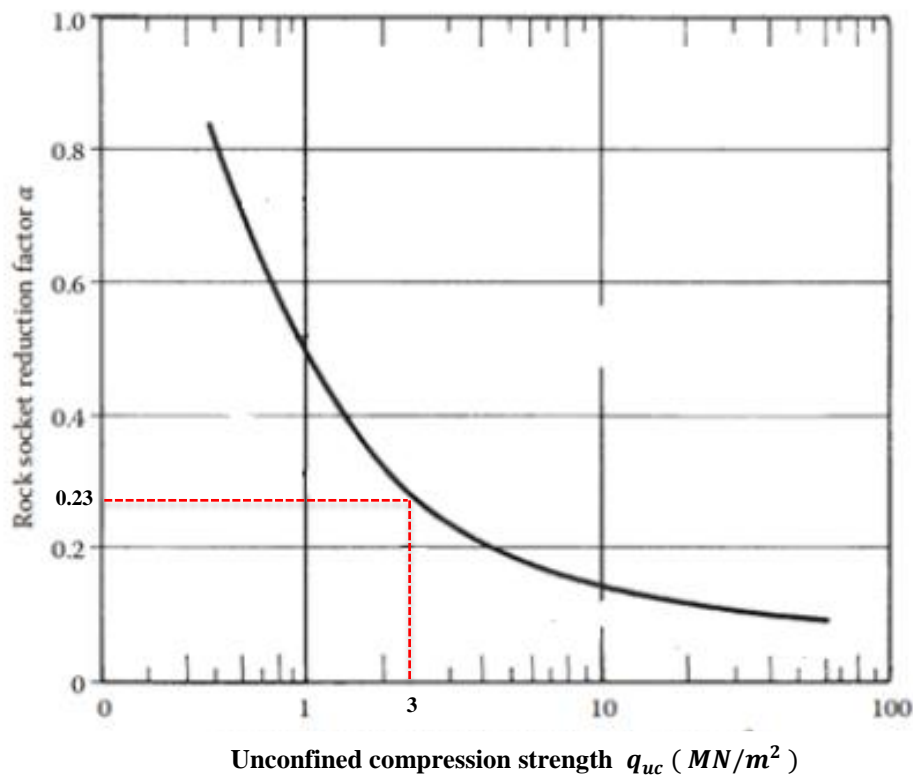


Figure 3. 4 The adhesion factor of intact weak rocks (mudstone, shale, sandstone, etc.) from Williams and Pells

Table 3.4 Mass factor J values corresponding to RQD

RQD(%)	Fracture frequency per meter	Mass factor
0 - 25	>15	0.2
25 - 50	15 - 8	0.2
50 - 75	8 - 5	0.2 - 0.5
75 - 90	5 - 1	0.5 - 0.8
90 - 100	1	0.8 - 1

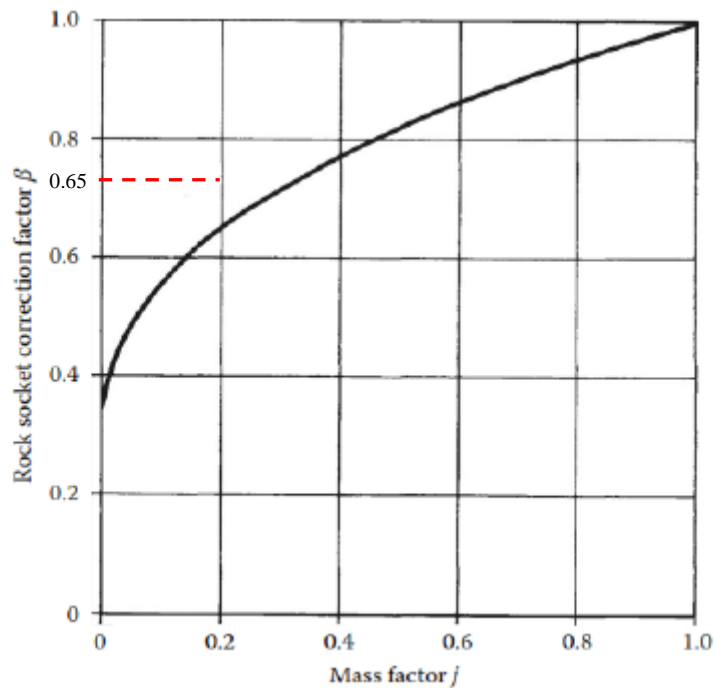


Figure 3. 5 The correction factor β in Williams and Pells method

$SF = 3$, $\alpha = 0.23$ from Fig.3.4 and $\beta = 0.65$ from Fig.3.5.

$$f_{sult} = \alpha \beta q_{uc} = 0.23 \times 0.65 \times 3 = 0.4485 \text{ MPa} = 448.5 \frac{\text{kN}}{\text{m}^2}$$

It has been shown that the pile socket length is 8 m and the pile diameter is 1.65 m in the viaduct pile foundation projects. Since the ratio of the pile socket length to the pile diameter is greater than 4 ($8/1.65=4.85$), the pile bearing capacity calculation has been made by considering only the pile ultimate frictional capacity.

$$Q_{sult} = 2\pi r L_{socket} f_{sult} = 2\pi \times \frac{1.65}{2} \times 8 \times 448.5 = 18598.86 \text{ kN}$$

$$W_{pile} = \pi r^2 L \gamma_{concrete} = \pi \times \left(\frac{1.65}{2}\right)^2 \times 12 \times 25 = 641.47 \text{ kN}$$

- **Single pile ultimate bearing capacity**

$$Q_{ult} = Q_{sult} + Q_{bult} - W_{pile} = 18598.86 + 0 - 641.47 = 17957.39 \text{ kN}$$

$$Q_{all} = \frac{Q_{ult}}{FS} = \frac{17957.39}{3} = 5985.8 \text{ kN}$$

In the structural analysis model of pile foundation, the socket length of pile is taken as 2 m (minimum socket length) .

$$Q_{sult} = 2\pi r L_{socket} f_{sult} = 2\pi \times \frac{1.65}{2} \times 2 \times 448.5 = 4649.71 \text{ kN}$$

$$Q_{bult} = q_{bult} A_b = q_{bult} \pi r^2$$

$$q_{bult} = N_q \sigma'_v + c N_c$$

$$q_{bult} = 5 \times 20 \times 13 + 817 \times 9 = 8653 \text{ kN/m}^2$$

$$Q_{bult} = q_{bult} A_b = 8653 \times \pi \left(\frac{1.65}{2}\right)^2 = 18502.25 \text{ kN}$$

$$W_{pile} = \pi r^2 L \gamma_{concrete} = \pi \times \left(\frac{1.65}{2}\right)^2 \times 12 \times 25 = 641.47 \text{ kN}$$

- **Single pile ultimate bearing capacity**

$$Q_{ult} = Q_{sult} + Q_{bult} - W_{pile} = 4649.71 + 18502.25 - 641.47 = 17957.39 \text{ kN}$$

One of the following approaches can be applied in calculating the bearing capacity of pile foundations according to TBEC-2020 (8.4.4.1).

(a) Bearing capacity of piles can be calculated by using the data obtained from pile static load tests.

(b) It can be calculated using soil properties from soil explorations/soil investigations.

(c) It can be calculated using the results obtained from dynamic loading tests validated by static loading tests.

The safety factors or strength coefficients which will be used in the calculation of base bearing capacity and skin friction resistance of pile foundations capacity are given in Table 4.5.

Table 3.5. Safety factors in calculating the pile bearing capacity

Strength Coefficients	Strength Coefficients Values (Safety Factors)	
	If no pile loading tests have been carried out	If pile loading tests have been carried out
Skin friction (compression)	1.5	1.3
Skin friction (tension)	1.6	1.4
Pile tip(base) resistance	2.0	1.5
Total bearing capacity (compression)	–	1.4

$$Q_{all} = \frac{Q_{sult}}{FS} + \frac{Q_{bult}}{FS} = \frac{Q_{sult}}{FS} + \frac{Q_{bult}}{FS} = \frac{18502.25}{2} + \frac{4649.71}{1.5}$$

$$Q_{all}^{compression} = 9251.125 + 3099.807 = 12350.93 \text{ kN}$$

$$Q_{all}^{tension} = \frac{Q_{bult}}{FS} = \frac{4649.71}{1.6} = 2906.07 \text{ kN}$$

- **Crushing Strength of Pile Concrete :**

$$\pi r^2 f'_c = \pi 0.825^2 \times 20\,000 \times 0.4 = 17105.97 \text{ kN /m}$$

where :

Ultimate base capacity : Q_{bult}

Ultimate frictional capacity : Q_{sult}

Coefficient of horizontal subgrade reaction

$$k_s = 1.6 \frac{E_s}{\text{Pile Diameter}} \quad \text{For cohesive soil} \quad \text{Eqn. (1.9)}$$

$$k_s = 3 \frac{E_s}{\text{Pile Diameter}} \quad \text{For cohesionless soil} \quad \text{Eqn. (1.10)}$$

Young's modulus of soil

$$E_s \left(\frac{kN}{m^2} \right) = 500c_u \quad \text{Banerjee and Driscoll (1976)} \quad \text{Eqn. (1.11)}$$

$$E_s \left(\frac{kN}{m^2} \right) = 766 N_f \quad \text{Schmertmann(1970)} \quad \text{Eqn. (1.12)}$$

where :

Field SPT number : N_f

Ultimate frictional capacity : Q_{sult}

$$E_s = 500c_u = 500 \times 175 = 87\,500 \frac{kN}{m^2}$$

$$k_s = 1.6 \times \frac{E_s}{\text{Pile Diameter}} = 1.6 \times \frac{87\,500}{1.65} = 84848.5 \text{ kN/m}^3$$

Table 3.6. Young's Modulus and coefficient of horizontal subgrade reaction

Soil Type	Depth (m)	C_u (kPa)	Young's Modulus E_s , (kN/m ²)	Coefficient of horizontal subgrade reaction k_h , (kN/m ³)
Fill Soil	0,00 - 4,00			-
Limestone	4,00 - 12,00	175	87,500	84,848

CHAPTER 4

4. ROUTE AND FEATURES OF THE PROJECT

4.1 Route and Features of the Project

Molla Gürani Viaduct is located in front of Elmalı Dam on the TEM(O-2 motorway) in Marmara Region of Turkey, within the boundaries of Istanbul province. (Figure 4.1). The viaduct was built between 1986 and 1990 by the IGL and STFA Joint Venture, with a loan from Japan for the construction of the Fatih Sultan Mehmet Bridge and the connection roads.



Figure 4. 1 Location description map

The coordinates of the viaduct are Latitude : 41.074572° , Longitude : 29.102464° which used for obtaining seismic design parameter from Disaster and Emergency Management Authority (AFAD) internet address <https://tdth.afad.gov.tr/>.

According to recent assessments, the probability of occurrence a major earthquake affecting Istanbul in the next 30 years is very high. If a seismic event of the same magnitude as the powerful November 12, 1999 Duzce earthquake is occur in Marmara region, impact of it may be dramatically higher than before. It is clear that the strengthening of bridges and viaducts against a possible Istanbul earthquake, has become an urgent necessity to mitigate earthquake damages and harmful effects. The seismic performance evaluation of the existing Molla Gürani viaduct and strengthening of it , was chosen as the subject of this study, considering the above-mentioned situations.

4.2 General Information about Molla Gürani(Elmalı) Viaduct



Figure 4. 2 Molla Gürani Viaduct

Construction Method	: Incremental Launching Method
Total Deck Length	: 498.8 m
Number of Span	: 9 (7 x 58 m + 2 x 46.4 m)
Girder Section	: Post Tensioned Box Girder

Skew Angle	: 0 °	
Number of Lanes	: 4	
Total width of a deck	: 20 m	
The width of right sidewalk	: 0.75 m	
The width of left sidewalk	: 1.25 m	
The height of sidewalks	: 0.30 m	
The clear roadway width	: 18 m (each viaducts)	
Pier Sections	: Rectangular Hollow Box	
Foundation	: P1, P2, P3, P4, P7, P8 are shallow and P5 , P6 are pile foundations.	
Design Truck	: HS20-44	AASHTO 1989 14 th Ed. (3.7.3)

4.3 Superstructure of Viaducts

Molla Gürani viaduct consists of two parallel viaducts, each carrying separate traffic directions. There is 1.50 m gap between two adjacent viaducts. Viaducts have 10 axes numbered from 0 to 9. Each viaduct has 9 spans. Seven mid-spans of the nine are 58 m long and the remaining two end spans are each 46.4 m long. The total length between the 0 and 9 axes is 498.8 m. (Figure 4.3 and 4.4).

The superstructure is continuous, rests on elastomeric bearing and expansion joints are only present at abutments. The deck is post tensioned box girder with an average total height of 5.03 m. The total width of each deck is 20 m. The right sidewalk width is 0.75 m and left sidewalk width is 1.25 m. The roadway width is 18 m curb to curb and there is a 6 cm thick bituminous wearing overlay on it. (Figure 4.3).

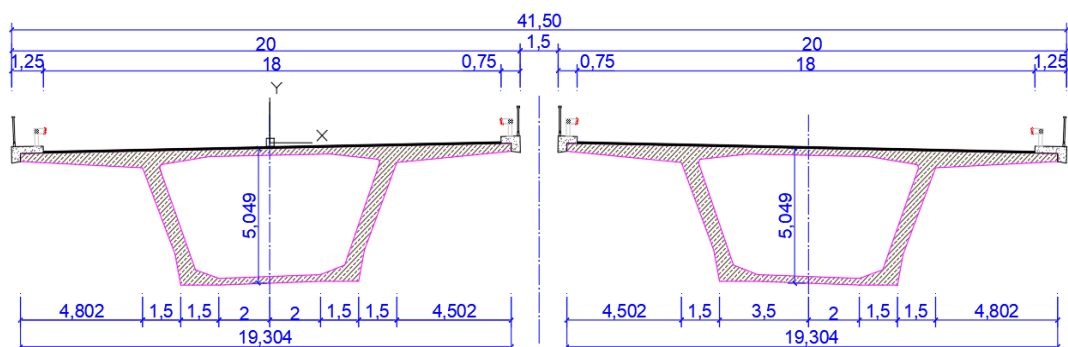


Figure 4.3. Box Girder Section at Span

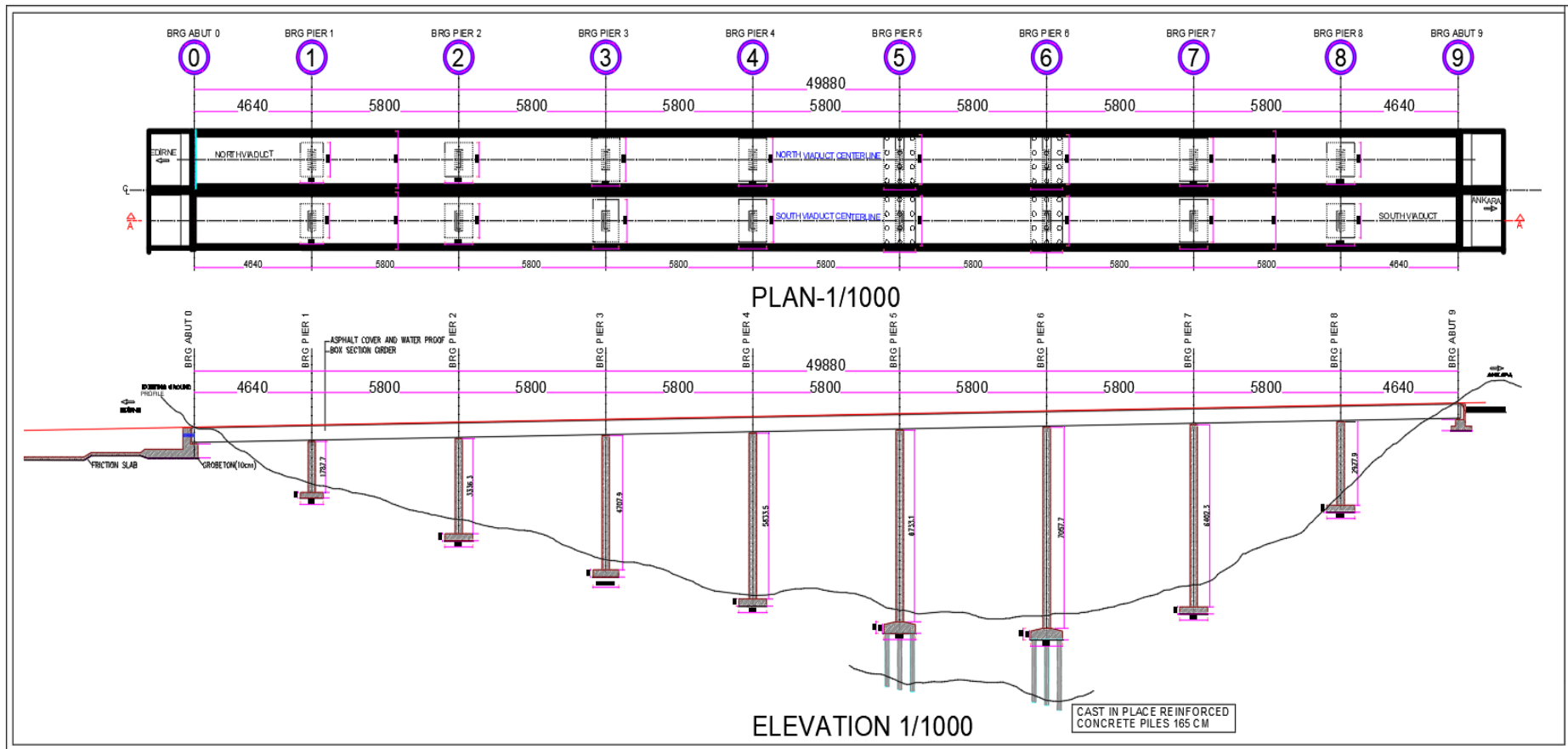


Figure 4.4. Viaduct Plan and Elevation

4.4 Typical Pier Sections and Substructure of Viaducts

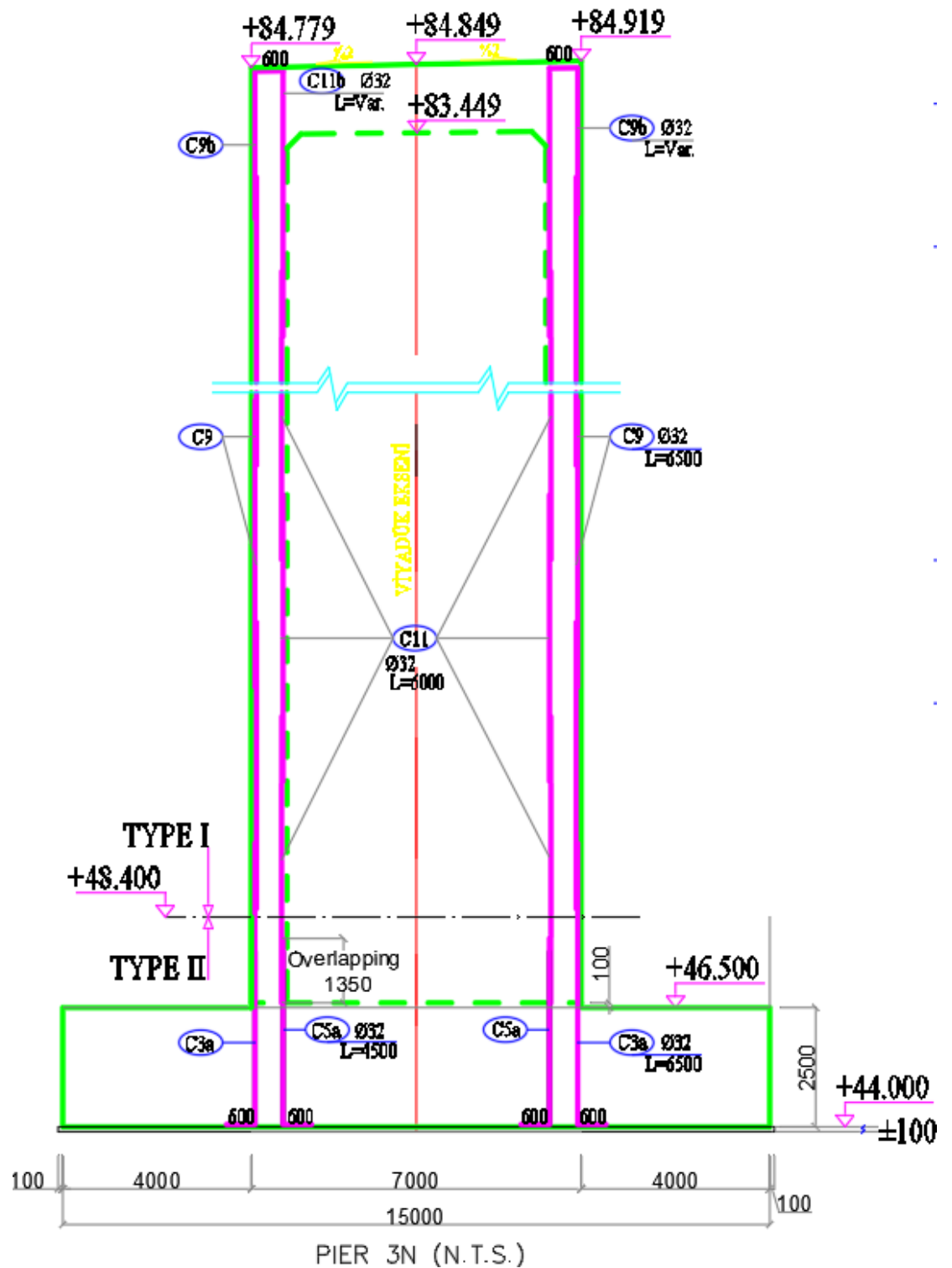


Figure 4.5. Typical Pier Section (North Viaduct Axis 3)

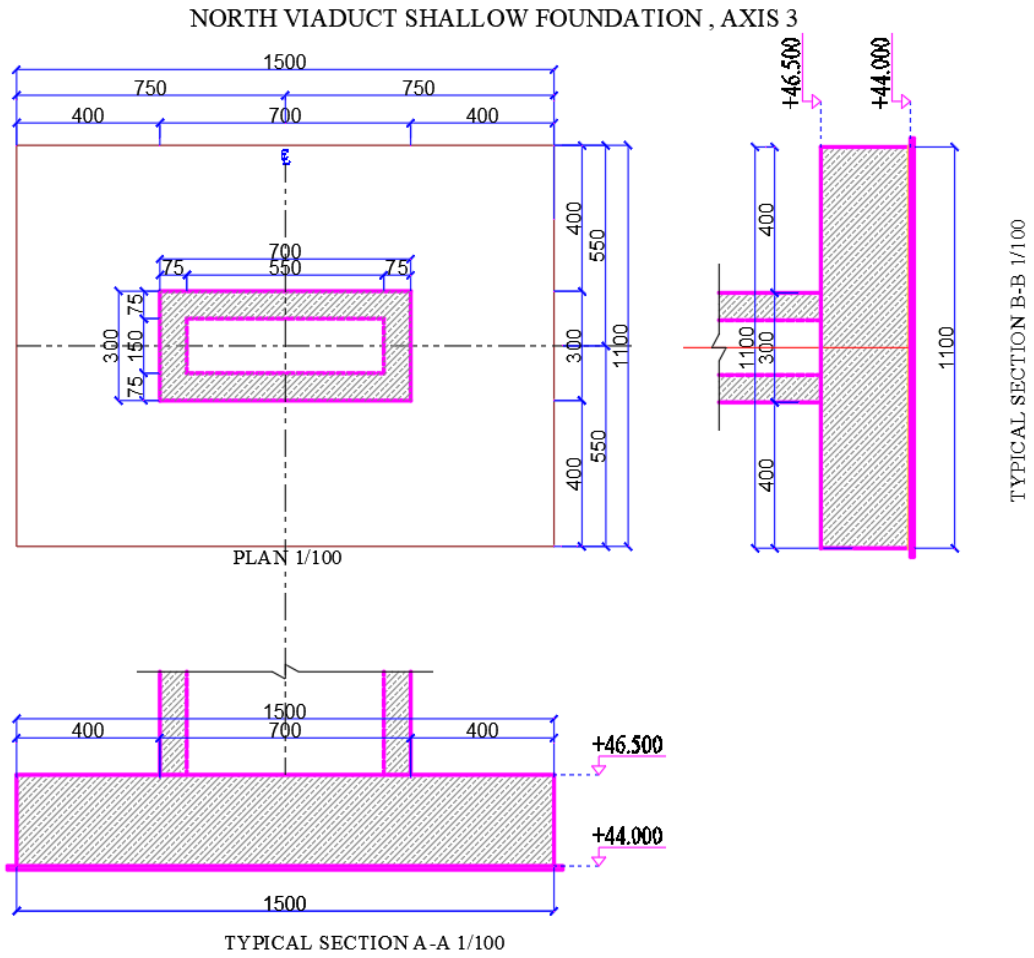


Figure 4.6. Foundation Plan and Typical Sections (North Viaduct Axis 3)

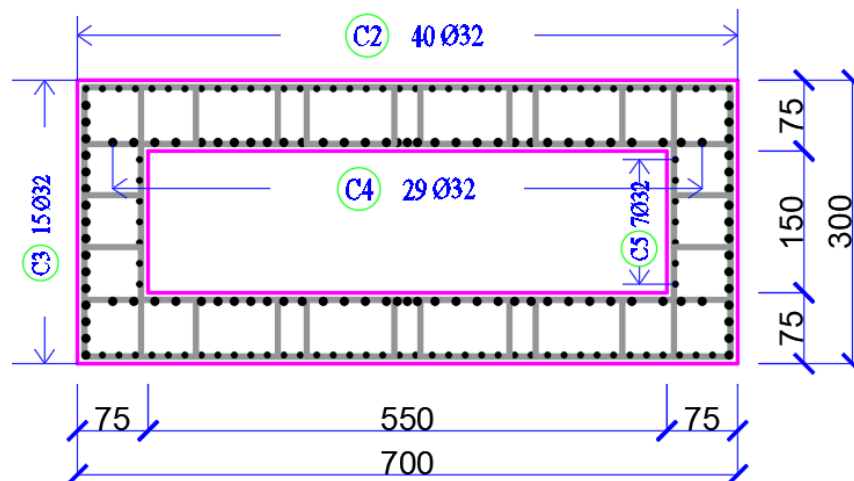


Figure 4.7. General Reinforcement Layout Type I (North Viaduct Axis 3)

- PIER 3 Cross Section Properties

Cross Sectional Area : 12.7500 m²

Principal moments and X-Y directions about centroid:

: I: 14.2031 m⁴ along [1.0000 0.0000]

: J: 64.9531 m⁴ along [0.0000 1.0000]

Table 4.1. Top Cross Section Reinforcement Ratio of North Viaduct Pier 3

Number of Bars	Diameter Φ [mm]	Bar Area A [cm ²]	Total Longitudinal Reinforcement Area A [cm ²]	Pose	Similar
15	32	8.0425	241.27	C3	2
7	32	8.0425	112.59	C5	2
40	32	8.0425	643.40	C2	2
29	32	8.0425	466.46	C4	2

Total Longitudinal Reinforcement Area 1463.7308 cm²
 Percent of Longitudinal Reinforcement 0.6970%

Table 4.2. Bottom Cross Section Reinforcement Ratio of North Viaduct Pier 3

Number of Bars	Diameter Φ [mm]	Bar Area A [cm ²]	Total Longitudinal Reinforcement Area A [cm ²]	Pose	Similar
9	32	8.0425	144.76	C3	2
5	32	8.0425	80.42	C5	2
23	32	8.0425	369.95	C2	2
21	32	8.0425	337.78	C4	2

Total Longitudinal Reinforcement Area 932.9274 cm²
 Percent of Longitudinal Reinforcement 0.7317%

Longitudinal reinforcement percentages that used to obtain the moment curvature relationship are given in Table 4.1&4.2 The concrete is assumed to be unconfined due to the large spacing of the transverse reinforcement. The section properties of the upper 1.40 m solid section of the viaduct piers are defined in the three-dimensional model of the viaduct and the moment curvature relationship.

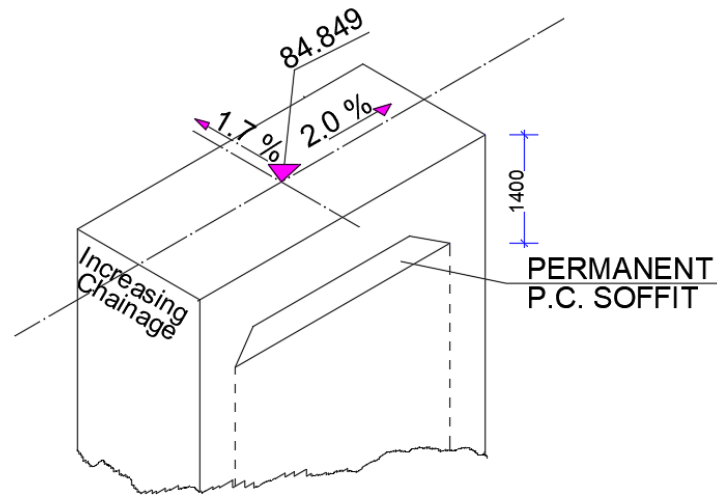


Figure 4.8. The detail of top Pier

Table 4.3. Foundation Type and Pier(Column Elevations) Heights

Axis	Foundation Type		Foundation Top Level [meter]		Column Top Level [meter]		Column Length [meter]	
	North	South	North	South	North	South	North	South
0	Shallow	Shallow	82.088	82.088	-	-	-	-
1	Shallow	Shallow	82.877	82.877	72.0	65.0	10.877	17.877
2	Shallow	Shallow	83.863	83.863	59.5	50.5	24.363	33.363
3	Shallow	Shallow	84.849	84.849	46.5	37.77	38.349	47.079
4	Shallow	Shallow	85.835	85.835	28.5	27.5	57.335	58.335
5	Pile	Pile	86.821	86.821	18.97	19.49	67.851	67.331
6	Pile	Pile	87.807	87.807	17.23	17.23	70.577	70.577
7	Shallow	Shallow	88.793	88.793	25.6	24.77	63.193	64.023
8	Shallow	Shallow	88.779	88.779	60.5	60.5	28.279	28.279
9	Shallow	Shallow	90.568	90.568	-	-	-	-

4.5 Elastomeric Bearings

There are two elastomeric bearings at each of the abutments and four on each piers. The reinforced bearings (consisting of layers of elastomer restrained at their interfaces by integrally bonded steel properties of the elastomeric bearings) that installed to viaduct has following properties:

Rubber : According to CNR-UNI 10018/85 Specification
: Shore A hardness 60 ± 5
Reinforced Steel : Fe 430 – UNI 7070
F : Fixed bearings (Algabloc NB), S : Sliding bearings (Algabloc NTm)
G : Sliding guided bearings (Algabloc NTu)

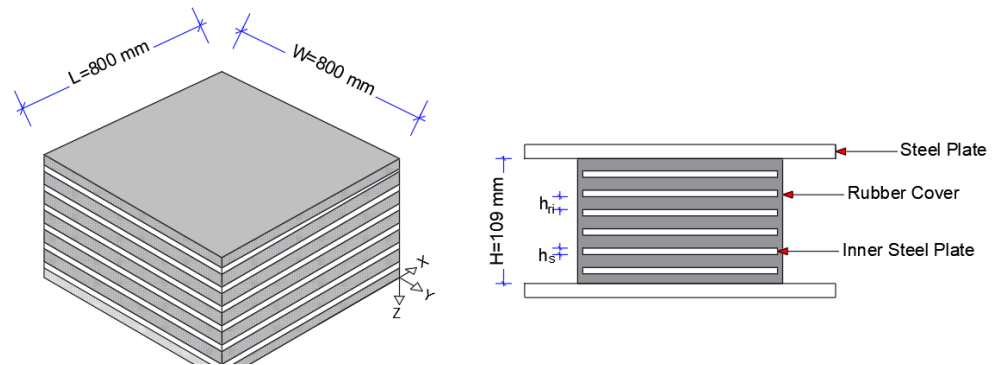


Figure 4.9. The detail of elastomeric bearings. (axes 0, 1, 2, 3, 9.)

Table 4.4. The dimensions of the elastomeric bearings

Axis	Dimensions of elastomeric bearings										Kh
	N	Width	Length	Height	nr	hri	ns	hs	hst	hrt	
		W (mm)	L (mm)	H (mm)							
0	2	800	800	109	5	16	6	4	24	85	8583.53
1	4	800	800	109	5	16	6	4	24	85	8583.53
2	4	800	800	109	5	16	6	4	24	85	8583.53
3	4	800	800	109	5	16	6	4	24	85	8583.53
4	4	800	800	129	6	16	7	4	28	101	7223.76
5	4	800	800	209	10	16	11	4	44	165	4421.82
6	4	800	800	209	10	16	11	4	44	165	4421.82
7	4	800	800	161	8	15	9	4	36	125	5836.80
8	4	800	800	189	9	16	10	4	40	149	4896.64
9	2	800	800	109	5	16	6	4	24	85	8583.53

The shear modulus of the reinforced elastomeric bearings is given between 0.9 - 1.38 MPa in the Table 14.7.6.2-1 of AASHTO LRFD Bridge Specifications 2007, 4th Edition. The arithmetic mean value of given values $G=1.14$ MPa was accepted as the shear modulus of the elastomeric bearings in the calculations. Upper

bound, lower bound and mean values of the shear modulus calculated and three different analyses based on these values are performed. All results of the three different cases compared with each other.

$$S = \frac{LW}{2 h_{r,i} (L + W)} = \frac{800 \times 800}{2 \times 16 \times (800 + 800)} = 12.50$$

$$E = 6GS^2 = 6 \times 1140 \times (12.50)^2 = 1,068,750 \frac{kN}{m^2}$$

$$K_h = \frac{A \cdot G}{h_{eff}} = \frac{0.64 \times 1140}{0.085} = 8,583.53 \frac{kN}{m}$$

$$K_v = \frac{E \cdot A}{h_{eff}} = \frac{1,068,750 \times 0.64}{0.085} = 8,047,058.82 \frac{kN}{m}$$

$$K_{r,x} = K_{r,y} = K_\theta = \frac{E \cdot I_x}{h_{eff}} = \frac{E \cdot I_y}{h_{eff}} = \frac{1,068,750 \times \frac{0.8 \times 0.8^3}{12}}{0.085} = 429,176.47 \frac{kNm}{rad}$$

The horizontal(longitudinal) stiffness coefficient of Pier 8 sliding elastomeric bearing is calculated as follows:

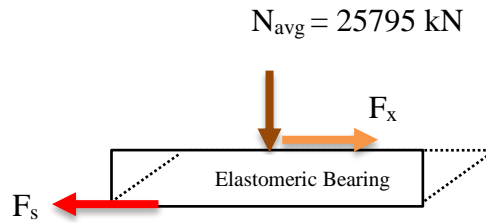


Figure 4.10. The horizontal stiffness coefficient of Pier 8 elastomeric bearings.


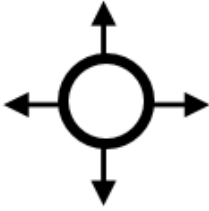

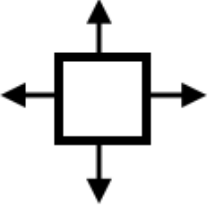



The friction coefficient of the elastomeric bearing is equal to 4 %. The average longitudinal displacement $u_x^{(8)} = 0.1984 m$ is obtained from the analysis results under DD1 earthquake ground motion level and it is used in the calculation of the horizontal stiffness of sliding bearing of Pier 8 .

$$F_x = F_s = \mu N_{avg} = 1031.8 kN \quad F_x^{(8)} = K_h^{(8)} u \quad , K_h^{(8)} = \frac{F_x^{(8)}}{u_x^{(8)}} = \frac{1031.8}{0.1984} = 1300 \frac{kN}{m}$$

where :

- N_{avg} : The average vertical force on the elastomeric sliding bearing.
- μ : Static friction coefficient of the elastomeric sliding bearing
- F_s : Elastomeric sliding bearing friction force in longitudinal direction
- F_x : Horizontal force in longitudinal direction
- N : Number of the elastomeric bearing in each axis
- G : Shear modulus of the elastomer (MPa)
- L : Length of a rectangular elastomeric bearing (Plan dimension of the bearing perpendicular to the axis of rotation under consideration (parallel to the global longitudinal bridge axis (mm))
- W : Width of the rectangular elastomeric bearing (Plan dimension of the bearing parallel to the axis of rotation under consideration (parallel to the global transverse bridge axis (mm))
- S_i : Shape factor of the thickest layer of the bearing. (S_i is taken as plan area of the elastomeric bearing layer divided by the area of the perimeter free to bulge)
- $h_{r,i}$: Thickness of i-th elastomeric layer in elastomeric bearing (mm)
- $h_{r,t}$: Total thickness of the elastomeric layers in elastomeric bearing (mm)
- n_r : Number of the internal elastomer layers
- h_s : Thickness of a single steel plate in elastomeric bearing (mm)
- h_{st} : Total thickness of the steel plates in elastomeric bearing (mm)
- n_s : Number of the steel plates in elastomeric bearing
- K_h : Horizontal stiffness coefficient of elastomeric bearing
- K_v : Vertical stiffness coefficient of elastomeric bearing
- K_θ : Rotational stiffness of elastomeric bearing

Table 4.5 Symbolic Representation of Bearing Function

Axis	Symbol	Bearing Type	Resists Vertical Load	Resists Horizontal Force Along Direction (In the horizontal)	Permits Translation Along Direction (In the horizontal plane)	Permits Rotation Axis (In the horizontal plane)
0		Fixed Pot	Yes	Any	No	Any
1		Free Sliding Pot-cum-PTFE	Yes	No	Any	Any
2		Guided Sliding Pot-cum-PTFE	Yes	Uni-directional	Uni-directional	Any
3		Free PTFE Sliding Assembly	Yes	No	Any	No
4		Guided PTFE Sliding Assembly	Yes	Uni-directional	Uni-directional	No
5		Pin	No	Any	No	Any
6		Metallic Guide	No	Uni-directional	Uni-directional	Uni-directional

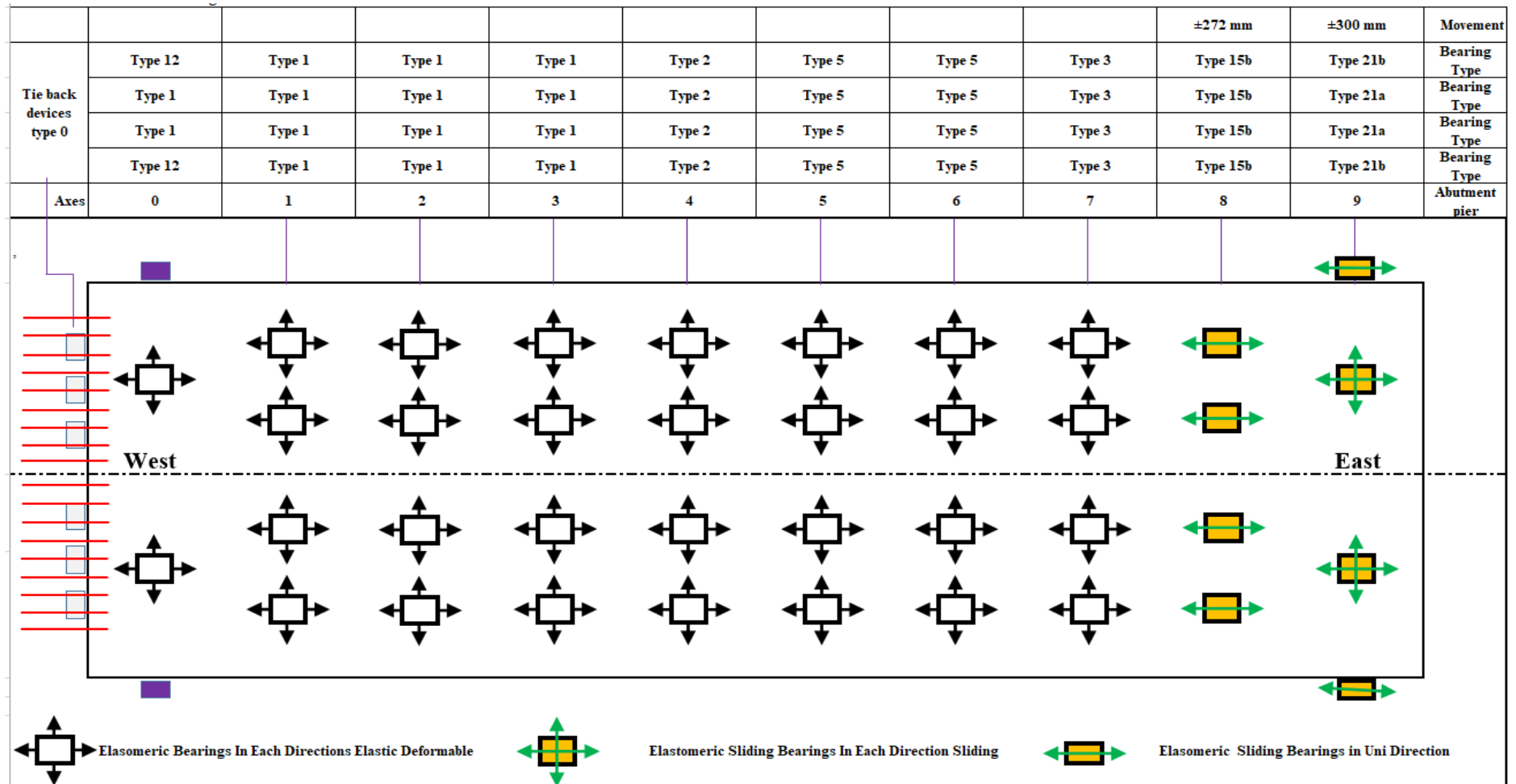


Figure 4.11 The function and configuration plan of the viaduct bearings

CHAPTER 5

5. EARTHQUAKE GROUND MOTION

5.1 Bridge Performance Earthquake Ground Motion Level

Four types of earthquake ground motion levels are identified in Turkey Bridge Earthquake Code (TBEC-2020)

5.1.1 Earthquake Ground Motion Level-1 (DD-1)

This earthquake ground motion level, provides spectral ordinates (PGA, S_A at $T=0.2$ and 1.0 s) for return periods of 2475 years with probability exceedance 2 % in 50 years. It represents the highest intensity, very infrequent earthquake ground motions that bridge structures within the scope of the code may be subjected to.

5.1.2 Earthquake Ground Motion Level-2 (DD-2)

DD-2 Earthquake Ground Motion describes a rare earthquake ground motion with 10% probability of spectral magnitudes exceeding 50 years and a corresponding the return period of 475 years. This earthquake ground motion is also called the standard design earthquake ground motion.

5.1.3 Earthquake Ground Motion Level-3 (DD-2a)

DD-2a Earthquake Ground Motion describes the frequent earthquake ground motion where the probability of exceedance of spectral magnitudes in 50 years is 30% (50% in 100 years) and the corresponding recurrence period is 144 years. Spectral acceleration data of this ground motion level are defined in Annex 2A of TBEC-2020.

5.1.4 Earthquake Ground Motion Level-4 (DD-3)

DD-3 Earthquake Ground Motion refers to frequent earthquake ground motions where the probability of spectral magnitudes exceeding 50% in 50 years and the return period of 72 years.

5.2 Standard Earthquake Ground Motion Spectrums

In TBEC, earthquake ground motion spectrums are defined for a 5% damping ratio based on a specific earthquake ground motion level, in a standard form or by implementing site-specific earthquake hazard analyses depending on the mapped spectral acceleration coefficients and local site parameter coefficients.

5.2.1 Determination of spectral acceleration coefficients

In TBEC-2018, dimensionless mapped spectral acceleration coefficients are given as short-period(0.2 sec.) response acceleration coefficient, S_s , and long-period(1 sec.) response acceleration coefficient, S_1 , for four different earthquake ground shaking hazard levels. The values of the mapped spectral acceleration coefficient can be obtained in a dimensionless form directly from the Turkish earthquake hazard map by selecting a point, where the structure will be built for any considered earthquake hazard level. After determining mapped values of S_s and S_1 , the design response acceleration coefficients S_{DS} and S_{D1} can be determined as follow:

$$S_{DS} = S_s F_s \quad ; \quad S_{D1} = S_1 F_1 \quad (5.1)$$

where :

F_s and F_1 are the local site coefficients, S_{DS} and S_{D1} are the design response acceleration coefficient for a short period and 1-second period.

5.2.2 Determination of the local soil effect parameters

The values of the local soil/site effect parameters F_s and F_1 defined for different soil classes in TBEC-2020 are given in Tables 5.1 and 5.2 respectively. These parameters are defined based on the local soil classes and the values of the mapped response acceleration parameters S_s and S_1 for a selected hazard level. For intermediate

values of the mapped spectral acceleration coefficient, straight-line interpolation can be used.

Table 5.1. Short period spectral region local soil effect coefficients, F_s

Local Site Class	Spectral Response Acceleration Coefficient at Short Period					
	$S_S \leq 0.25$	$S_S = 0.50$	$S_S = 0.75$	$S_S = 1.00$	$S_S = 1.25$	$S_S \geq 1.50$
ZA	0.8	0.8	0.8	0.8	0.8	0.8
ZB	0.9	0.9	0.9	0.9	0.9	0.9
ZC	1.3	1.3	1.2	1.2	1.2	1.2
ZD	1.6	1.4	1.2	1.1	1	1
ZE	2.4	1.7	1.3	1.1	0.9	0.8
ZF	Site-specific geotechnical investigation is required. It will be carried out according to TBEC-2020 section 6.6.					

Table 5.2. Long period spectral region local soil effect coefficients, F_1

Local Site Class	Spectral Response Acceleration Coefficient for 1.0 Second Period					
	$S_1 \leq 0.10$	$S_1 = 0.20$	$S_1 = 0.30$	$S_1 = 0.40$	$S_1 = 0.50$	$S_1 \geq 0.60$
ZA	0.8	0.8	0.8	0.8	0.8	0.8
ZB	0.8	0.8	0.8	0.8	0.8	0.8
ZC	1.5	1.5	1.5	1.5	1.5	1.4
ZD	2.4	2.2	2	1.9	1.8	1.7
ZE	4.2	3.3	2.8	2.4	2.2	2.0

5.2.3 Horizontal Earthquake Design Spectrum

The horizontal elastic design spectral accelerations $S_{ac}(T)$, which are the ordinates of the horizontal elastic design acceleration spectrum, are defined in Equation (5.2) in terms of gravitational acceleration [g] depending on the natural vibration period (Figure 5.1).

$$\begin{aligned}
S_{ae}(T) &= \left(0.4 + 0.6 \frac{T}{T_A}\right) S_{DS} & (0 \leq T \leq T_A) \\
S_{ae}(T) &= S_{DS} & (T_A \leq T \leq T_B) \\
S_{ae}(T) &= \frac{S_{D1}}{T} & (T_B \leq T \leq T_L) \\
S_{ae}(T) &= \frac{S_{D1} T_L}{T^2} & (T_L \leq T)
\end{aligned} \tag{5.2}$$

where :

T : the natural vibration period
 T_A and T_B : the corner periods that are given depending on S_{DS} and S_{D1} by Equation (5.3).

$$T_A = 0.2 \frac{S_{D1}}{S_{DS}} ; \quad T_B = \frac{S_{D1}}{S_{DS}} \tag{5.3}$$

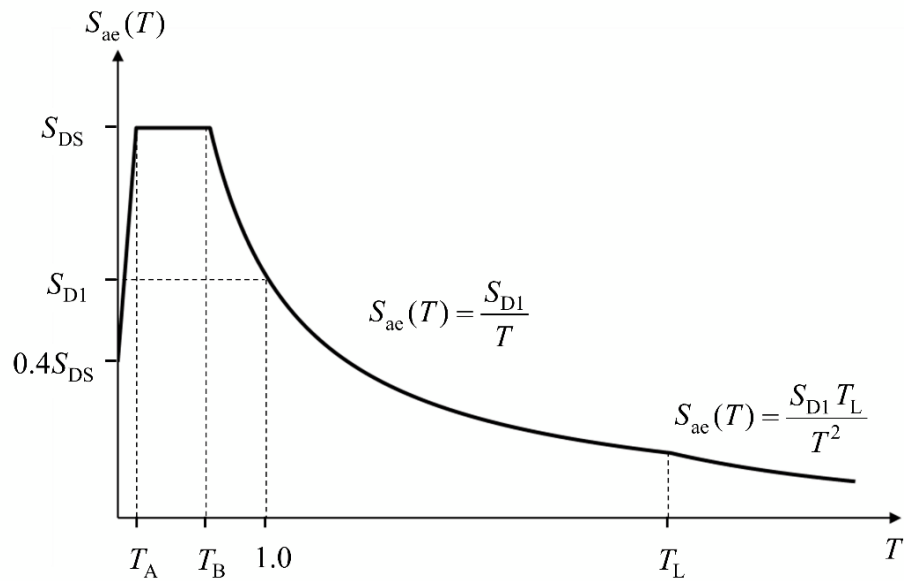


Figure 5.1. Horizontal elastic design spectrum (TBEC-2020)

The horizontal design spectral displacements, which are the ordinates of the horizontal earthquake design displacement spectrum for any earthquake ground motion level under consideration, are defined by Eq.(5.4) in meters [m] based on the natural vibration period (Figure 5.2).

$$S_{de}(T) = \frac{T^2}{4\pi^2} g S_{ae}(T) \tag{5.4}$$

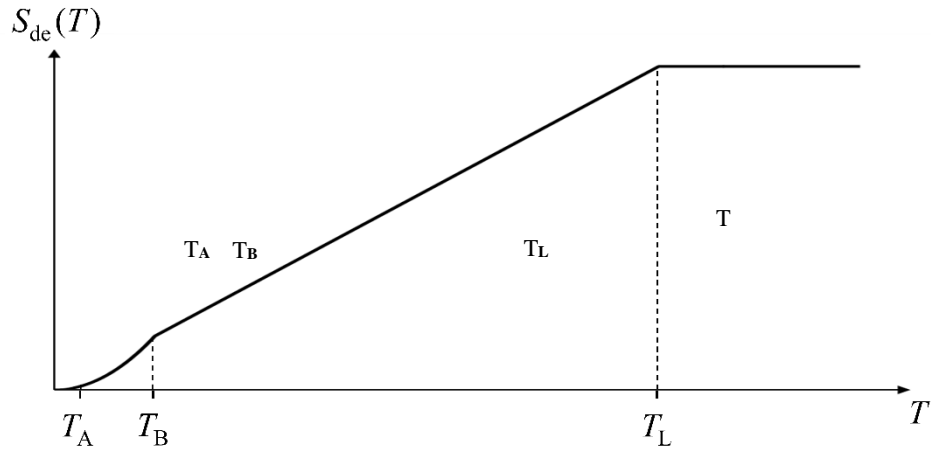


Figure 5.2. Horizontal elastic design displacement spectrum(TBEC-2020)

5.2.4 Horizontal Elastic Design Spectrum of Molla Gürani Viaduct

The map spectral acceleration coefficients S_s and S_1 values obtained from the map in Disaster and Emergency Management Authority (AFAD) website at <https://tdth.afad.gov.tr/>, for DD-1, DD-2 and DD-3 earthquakes are as follows.

$$DD-1 = \begin{cases} S_s = 1.316 \\ S_1 = 0.365 \end{cases}, DD-2 = \begin{cases} S_s = 0.738 \\ S_1 = 0.211 \end{cases}, DD-3 = \begin{cases} S_s = 0.292 \\ S_1 = 0.088 \end{cases}$$

The design spectral acceleration coefficients for Local Soil Class ZC specified in the Geotechnical Report were obtained using the Local Soil Effect Coefficients given in Table 5.1&5.2 or in Table 2.1 of the TBEC 2020, and are as follows:

$$DD-1 = \begin{cases} S_{DS} = S_s F_s = 1.316 \times 1.200 = 1.579 & \text{TBEC(2.1)} \\ S_{D1} = S_1 F_1 = 0.365 \times 1.500 = 0.548 & \text{TBEC(2.2)} \end{cases}$$

F_s values for DD-2 Earthquake Ground Motion Level is calculated by linear interpolation of values given in Table 5.1&5.2.

$$F_s = 1300 + \frac{(0.738 - 0.50)}{(0.75 - 0.50)} (1.200 - 1.300) = 1.2048 \cong 1.205$$

$$DD-2 = \begin{cases} S_{DS} = S_s F_s = 0.738 \times 1.205 = 0.889 & \text{TBEC(2.1)} \\ S_{D1} = S_1 F_1 = 0.211 \times 1.500 = 0.317 & \text{TBEC(2.2)} \end{cases}$$

$$DD-2a = \begin{cases} S_{DS} = S_S F_S = 0.410 \times 1.300 = 0.533 & \text{TBEC(2.1)} \\ S_{D1} = S_1 F_1 = 0.121 \times 1.300 = 0.182 & \text{TBEC(2.2)} \end{cases}$$

$$DD-3 = \begin{cases} S_{DS} = S_S F_S = 0.292 \times 1.300 = 0.380 & \text{TBEC(2.1)} \\ S_{D1} = S_1 F_1 = 0.088 \times 1.500 = 0.132 & \text{TBEC(2.2)} \end{cases}$$

Spectral Acceleration coefficients $S_{S,144}$ and $S_{1,144}$ for DD-2a Earthquake Ground Motion Level are calculated by logarithmic linear interpolation by using following equations given in Annex 2A of the TBEC.

$$\frac{S_{a,R1}}{S_{a,R2}} = \left(\frac{T_{R,1}}{T_{R,2}} \right)^k \quad \text{TBEC(2A.1)}$$

Taking logarithm of the both sides;

$$\log \frac{S_{a,R1}}{S_{a,R2}} = k \log_{10} \frac{T_{R1}}{T_{R2}} \quad \text{TBEC(2A.2)}$$

obtained. This relationship expresses a linear relationship between the return periods and spectral accelerations in the log-log axis set with the slope k. The spectral acceleration coefficients, S_S and S_1 values of DD-2 and DD-3 earthquake ground motion levels with 475 and 72 years return periods are used to obtain k_s short period region and k_1 , 1 second period region slopes.

$$k_s = 1.22 \log_{10} \frac{S_{S,475}}{S_{S,72}} \quad , \quad k_1 = 1.22 \log_{10} \frac{S_{1,475}}{S_{1,72}} \quad \text{TBEC(2A.3)}$$

$$k_s = 1.22 \log_{10} \frac{0.738}{0.292} = 0.483208212 \quad ,$$

$$k_1 = 1.22 \log_{10} \frac{0.211}{0.088} = 0.460838679$$

For the DD-2a earthquake level with a return period of 144 years, the map spectral acceleration coefficients of $S_{S,144}$ and $S_{1,144}$ are taken as $T_{R1} = 144$ years, $T_{R2} = 72$ years and thus $T_{R1} / T_{R2} = 2.0$ from Equation(2A.1) to 72 based on the map spectral acceleration coefficients of the annual DD-3 earthquake level, it was obtained as follows:

$$S_{S,144} = (2.0)^{k_s} S_{S,72} \quad ; \quad S_{1,144} = (2.0)^{k_1} S_{1,72} \quad \text{TBEC(2A.4)}$$

$$S_{S,144} = (2)^{0.483208212} 0.292 = 0.408171819$$

$$S_{1,144} = (2)^{0.460838679} 0.088 = 0.121180680$$

Alternatively, the kS and k1 slopes calculated by Equation (2A.3) are put into their places in the logarithmic expression of Equation (2A.4), and the map spectral acceleration coefficients SS,144 and S1,144 for the DD-2a earthquake level, may be obtained as expressed below:

$$\begin{aligned} \log_{10} S_{S,144} &= 0.633 \log_{10} S_{S,72} + 0.367 \log_{10} S_{S,475} \\ \log_{10} S_{1,144} &= 0.633 \log_{10} S_{1,72} + 0.367 \log_{10} S_{1,475} \end{aligned} \quad (2A.5)$$

$$\begin{aligned} \log_{10} S_{S,144} &= 0.633 \log_{10} S_{S,72} + 0.367 \log_{10} S_{S,475} \\ \log_{10} S_{S,144} &= 0.633 \log_{10} 0.292 + 0.367 \log_{10} 0.738 = -0.38683597 \\ S_{S,144} &= 0.410359063 \end{aligned}$$

$$\begin{aligned} \log_{10} S_{1,144} &= 0.633 \log_{10} S_{1,72} + 0.367 \log_{10} S_{1,475} \\ \log_{10} S_{1,144} &= 0.633 \log_{10} 0.088 + 0.367 \log_{10} 0.211 = -0.916130807 \\ S_{1,144} &= 0.121302343 \end{aligned}$$

Table 5.3 Peak Ground Acceleration and Spectral Acceleration Values

Design Earthquake Ground Motion Level	Return Period (years)	Geometric Mean Values (SaGM)		
		PGA	Ss	S1
DD-1	2475	0.538	1.316	0.365
DD-2	475	0.306	0.738	0.211
DD-2a	144	0.174	0.410	0.121
DD-3	72	0.126	0.292	0.088

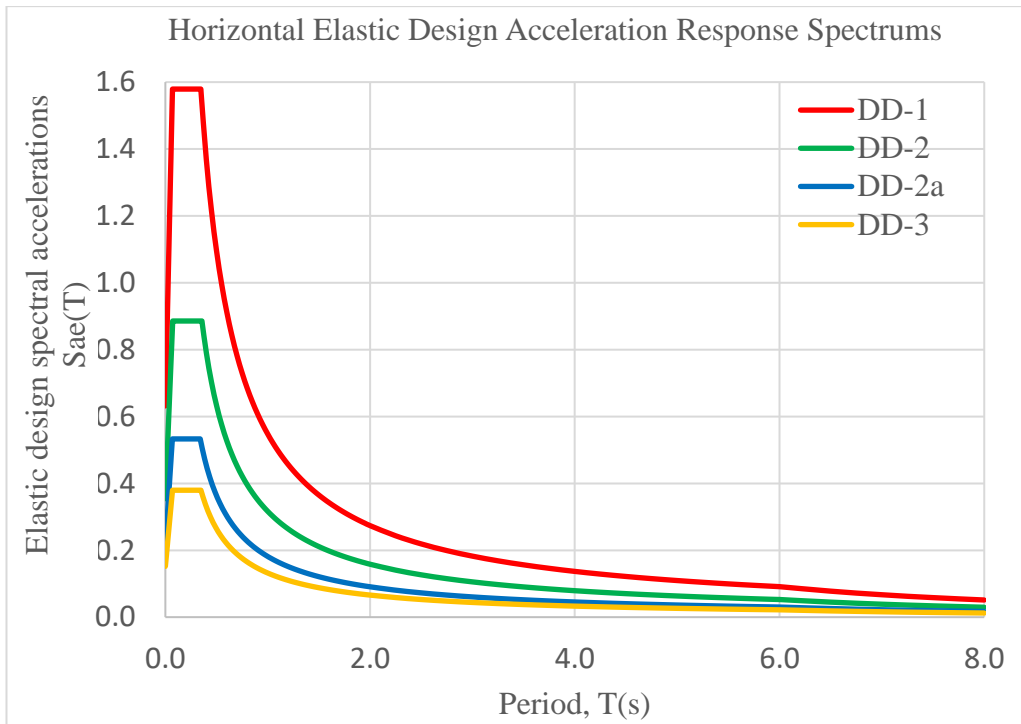


Figure 5.3. TBEC 2020 Design Acceleration Response Spectrums

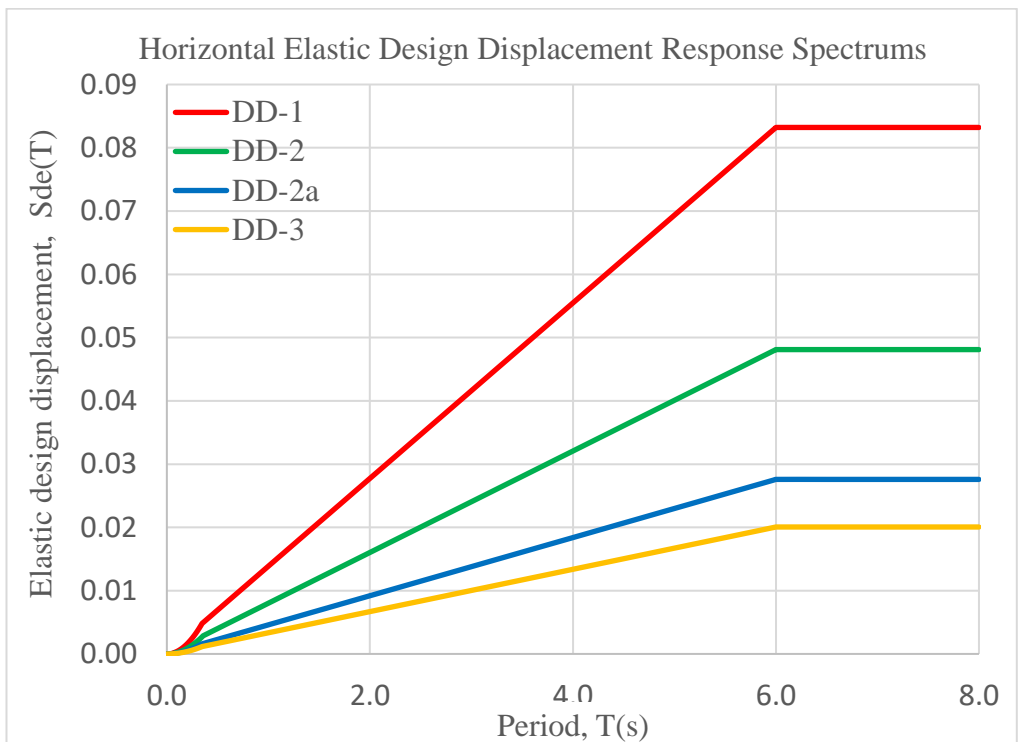


Figure 5.4. TBEC 2020 Design Displacement Response Spectrums

CHAPTER 6

6. SEISMIC PERFORMANCE EVALUATION

6.1 Bridge Importance Classes in TBEC-2020

Standard highway bridges are categorized into three main classes in terms of following factor:

- Usage
- Expected earthquake performance during and after the earthquake.
- Degree of Importance

6.1.2 BIC(KÖS)=1 Important and Special Bridges

- a) Standard bridges that have strategic importance in terms of security/defense.
- b) Critical bridges for post-earthquake emergency response: Standard bridges that provide direct access to hospitals, emergency response centers, ports and airports within a 10 km radius in residential areas and have no alternatives.
- c) Bridges whose piers are in water constantly and there is no possibility of intervention after construction (sea, lake, dam lake).

6.1.3 BIC(KÖS)=2 Normal Bridges

All other standard bridges except BIC = 1 and BIC = 3.

6.1.4 BIC(KÖS)=3 Simple(Other) Bridges

- a) Standard bridges with a total length of less than 100 m and a pier height of less than 10 m, which are not important in terms of emergency transportation after the earthquake, secondary, with maximum three spans, not on the curve.
- b) Single span standard bridges.
- c) Standard pedestrian bridges.

In TBEC-2020, bridges are categorized as follows according to their degrees of complexity in analysis:

- Complex Bridges
- Single Span Straight Bridges
- Other Bridges

6.2 Seismic Design Category

Seismic Design Classes (SDC) to be used for the classification of calculation and evaluation methods to be applied in standard bridges, Table 6.1' for DD-2 Earthquake Ground Motion Level defined in 5.1.2., depending on the Short Period Design Spectral Acceleration Coefficient(S_{DS}) defined in 5.2.1. will be determined accordingly.

Table 6.1 Seismic(Earthquake) Design Category(Class) (SDC)

Short Period (0.2 sec.) Design Spectral Acceleration Coefficient (S_{DS}) , at DD-2 Earthquake Ground Motion Level	Earthquake Design Class
$S_{DS} < 0.33$	SDC = 4
$0.33 \leq S_{DS} < 0.67$	SDC = 3
$0.67 \leq S_{DS} < 1.00$	SDC = 2
$1.00 \leq S_{DS}$	SDC = 1

In case the ground conditions along the bridge are variable, the design spectral acceleration coefficient corresponding to the weakest local soil class shall be used, for the sole purpose of determining the earthquake design class.(TBEC-2020 Section 3.9).

Even though $0.67 \leq SDS=0.889 \leq 1.00$ for DD-2 Earthquake Ground Motion Level, Seismic Design Category of viaduct is assumed as $SDC=I$. Molla Gürani Viaduct superstructure is supported by elastomeric bearings but only circular bearings are accepted as an type of seismic isolation bearings in TBEC-2020 Annex 1 Seismic Isolation Bridge Design Specification Section 5.1.

The selection of appropriate analysis method based on bridge seismic design category in TBEC-2020 given in Table 6.2.

Table 6.2 Analysis and Evaluation Methods(TBEC-2020 Section 3.8)

Bridge Importance Category (KÖS=IC)	Analysis and Evaluation Stage	Earthquake Ground Motion Level	Seismic Design Category(DTS=SDC)		
			DTS=SDC=1	DTS=SDC=2,3	DTS=SDC=4
KÖS=1	Stage 1	DD-2a	Method 1 Linear Method / Strength Based Evaluation	Method 1 Linear Method / Strength Based Evaluation	Method 1 Linear Method / Strength Based Evaluation
	Stage 2	DD-1	Method 2.3 Nonlinear Time History Analysis(NLTH) / Displacement Based Evaluation	Method 2.1 Linear Method(Mixed Method) / Displacement Based Evaluation	-----
KÖS=2	Stage 1	DD-3	Method 1 Linear Method / Strength Based Evaluation	Method 1 Linear Method / Strength Based Evaluation	Method 1 Linear Method / Strength Based Evaluation
	Stage 2	DD-1	Method 2.2 Nonlinear Pushover Analysis / Displacement Based Evaluation	Method 2.1 Linear Method(Mixed Method) / Displacement Based Evaluation	-----
KÖS = 3	Stage 1	DD-3	Method 1 Linear Method / Strength Based Evaluation	Method 1 Linear Method / Strength Based Evaluation	Method 1 Linear Method / Strength Based Evaluation

6.3. Bridge Performance Levels And Performance Targets

6.3.1 Bridge Performance Levels

In TBEC 2020, four bridge structural performance levels are defined as follows, based on predicted or expected earthquake damage, applicable to special and standard bridges:

(1) Immediate Occupancy (IO) Performance Level : This performance level corresponds to the state where no or negligible damage occur in the bridge structures and/or in their main structural system elements under an earthquake. Immediately after the earthquake, emergency response vehicles will be allowed to pass. It is foreseen that normal traffic flow will be provided in a very short time following the examinations to be made.

(2) Limited Damage (MD) Performance Level : This performance level corresponds to the limited and easily repairable damage level in the bridge main structural system elements. This level of damage will not be used for new bridges, but will only be used in the first stage performance evaluation of existing bridges and, if necessary, in retrofitting design.

(3) Controlled Damage (CD) Performance Level : This performance level corresponds to the controlled damage level in the bridge main structural system elements, which is not too heavy and is mostly repairable. It is possible for the structure to be out of service for a while during the repair. In this case, short-term service interruptions on the bridge may be expected. After the earthquake, it will be possible to allow the passage of emergency response vehicles with limited repairs.

(4) Collapse Prevention (CP) Performance Level : This performance level corresponds to the pre-collapse situation where extensive damage occurred in the structural system elements of the bridge. Partial or complete collapse of the bridge is prevented. It may be accepted that limited or controlled passage of the emergency response vehicles would be possible. However, It may not be to use the bridge in the long term.

The provisions specified in TBEC-2020 are given as the minimum requirements for the new bridges that will be constructed in the areas of high seismic risk and for the seismic performance evaluation and strengthening of existing bridges. Additional provisions may be needed to achieve higher performance criteria for repairable or minimum damage attributed to essential or critical bridges.

6.3.2 Bridge Performance Targets

Bridge Performance Targets for special bridges and standard bridges under earthquake effect refer to “targeted bridge performance levels under certain earthquake ground motion levels”. Based on the two-stage design explained in 3.6.1 and 3.6.2 of TBEC-2020, Bridge Performance Targets defined according to Bridge Importance Classes and Earthquake Ground Motion Levels are summarized in Table 6.3.

Table 6.3 Bridge Performance Targets for Special and Standard Bridges

Bridge Performance Target			
Earthquake Ground Motion Level	Bridge Importance Category		
	KÖS=1	KÖS=2	KÖS=3
DD-3	-----	IO	IO
DD-2a	IO	-----	
DD-1	CD	CP	-----

where :

- IO : Immediate Occupancy Performance Level
- CD : Controlled Damage Performance Level
- CP : Collapse Prevention Performance Level

6.3.3 Near fault effect

The perpendicular distance between the Molla Gürani viaduct longitudinal axis and nearest fault line (the northern branch of the North Anatolian Fault Zone passing through the Marmara Sea) is about 28.27 km.(Figure 6.1)

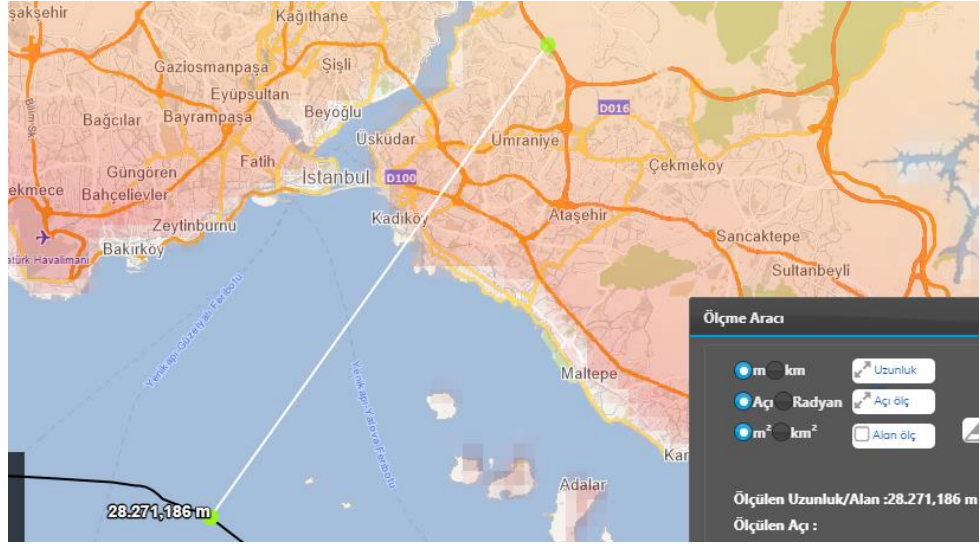


Figure 6.1 Distance to nearest fault line

CHAPTER 7

7. MATERIAL PROPERTIES

7.1 Concrete Material

According to TBEC-2020 9.1.2.3.b, the material strengths of existing bridge elements will be determined by tests to be carried out on concrete samples to be taken from these elements in accordance with the conditions specified in TS EN 12504-1. Between the mean minus standard deviation value and 0.85 times the mean value, the larger one will be taken as the existing concrete strength (f_{cm}).

The material properties given in Table 7.1 were used in the analyses since the compressive strengths in the current situation were not known and concrete samples couldn't taken.

Table. 7.1. Concrete Material Properties According to As-built projects.

Concrete Class	$f_{ck,cylinder}$	$f_{ck,cube}$	Elasticity Modulus of Concrete $E_c=5000(f'c)(1/2)$	Structural Element
	[MPa]	[MPa]	[MPa]	
C20/25	20	25	22361	Pile Foundation
C25/30	25	30	25000	Piers, Shallow Foundation
C35/45	35	45	29580	Box Girder, R.C. Slab, Bearing Pedestals

Weight per unit volume of concrete is taken as 25 kN/m^3 .

where:

- $f_{ck,cylinder}$: 28 days characteristic cylinder compressive strength of concrete[MPa]
- $f_{ck,cube}$: 28 days characteristic cube compressive strength of concrete[MPa]
- E_c : Elasticity Modulus of Concrete

7.2 Unconfined and Confined Concrete Models

Mander's stress-strain model, as shown in Figure 7.1 used to determine the capacity of concrete members according to TBEC annex 2020 5A.1. Mander et al. (1984) have proposed a unified stress-strain approach for confined concrete applicable to both circular and rectangular shaped transverse reinforcement. This stress-strain model is based on an equation suggested by Popovics (1973).

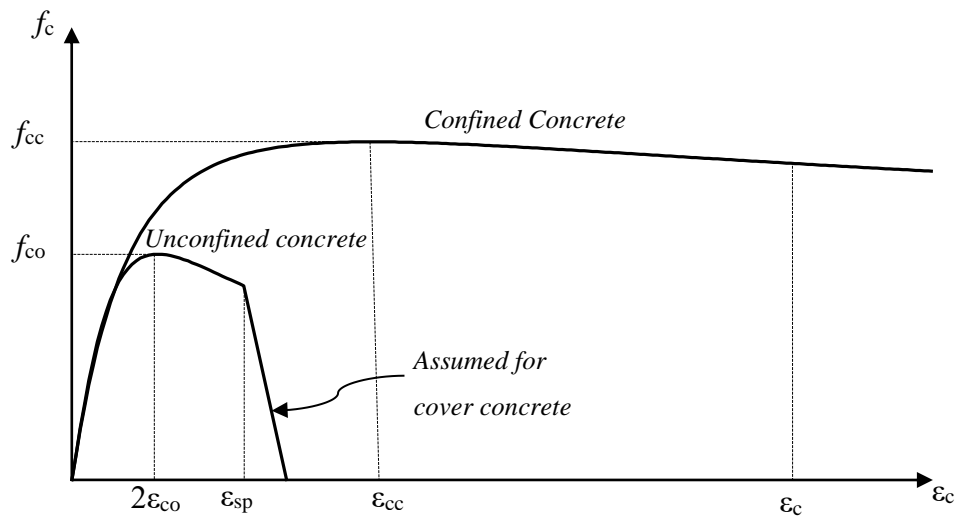


Figure 7.1 Stress-strain model of concrete

For a slow (quasi-static) strain rate and monotonic loading, the longitudinal compressive concrete stress f_c is given as a function of concrete compressive unit strain ϵ_c by Eq. (5.A.1) in TBEC-2020.

$$f_c = \frac{f_{cc} \times r}{r - 1 + x^r} \quad (5A.1)$$

The relations for the normalized concrete unit strain x and variable r in Eq.(5A.1) are given in Eq.(5A.2) and Eq.(5A.3).

$$x = \frac{\varepsilon_c}{\varepsilon_{cc}} \quad ; \quad \varepsilon_{cc} = \varepsilon_{co}[1+5(\lambda_c - 1)] \quad ; \quad \varepsilon_{co} = 0.002 \quad (5A.2)$$

$$r = \frac{E_c}{E_c - E_{sec}} \quad ; \quad E_c \cong 5000\sqrt{f_{co}} \text{ [MPa]} \quad ; \quad E_{sec} = \frac{f_{cc}}{\varepsilon_{cc}} \quad (5A.3)$$

The relation between confined concrete strength f_{cc} and unconfined concrete strength f_{co} is given by Eq.(5A.4).

$$f_{cc} = \lambda_c f_{co} \quad ; \quad \lambda_c = 2.254 \sqrt{1 + 7.94 \frac{f_e}{f_{co}} - 2 \frac{f_e}{f_{co}} - 1.254} \quad (5A.4)$$

Here for rectangular and circular sections effective confinement pressure f_e had been defined as follows :

(a) The effective confinement pressure in rectangular sections can be taken as the average of the values given in **Eq.(5A.5)** for two perpendicular directions:

$$f_{ex} = k_e \rho_x f_{ywk} \quad ; \quad f_{ey} = k_e \rho_y f_{ywk} \quad (5A.5)$$

$$\rho_x = \frac{A_{swx}}{h_o s} \quad ; \quad \rho_y = \frac{A_{swy}}{b_o s} \quad (5A.6)$$

$$k_e = \left(1 - \frac{\sum a_i^2}{6b_o h_o}\right) \left(1 - \frac{s}{2b_o}\right) \left(1 - \frac{s}{2h_o}\right) \left(1 - \frac{A_s}{b_o h_o}\right)^{-1} \quad (5A.7)$$

where :

- f_{ex} : The effective lateral confining stresses in the x direction
 f_{ey} : The effective lateral confining stresses in the y direction
 k_e : The confinement effectiveness coefficient
 f_{ywk} : The characteristic yield strength of the transverse reinforcement
 ρ_x : The volumetric ratio of the transverse reinforcement in x direction
 ρ_y : The volumetric ratio of the transverse reinforcement in y direction.
 a_i : The distance between to axes(center line) of the longitudinal reinforcements at cross-section perimeter
 b_o : The concrete core dimension to center line of perimeter ties in x direction
 h_o : The concrete core dimension to center line of perimeter ties in y direction
 s : Center to center spacing or pitch of spiral or circular hoop
 A_s : The longitudinal reinforcement area in the section
 A_{swx} : The transverse reinforcement area in x direction.
 A_{swy} : The transverse reinforcement area in y direction.

(b) The effective confinement pressure for circular sections confined by spirals or circular hoops is given by Eq.(5A.8)

$$f_e = \frac{1}{2} k_e \rho_s f_{ywk} \quad (5A.8)$$

$$\rho_s = \frac{4A_{sp}}{D_o s} \quad (5A.9)$$

The confinement effectiveness coefficient k_e is given by Eq.(5A.10a), for circular sections confined by circular hoops.

$$k_e = \left(1 - \frac{s}{2D_o}\right)^2 \left(1 - \frac{A_s}{\pi D_o^2 / 4}\right)^{-1} \quad (5A.10a)$$

The confinement effectiveness coefficient k_e is given by Eq.(5A.10b), for circular sections confined by spirals

$$k_e = \left(1 - \frac{s}{2D_o}\right) \left(1 - \frac{A_s}{\pi D_o^2 / 4}\right)^{-1} \quad (5A.10b)$$

where :

- ρ_s : Ratio of the volume of transverse confining reinforcement to the volume of confined concrete core
- A_{sp} : Area of transverse(stirrup or spiral) reinforcement bar
- D_o : The cross-section diameter between bar centers of stirrups or spiral that confined the core concrete (diameter of spiral between bar centers)

The equation Eq.(5A.1) given for confined concrete is also valid for unconfined concrete in the region up to $\varepsilon_c = 0.004$. Since the effective confinement pressure of unconfined concrete is equal to zero ($f_e = 0$), and accordingly λ_c (the ratio of compressive strength of confined concrete to unconfined concrete compressive strength) will be equal to $\lambda_c=1$ from Eq.(5A.4).

$$\lambda_c = 2.254 \sqrt{1 + 7.94 \frac{f_e}{f_{co}}} - 2 \frac{f_e}{f_{co}} - 1.254$$

$$\lambda_c = 2.254 \sqrt{1 + 7.94 \times 0} - 2 \times 0 - 1.254 = 2.254 - 1.254 = 1$$

than from Eq.(5A.2)

$$\varepsilon_{cc} = \varepsilon_{co} [1 + 5(\lambda_c - 1)] = \varepsilon_{co} [1 + 5(1 - 1)] = \varepsilon_{co}$$

and from Eq.(5A.4);

$$f_{cc} = \lambda_c f_{co} = 1 \times f_{co} = f_{co}$$

It is defined as $f_c = 0$ at $\epsilon_c = 0.005$. In the range of $0.004 < \epsilon_c \leq 0.005$, the stress-strain relationship is linear.

7.3 Steel Material Properties

In the seismic performance assessment of the existing structures, the designer should use actual test data if available. In our case of study there is no reinforcing steel samples were taken from the field, that's why the following steel reinforcement properties is used in the analyses.

Table 7.2 Mechanical Properties of Steel Reinforcement

	f_{sy} (MPa)	ϵ_{sy}	ϵ_{sh}	ϵ_{su}	f_{su} (MPa)	E_s (MPa)
S420	420	0.0021	0.008	0.08	500	200 000
B420C	420	0.0021	0.008	0.08	500	200 000
B500C	500	0.0025	0.008	0.08	650	200 000

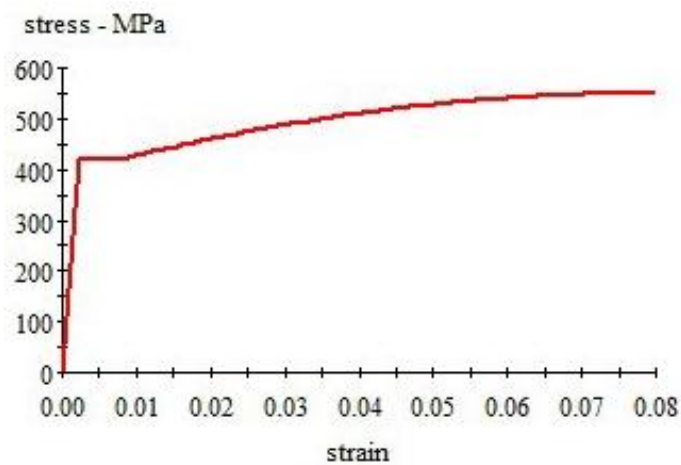


Figure 7.2 Stress-strain model of reinforcing steel B420C

Stress-strain equations

$$\text{for strain } f_s = E_s \epsilon_s \quad (\epsilon_s \leq \epsilon_{sy})$$

$$\text{for strain } f_s = f_{sy} \quad (\epsilon_{sy} < \epsilon_s \leq \epsilon_{sh})$$

$$\text{for strain } f_s = f_{su} - (f_{su} - f_{sy}) \frac{(\epsilon_{su} - \epsilon_s)^2}{(\epsilon_{su} - \epsilon_{sh})^2} \quad (\epsilon_{sh} < \epsilon_s \leq \epsilon_{su})$$

where :

- E_s : Modulus of elasticity
- f_{sy} : Yield stress ϵ_{sy} : Yield Strain
- ϵ_{sh} : Strain at Strain Hardening ϵ_{su} : Failure Strain

7.4 Moment Curvature Relationship

The flexural behavior of a reinforced concrete cross section (a non-linear material) can best be studied by using its moment curvature relationship. If the moment-curvature relationship is available , one can predict the strength and the stiffness , as well as the ductility characteristics of the cross-section.

In generation of a moment-curvature relationship for a reinforced concrete section , principles of mechanics of deformable bodies hold.

Need to consider :

- forces, equilibrium (system level and section level)
- geometry of deformations, displacement compatibility
- relationships between forces and deformations (stress-strain relationships)

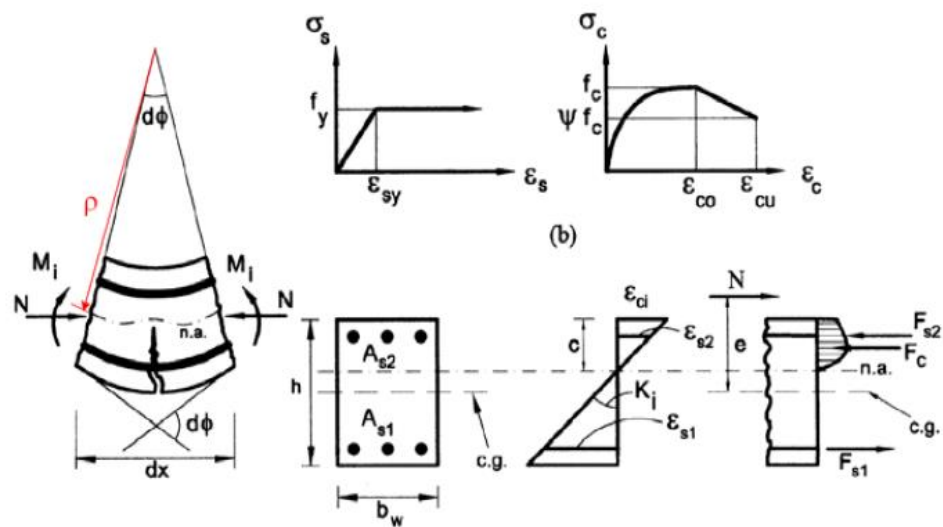


Fig. 7.3 Moment-Curvature relationship a reinforced concrete cross-section.

From mechanics of deformable solids can be written following relations

$$\frac{d^2 y}{dx^2} = \frac{1}{\rho} = K = \frac{d\theta}{dx} \quad (7.1)$$

$$K = \frac{\epsilon_x}{y} = \frac{\epsilon_{ci}}{c} \quad (7.2)$$

where:

$y(x)$: deflection of the member in flexure (beam)

$\theta(x)$: rotation of the beam

ρ : radius of curvature

K : curvature

ϵ_x : normal strain on a fiber located at a vertical distance of y from the neutral axis of the beam

ϵ_{ci} : extreme fiber strain

c : depth of neutral axis

Consider the following M-K relationships for the R/C column cross-section below:

- M-K relation changes with level of a axial load
- Indicates moment capacity of a section as well as ductility (rotation capacity – plastic hinge)
- M-K under zero axial load can be approximated as a bilinear relationship (elasto-plastic behavior)
- $K_u / K_y \rightarrow$ Curvature ductility ratio
- Area under the M-K diagram a measure of the energy dissipation capacity (seismic design)

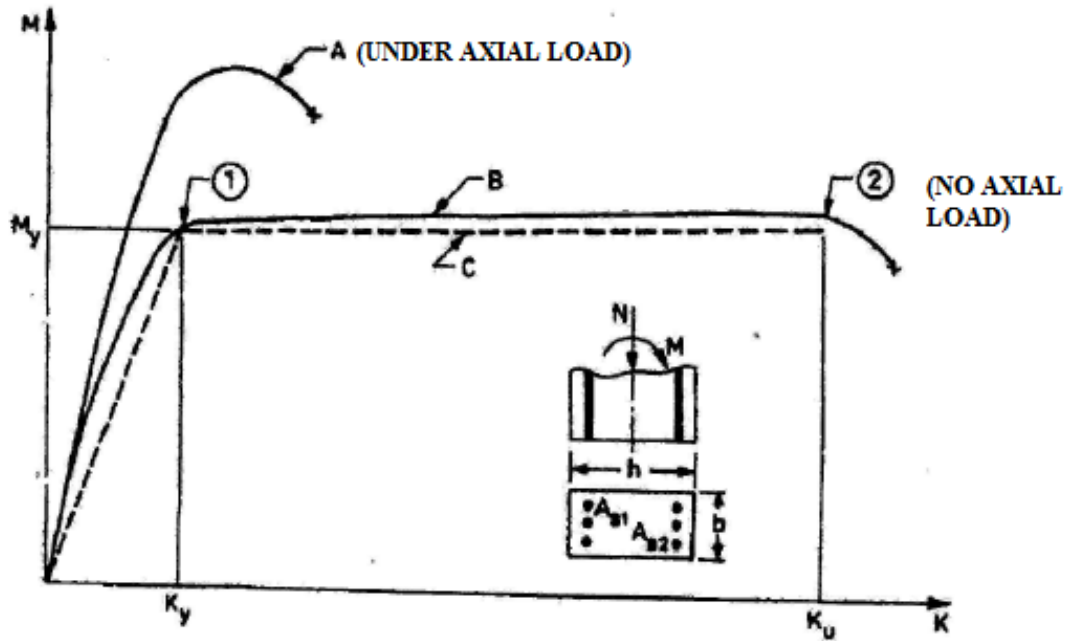


Fig. 7.4 Moment-Curvature relationship a reinforced concrete column cross-section.

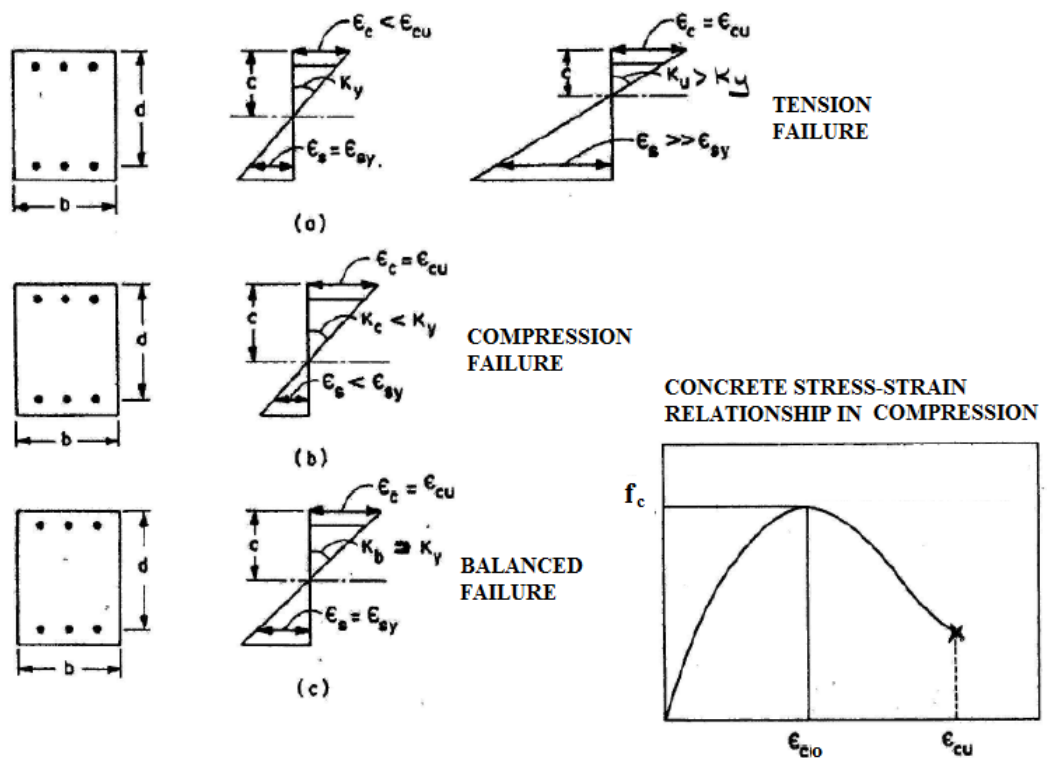


Fig. 7.5 Types of failures in RC members (related to ductility) (K.Orakcal)

- Tension Failure : Steel yields in tension prior to crushing of concrete (ductile behavior)
- Compression Failure : Concrete crushes in compression before steel yields (brittle behavior)
- Balanced Failure : Crushing of concrete and yielding of steel occur simultaneous (brittle behavior)

Crushing of concrete usually define when the strain at the extreme concrete fiber in compression reaches the crushing strain, ϵ_{cu}

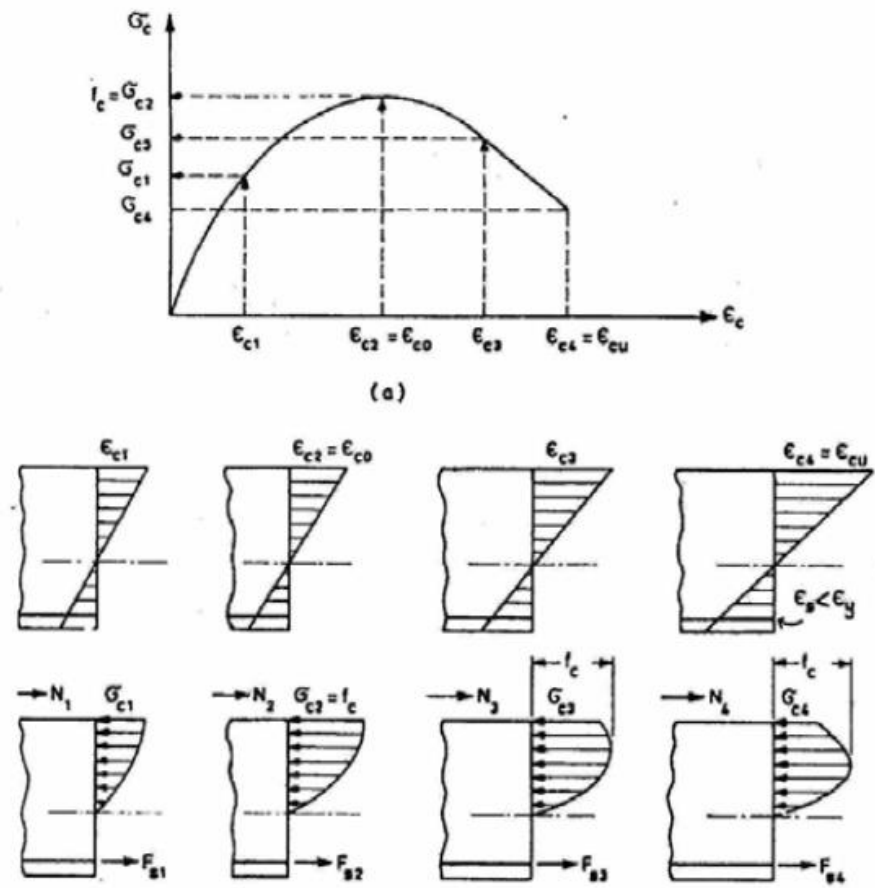


Fig. 7.6 Internal Stress Distribution (K.Orakcal)

Basic Assumptions

- Plane sections before bending remain plane after bending (not true for deep beams $h > 4b$)
- Fiber to fiber redistribution takes place as the moment on the section (as well as curvature) increases.
- Concrete fibers in compression follow the stress-strain relationship for concrete in compression.
- Depth of neutral axis changes.
- Always need to maintain equilibrium of forces on the section

❖ Generation of moment-curvature relationship for beams:

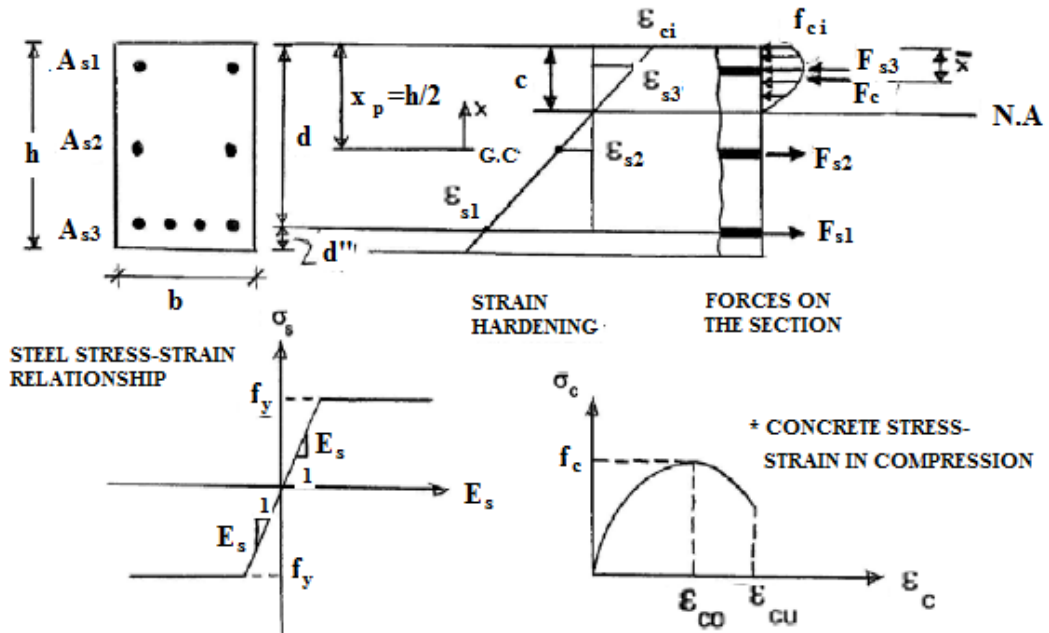


Fig. 7.7 Moment – Curvature relationship for beams (U. Ersoy)

Strain hardening in steel and tensile strength of concrete can possibly be neglected and simple material models can possibly be used.

For example :

Material models

$$\sigma_{si} = E_s \varepsilon_{si} \leq f_y$$

$$E_s = 200,000 \text{ MPa}$$

$$\text{if } \varepsilon_c \leq 0.002$$

$$\sigma_c = f_c \left[\frac{2\varepsilon_c}{0.002} - \left(\frac{\varepsilon_c}{0.002} \right)^2 \right]$$

$$\text{if } \varepsilon_c \geq 0.002$$

$$\sigma_c = f_c [1.15 - 75\varepsilon_c] \quad \text{straight - line}$$

$$\text{(For } \varepsilon_{co} = 0.002, \quad \varepsilon_{cu} @ 0.85f_c = 0.004)$$

The effects of strain hardening, concrete tensile strength and confinement in the analysis can be considered in the analysis.

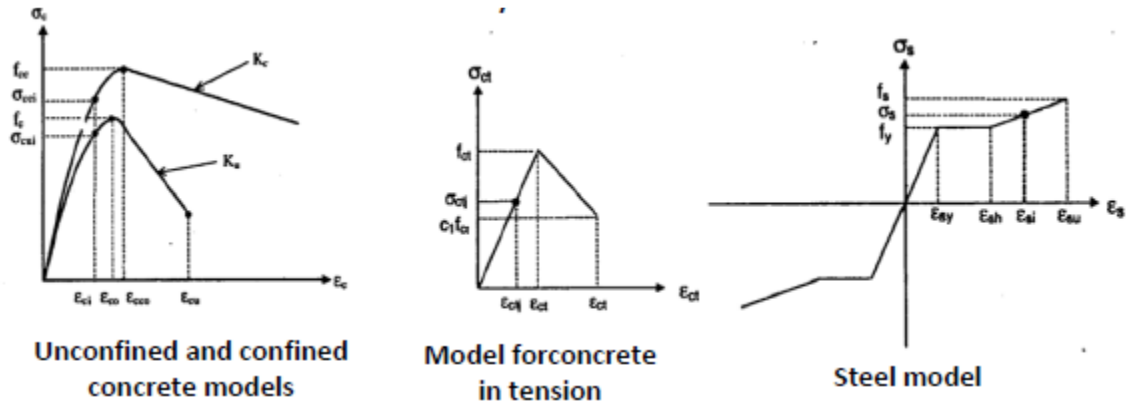


Fig. 7.8 Material models

- **Sectional equilibrium and compatibility**

Sectional equilibrium : $F_c + F_{s3} - F_{s2} - F_{s1} = 0$

Moment of the internal forces about the

geometric centroid (G.C) of the section : $M = F_{s1} \left(\frac{h}{2} - d'' \right) + F_{s3} \left(\frac{h}{2} - d'' \right) - F_c (x_p - \bar{x})$

Compatibility equations (similar triangles) : $\varepsilon_{si} = -\varepsilon_{ci} \left[\frac{(x_p - c) - x_i}{c} \right]$

for rectangular section $x_p = \frac{h}{2}$

Compatibility equations (similar triangles) : $\epsilon_{si} = \epsilon_{ci} \left[1 + \frac{x_i - \frac{h}{2}}{c} \right]$

Therefore $\sigma_{si} = E_s \epsilon_{si} = E_s \epsilon_{ci} \left[1 + \frac{x_i - \frac{h}{2}}{c} \right] \leq f_y$

Using these relations, can develop a trial-and-error solution to find a point on the M-K diagram.

1. Select an extreme fiber compressive strain, (E.G., start with $\epsilon_{ci}=0.001$)
2. Assume a neutral axis depth, c (E.G., $c=0.2d$)
3. Compute steel strains $\epsilon_{s1}, \epsilon_{s2}, \epsilon_{s3}, \dots$
4. Compute steel stresses $\sigma_{s1}, \sigma_{s2}, \sigma_{s3}, \dots$
5. Compute steel forces $F_{si} = \sigma_{si} A_{si}$
6. Compute the concrete force F_c . The resultant concrete force is equal to the volume under the stress distribution.
7. Check force equilibrium at the section
 - If force equilibrium is satisfied within a small tolerance, continue.
 - If not satisfied, go back to step 2 and assume another value for c (based on the unbalanced compression or tension force) until equilibrium is satisfied.
8. Compute the moment of the internal forces
9. Compute curvature, $K = \epsilon_{si} / c$
10. Go back to step 1 and select another value for ϵ_{ci} .

7.4.1 Generation Moment-Curvature relation for a given beam section

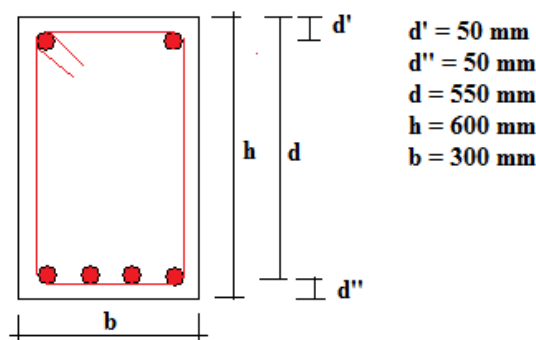
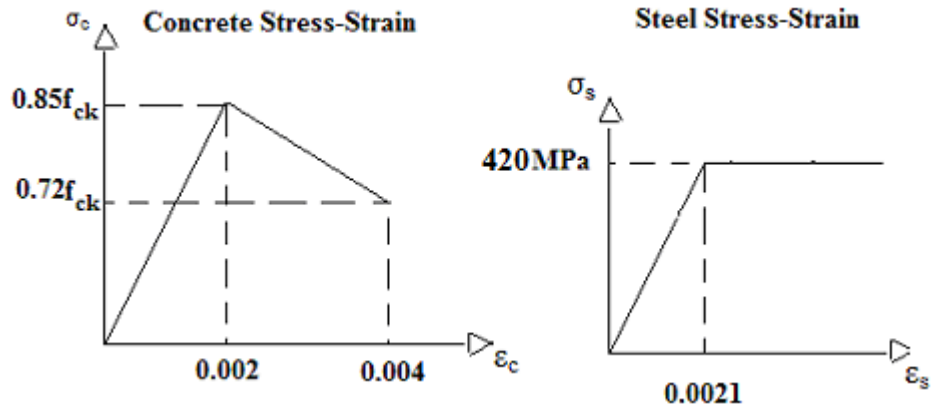


Fig. 7.9 A rectangular beam section

$$f_{ck} = 27\text{MPa}, \quad f_{yk} = 420\text{MPa}$$

$$A_s = 2124\text{mm}^2(4\phi 26), \quad A'_s = 1062\text{mm}^2(2\phi 26),$$

- **Material models**



Tensile strength of concrete is neglected . For both tension end compression

Fig. 7.10 Reinforcing steel and concrete material models

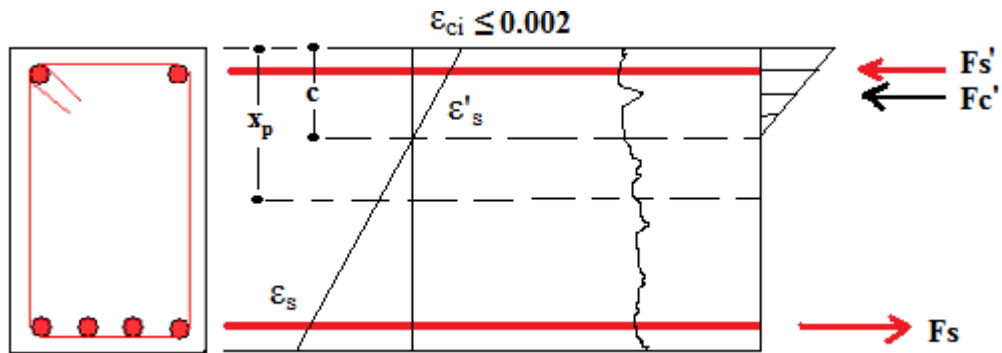


Fig. 7.11 Stresses, Strains and Forces in the section

Assume $\epsilon_{ci}=0.001$

Table 7.3 Reinforcing Steel Stresses and Strains

ϵ_{ci}	ϵ_{cu}	c	b	d	d'	h	A_s	A'_s	E_s	f_{yk}	f_{ck}	σ_c	$A_s \cdot f_{yk}$	$A'_s \cdot f_{yk}$
0,001	0,004	120	300	550	50	600	2123,717	1062	2e+5	420	27	11,5	891,96	445,98
0,001	0,004	200	300	550	50	600	2123,717	1062	2e+5	420	27	11,5	891,96	445,98
0,001	0,004	250	300	550	50	600	2123,717	1062	2e+5	420	27	11,5	891,96	445,98
0,001	0,004	235	300	550	50	600	2123,717	1062	2e+5	420	27	11,5	891,96	445,98
0,001	0,004	234,5	300	550	50	600	2123,717	1062	2e+5	420	27	11,5	891,96	445,98

Table 7.4 Forces in the section from reinforcing steel and concrete

c (mm)	ϵ_s	ϵ'_s	F_s (kN)	F'_s (kN)	F_c (kN)	$F_c+F'_s-F_s$ (kN)
120	0,00358	0,00058	892	124	207	-562
200	0,00175	0,00075	743	159	344	-240
250	0,00120	0,00080	510	170	430	91
235	0,00134	0,00079	569	167	404	2
234,7	0,00135	0,00079	571	167	404	0

From results c is obtained $c= 235$ mm. Total moment about the geometric centroid of section and curvature:

$$M = F_c(x_p - \frac{c}{3}) + F'_s(\frac{h}{2} - d') + F_s(\frac{h}{2} - d'')$$

$$M = 89588,72 + 41796,55 + 142864,09 = 274249,36\text{Nm}$$

$$M = 274,3\text{kNm} \quad K = \frac{\epsilon_{ci}}{c} = \frac{0,001}{0,235} = 0,004255\text{rad/m}$$

Neither compression reinforcement nor tension reinforcement are yielded. Assuming the $\epsilon_{ci} = 0.004$ (ultimate ; crushing) same steps repeated and the total moment in the section and curvature are obtained as follows:

$$M = 429 \text{ kNm} \quad K = 6,65 \text{ rad/m} \quad c=97 \text{ mm}$$

Assuming that $\epsilon_s = 0,0021$ and $\epsilon_{ci} \leq 0.002$ (linear distribution of σ_c above the neutral axis) if we try to find yield point on the M-K diagram (when steel strain equal to yield strain $\epsilon_s = \epsilon_y = 0,0021$)

Total moment about the geometric centroid of section and curvature:

$$M = F_{c1}(x_p - \frac{c}{4}) + F_{c2}(x_p - \frac{c}{3}) + F_{c3}(x_p - \frac{2c}{3}) + F'_s(\frac{h}{2} - d') + F_s(\frac{h}{2} - d'')$$

$$M = 451\text{kNm} \quad K = \frac{\epsilon_{ci}}{c} = \frac{0,004}{0,097} = 0,0412\text{rad/m}$$

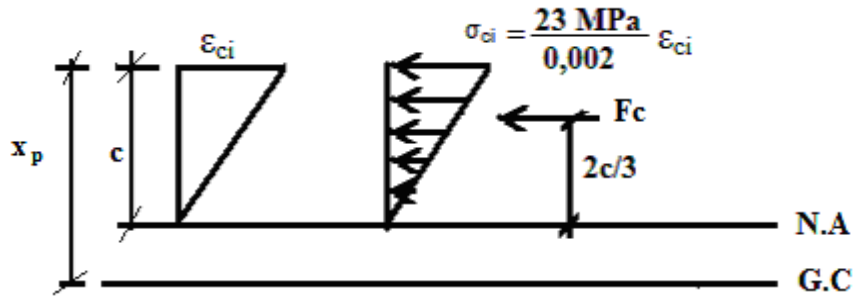


Fig. 7.12 Linear distribution of σ_c

The depth of the neutral axis c is the same when $\epsilon_{ci}=0,001$ and $\epsilon_s=0,0021$ ($c=235$ mm). This is expected since we have a section behaving linear elastically for both cases (both concrete and steel stress-strain relationships are in the linear range)

For a linear elastic section:

$$K=M/EI \quad \text{and} \quad EI=M/K$$

$$\text{For } \epsilon_{ci}=0,001 \quad EI = (274,3 \text{ kNm}) / (0,004255 \text{ rad/m}) = 64,5 \cdot 10^3 \text{ kNm}$$

$$\text{For } \epsilon_s=0,0021 \quad EI = (429 \text{ kNm}) / (0,00665 \text{ rad/m}) = 64,5 \cdot 10^3 \text{ kNm}$$

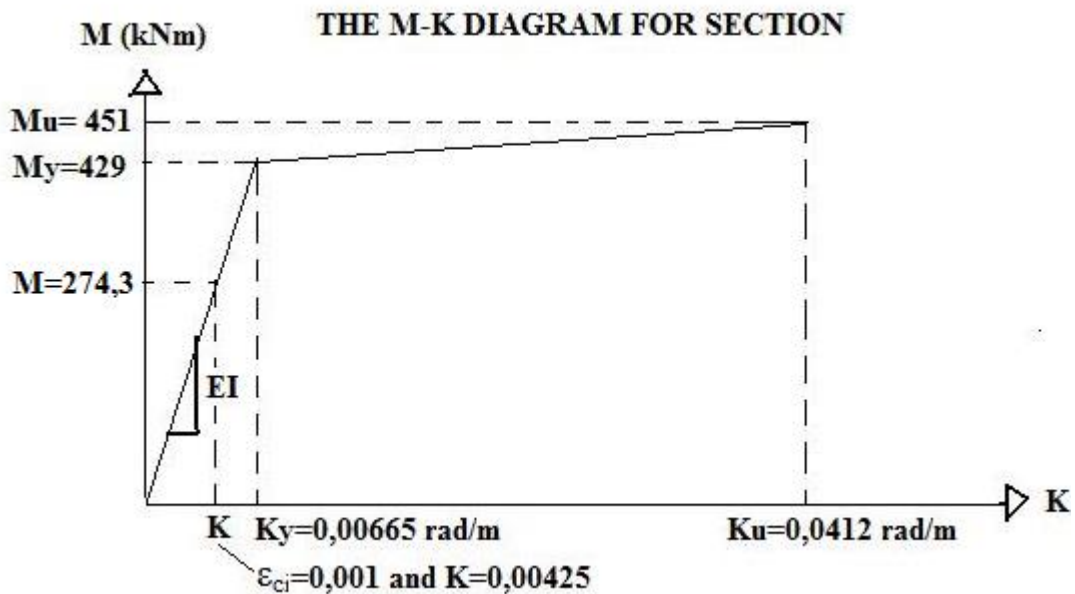


Fig. 7.13 Moment – Curvature diagram for a given section

Moment-Curvature diagram for cross section should be obtained by any program that available in literature instead of hand calculation.

7.4.2 Cross Sectional Analysis of column of Molla Gürani Viaduct piers.

Table 7.5 Moment-Curvature Analysis Results of Column of Molla Gürani Piers

Axes	Transverse Direction (M2)		Longitudinal Direction (M3)		Level	Location
	M-Moment	ϕ -Curvature	M-Moment	ϕ -Curvature		
1	209,000	5.23E-04	89,510	1.16E-03	Yield	Bottom
	222,500	4.27E-03	97,260	1.01E-02	Ultimate	
1	203,000	5.20E-04	87,010	1.16E-03	Yield	Top
	217,900	4.45E-03	95,220	1.03E-02	Ultimate	
2	221,700	5.30E-04	94,850	1.17E-03	Yield	Bottom
	232,300	3.90E-03	101,600	9.60E-03	Ultimate	
2	203,800	5.20E-04	87,350	1.16E-03	Yield	Top
	218,600	4.43E-03	95,490	1.03E-02	Ultimate	
3	234,500	5.38E-04	100,200	1.19E-03	Yield	Bottom
	241,700	3.55E-03	105,900	9.09E-03	Ultimate	
3	203,700	5.20E-04	87,320	1.16E-03	Yield	Top
	218,500	4.43E-03	95,460	1.03E-02	Ultimate	
4	307,200	5.76E-04	134,000	1.23E-03	Yield	Bottom
	309,500	2.58E-03	140,200	7.95E-03	Ultimate	
4	205,700	5.21E-04	88,150	1.16E-03	Yield	Top
	220,000	4.37E-03	96,150	1.02E-02	Ultimate	
5	316,300	5.83E-04	138,000	1.24E-03	Yield	Bottom
	316,500	2.46E-03	143,200	7.77E-03	Ultimate	
5	205,400	5.21E-04	88,010	1.16E-03	Yield	Top
	219,800	4.38E-03	96,040	1.02E-02	Ultimate	
6	318,700	5.85E-04	139,100	1.24E-03	Yield	Bottom
	318,900	2.42E-03	144,000	7.72E-03	Ultimate	
6	206,500	5.22E-04	88,490	1.16E-03	Yield	Top
	220,700	4.34E-03	96,420	1.02E-02	Ultimate	
7	312,500	5.80E-04	136,400	1.24E-03	Yield	Bottom
	312,800	2.51E-03	142,000	7.85E-03	Ultimate	
7	205,800	5.21E-04	88,180	1.16E-03	Yield	Top
	220,100	4.36E-03	96,170	1.02E-02	Ultimate	
8	226,300	5.33E-04	96,760	1.18E-03	Yield	Bottom
	235,800	3.77E-03	103,200	9.41E-03	Ultimate	
8	205,500	5.21E-04	88,050	1.16E-03	Yield	Top
	219,900	4.37E-03	96,070	1.02E-02	Ultimate	

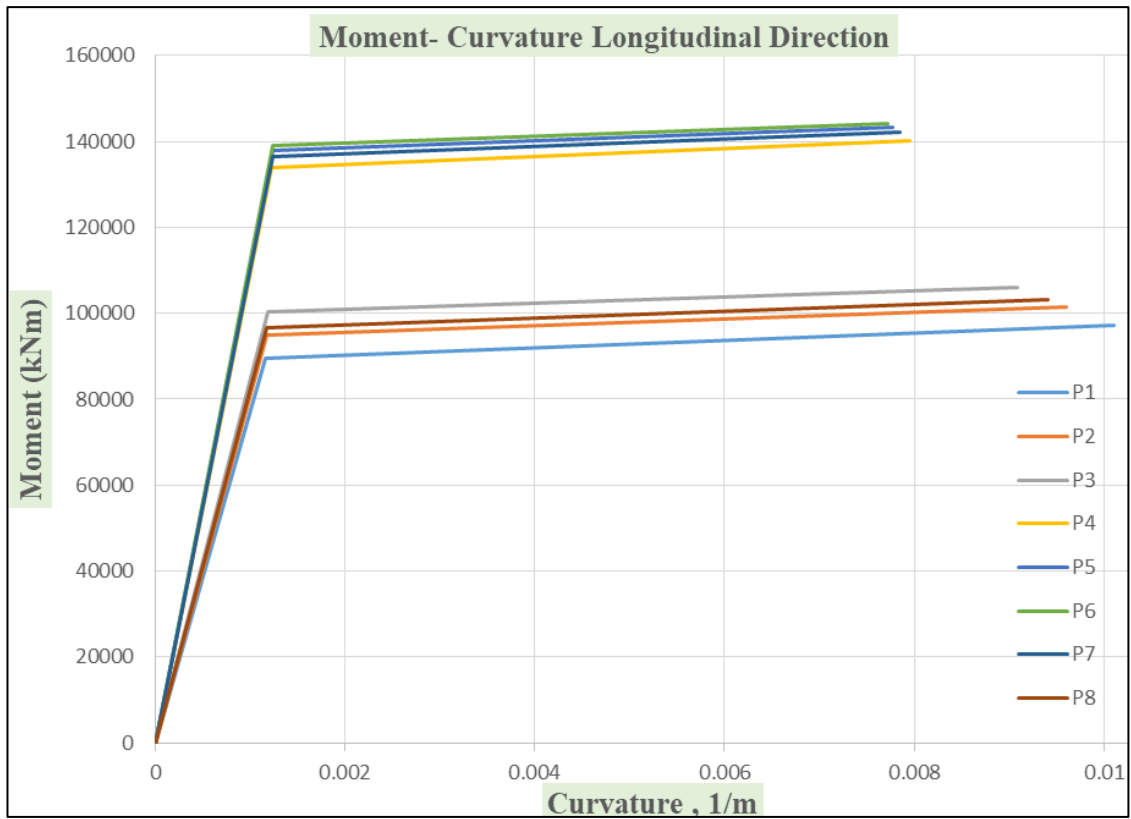


Fig. 7.14 Moment–Curvature diagrams of Pier Columns in Longitudinal Direction

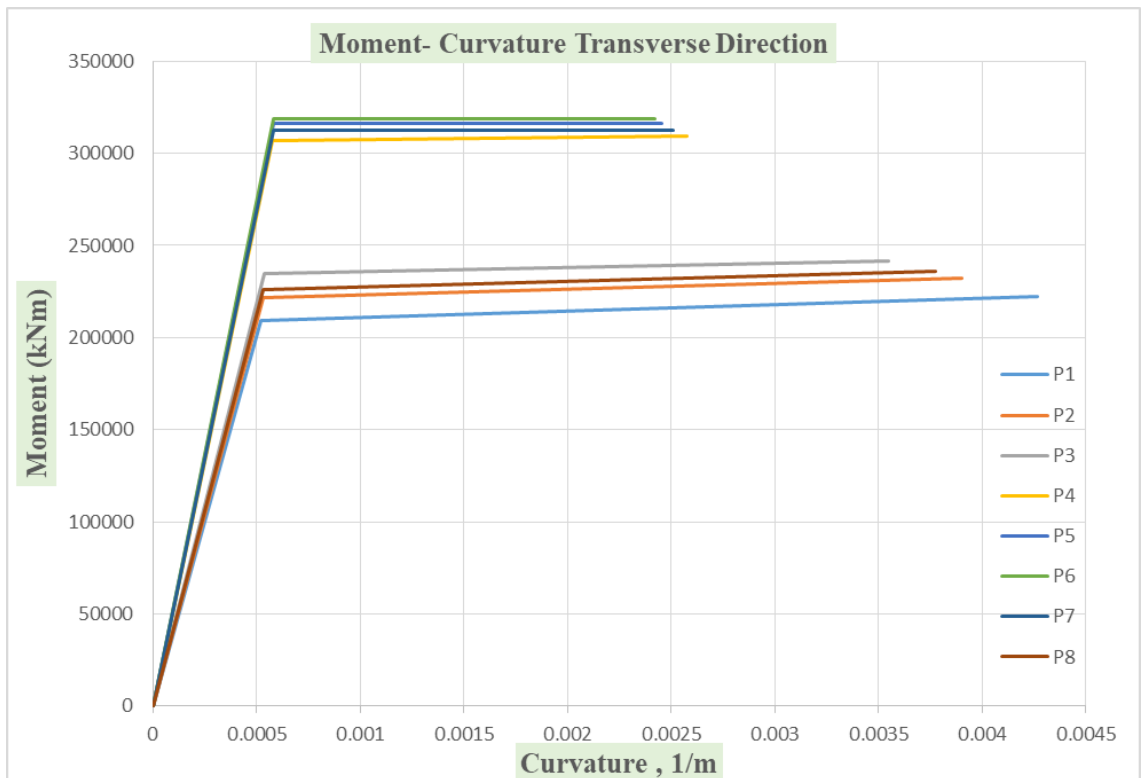
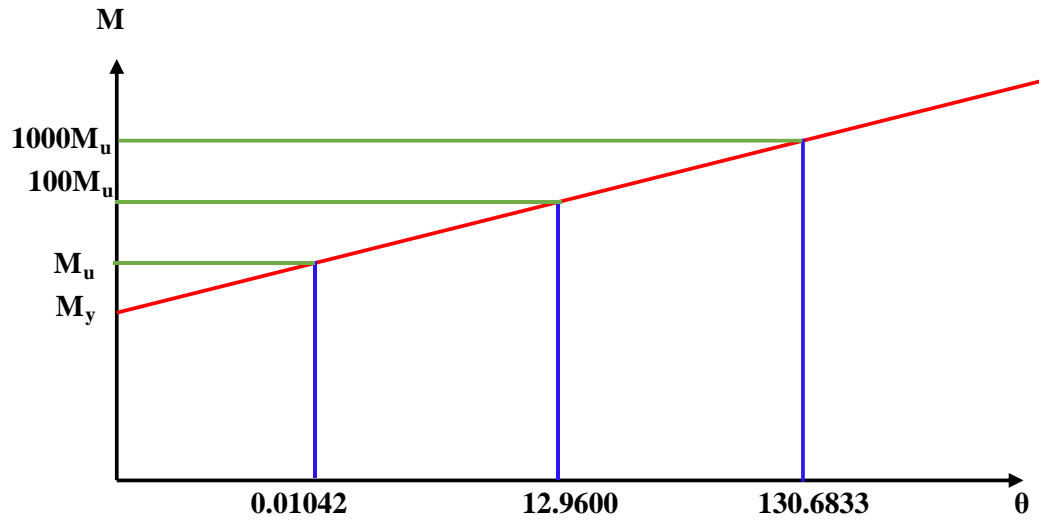


Fig. 7.15 Moment–Curvature diagrams of Pier Columns in Transversal Direction

7.4.3 Bilinearization of Moment-Curvature

Moment Curvature Axis 1 Longitudinal Direction(Global X Direction)



L_p : 1.166 m
Effective Yield Moment : 8.95E+04 kNm
Effective Yield Curvature : 1.16E-03 1/m
Ultimate Moment : 9.73E+04 kNm
Ultimate Curvature : 1.01E-02 1/m

SAP2000 Hinge Properties Input Values

Moments [kN/m]	Rotations [rad]
89,510	0
97,260	0.01042
9,726,000	12.9600
97,260,000	130.6833

XTRACT Analysis Report -

For use only in an academic or research setting.

Section Name: Axis-1
Loading Name: Longitudinal
Analysis Type: Moment Curvature

E.A

11.01.2022
Molla Gurani North Viaduct
Rectangular Hollow Column Sect
Page __ of __

Section Details:

X Centroid: -12.60E-6 m
Y Centroid: -3954E-6 m
Section Area: 12.75 m²

Loading Details:

Constant Load - P: 29.41E+3 kN
Incrementing Loads: Mxx Only
Number of Points: 31
Analysis Strategy: Displacement Control

Analysis Results:

Failing Material: Concrete Cover
Failure Strain: 4.000E-3 Compression
Curvature at Initial Load: .3378E-14 1/m
Curvature at First Yield: .9591E-3 1/m
Ultimate Curvature: 10.10E-3 1/m
Moment at First Yield: 73.94E+3 kN-m
Ultimate Moment: 97.26E+3 kN-m
Centroid Strain at Yield: .7285E-3 Ten
Centroid Strain at Ultimate: 10.98E-3 Ten
N.A. at First Yield: .7596 m
N.A. at Ultimate: 1.087 m
Energy per Length: 886.7 kN
Effective Yield Curvature: 1.161E-3 1/m
Effective Yield Moment: 89.51E+3 kN-m
Over Strength Factor: 1.087
EI Effective: 7.71E+10 N-m²
Yield EI Effective: 8.67E+8 N-m²
Bilinear Hardening Slope: 1.124 %
Curvature Ductility: 8.700

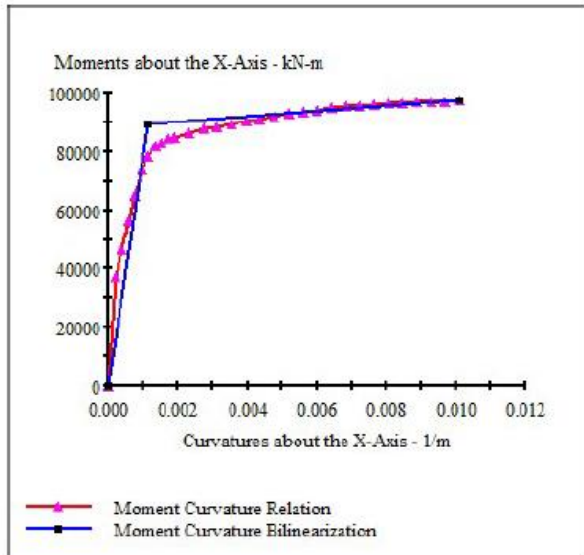
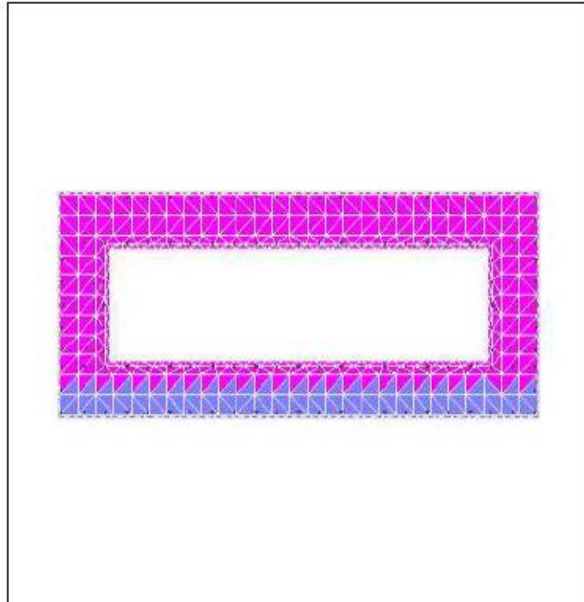


Fig. 7.16 Moment–Curvature Relation of Pier 1 Columns in Longitudinal Direction

7.4.4 Verification of the Results

Molla Gurani Viaduct Pier-1 column height is $L = 10.88$ m . Calculation of plastic rotation capacity, yield and ultimate displacements, and member ductility factors shown below:

- Plastic Hinge Length

$$L_p = \begin{cases} 0.08L + 0.022f_{ye}d_{bl} \geq 0.044f_{ye}d_{bl} & (f_{ye} \text{ in MPa}) \\ 0.08L + 0.15f_{ye}d_{bl} \geq 0.3f_{ye}d_{bl} & (f_{ye} \text{ in ksi}) \end{cases}$$

$$L_p = 0.08 \times 10880 + 0.022 \times 420 \times 32 = 1166.1 \text{ mm} \geq 0.044 \times 420 \times 32 = 591.4 \text{ mm}$$

- Plastic Rotation Capacity

$$\theta_p = L_p \Phi_p = L_p (\Phi_u - \Phi_y) = 1,166(0.0101 - 0.001161) = 0.01042 \text{ rad}$$

- Yield Displacement

$$\Delta_y = \frac{\Phi_y L^2}{3} = \frac{0.001161 \times 10.88^2}{3} = 45.81 \text{ mm}$$

- Plastic Displacement

$$\Delta_p = \left(\frac{M_u}{M_n} - 1 \right) \Delta_y + L_p (\Phi_u - \Phi_y) (L - 0.5L_p)$$

$$\Delta_p = \left(\frac{97260}{89510} - 1 \right) \times 45.81 + 0.01042 \times (10880 - 0.5 \times 1161) = 111.26 \text{ mm}$$

- Total Displacement

$$\Delta_u = \Delta_y + \Delta_p = 45.81 + 111.26 = 157.07 \text{ mm}$$

- Member Displacement Ductility

$$\mu_s = \frac{157.07}{48.81} = 3.43$$

- Member Ductility Capacity (Curvature Ductility)

$$\mu_\phi = \frac{0.00101}{0.001161} = 8.7$$

7.5.1 Weight of Girder Section (Span)

Box Girder Span Section	: 15.2538 m ² x 25 kN/m ³	= 381.35 kN/m
Bituminous wearing overlay	: 0.06 m x 18 m x 23 kN/m ³	= 24.84 kN/m
Right Sidewalk	: 0.46 m ² x 25 kN/m ³	= 11.50 kN/m
Left Sidewalk	: 0.32 m ² x 25 kN/m ³	= 8.00 kN/m
Guardrail	: 2x1.5 kN/m	= 3 kN/m
Total Weight	: 428.69 kN/m (per unit meter of viaduct)	

7.5.2 Weight of Girder Section (Support)

Box Girder	: 19.8689 m ² x 25 kN/m ³	= 496.72 kN/m
Bituminous wearing overlay	: 0.06 m x 18 m x 23 kN/m ³	= 24.84 kN/m
Right Sidewalk	: 0.46 m ² x 25 kN/m ³	= 11.50 kN/m
Left Sidewalk	: 0.32 m ² x 25 kN/m ³	= 8.00 kN/m
Guardrail	: 2 x 1.5 kN/m	= 3.00 kN/m
Total Weight	: 544.06 kN/m (per unit meter of viaduct)	

7.5.3 Total Weight of One Span

Total length of a mid span	: 58 m
Span box girder cross section length	: 48 m
Support cross section length	: 3.20 m (1.60 x 2)
Tapered (variable) nonprismatic box girder section length	: 6.80 m (3.40 x 2)
Span Unit Weight (48 m)	: 428.69 kN/m x 48 m = 20577.12 kN
Support Unit Weight (2x1.6=3.2 m)	: 544.06 kN/m x 3.2 m = 1740.992 kN
Nonprismatic section (3.4x2=6.8 m)	: (428.69+544.06)/2 x 6.8 m = 3307.35 kN
1 Span Total Weight	: 20577.12 + 1740.992 + 3307.35 = 25625.462 kN

CHAPTER 8

8. SEISMIC PERFORMANCE ASSESSMENT OF THE MOLLA GÜRANI VIADUCT

8.1 Seismic Performance Assessment

A two-stage evaluation and design approach has taken as a basis for the assessment of the seismic performance of existing Molla Gürani Viaduct according to TBEC-2020 Section 9. First of all three dimensional mathematical model of the viaduct is prepared. The detailed description of modelling is given in section 8.2.

The axial loads at each piers determined by performing nonlinear static analysis under the non-seismic loads. The moment-curvature relationship of the piers sections are obtained using the axial loads by XTRACT cross-section analysis program.

Nonlinear Time History Analysis of the existing Viaduct is performed. The initial deformed state of the structure due to the non-seismic loads is required before starting the nonlinear dynamic analyses. Nonlinear time history analyses are initiated on the basis of internal forces obtained from nonlinear static analysis.

Two orthogonal components of the ground motion set were used simultaneously in each analysis. $2 \times 7 = 14$ dynamic analyses were performed. The analysis was repeated by turning the application direction of the recordings 90 degrees. A total of 28 time history analyses were made and evaluated. The mean of the maximum absolute values of the structural response results from each analysis was calculated to be used to control the permitted deformation capacities.

8.2 Modelling of the Viaduct

8.2.1 Modelling of the Viaduct Superstructure

The deck of the viaduct is modeled with beam-column elements in order to represent the three-dimensional behavior of the entire deck cross section along the viaduct axis, according to TBEC-2020 Article 4.3.2.4, since the ratio of the shortest bridge span (46.4 m) to the bridge width ($46.4/20=2.32>2.0$) is greater than two. The characteristic features of the deck section are calculated and defined to the beam-column element assigned to the deck center of gravity.

8.2.2 Modelling of the Viaduct Piers

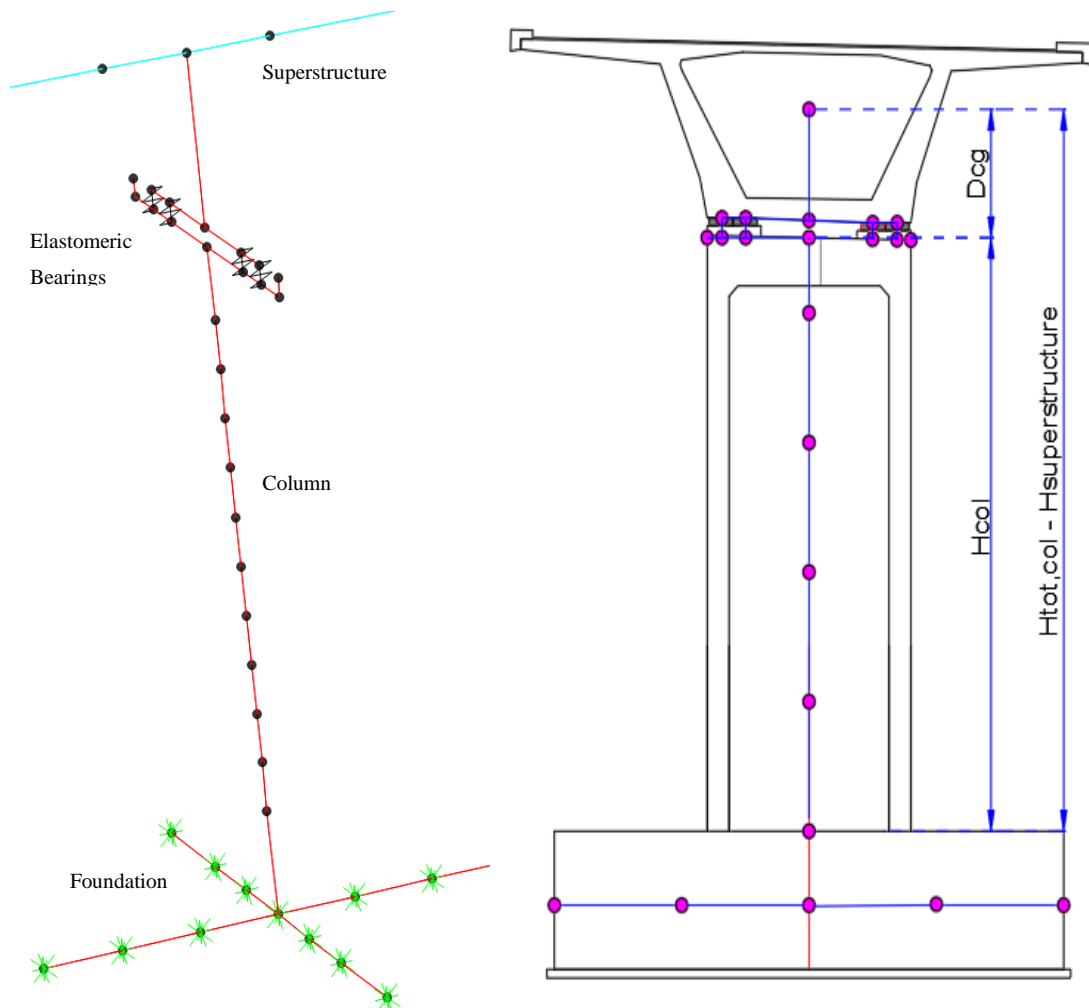


Figure 8.1 Pier Column Discretization

The clear height of the column H_{col} is taken according to Figure 8.1. The top of the column is defined at a distance of D_{cg} (difference between the top of column and the vertical centroid of the superstructure cross section) above the clear height of the bridge column as shown in Figure 8.1

Inelastic three dimensional beam-column elements used to model the each of pier columns of the viaduct. A beam-column element connects the nodes at the geometric centroid of the rectangular hollow column cross section using a minimum of five elements to model the column, according to TBEC-2020 (4.3.2.4)

The cracked section properties (Table 8.1) are used in the modelling of the columns. The property modifiers are applied to the column (frame elements) as shown in Figure 8.2

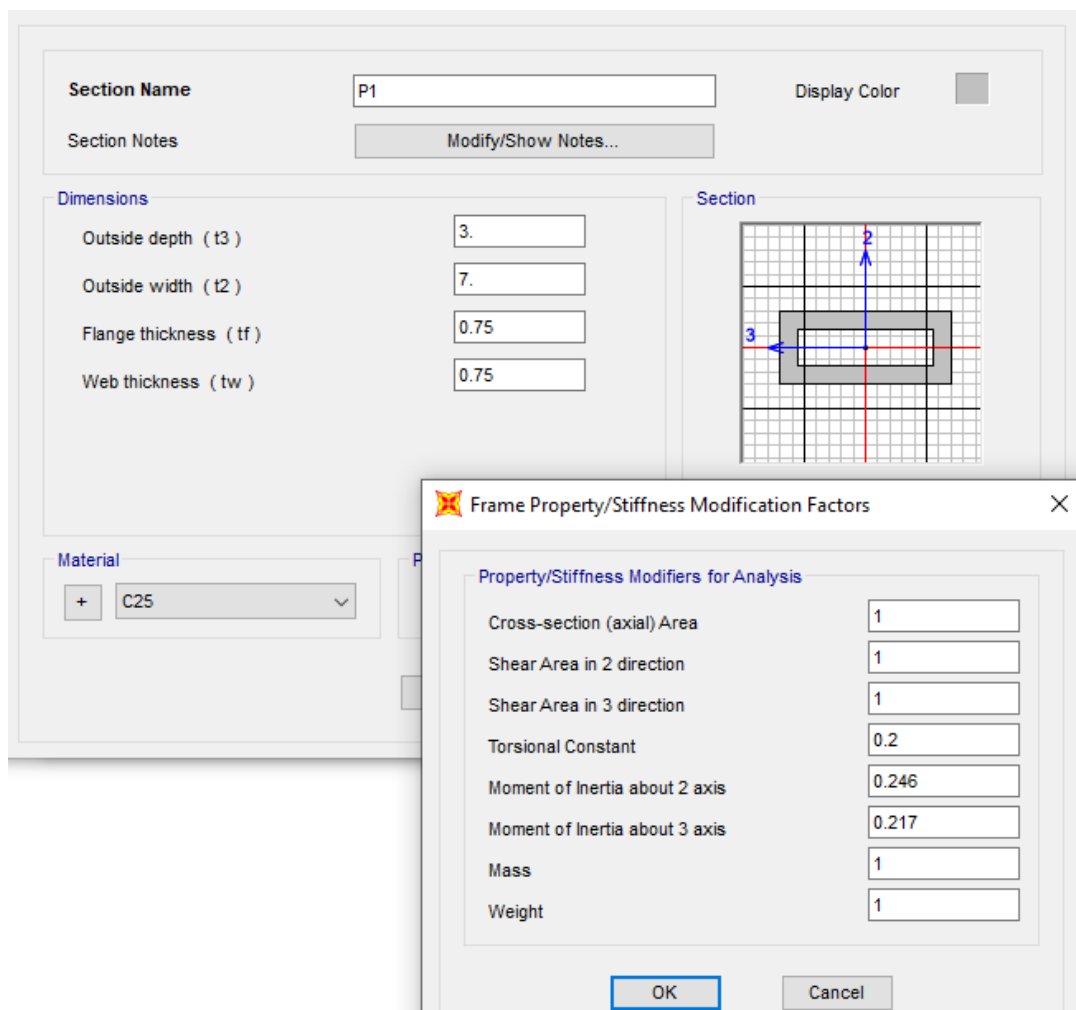


Figure 8.2 SAP2000 Section Property /Stiffness Modification

Table 8.1 Pier Columns Cracked Section Stiffness Modification Ratios

Axis	EI_{xx}	EI_{yy}	EI_{xx}	EI_{yy}	I_{22}	I_{33}
	N-m2	N/m2	N/m2	N/m2		
1	3.55E+11	1.62E+12	7.71E+10	4.00E+11	0.246	0.217
2	3.55E+11	1.62E+12	8.09E+10	4.18E+11	0.257	0.228
3	3.55E+11	1.62E+12	8.46E+10	4.36E+11	0.269	0.238
4	3.55E+11	1.62E+12	1.09E+11	5.33E+11	0.328	0.307
5	3.55E+11	1.62E+12	1.11E+11	5.43E+11	0.334	0.313
6	3.55E+11	1.62E+12	1.12E+11	5.45E+11	0.336	0.315
7	3.55E+11	1.62E+12	1.10E+11	5.39E+11	0.332	0.310
8	3.55E+11	1.62E+12	8.22E+10	4.25E+11	0.262	0.231

8.2.3 Modelling of the Abutments

The translational movement of the box girder in the longitudinal direction is restrained by anchoring devices (Gewi Bars 40 mm ST500/600) and shear keys in the 0 axis of the Molla Gürani Northern Viaduct. (Figure 8.3). Gewi tie bars are modeled as multi-elastic link elements on both sides (right-left) of the bridge superstructure girder section.

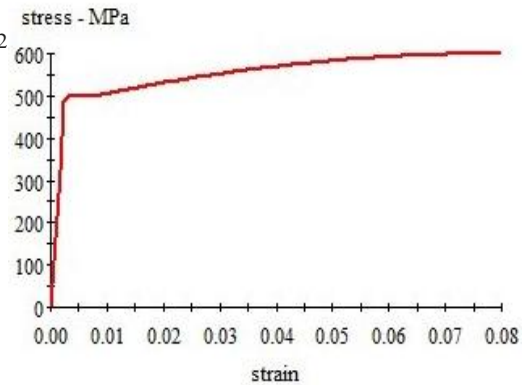


Figure 8.3 Tie(tension) bars

8.2.4 Modelling of the Tie Bars and Shear Keys at Abutments

Tie bars are modelled as multilinear elastic link elements and the effective stiffness that calculated below used in the model. The shear keys are modelled as a link/support property / gap elements.

Diameter of a tie bar : D = 40 mm
 Area of 58 Gewi bars : 72884.95 mm²
 Yield Stress : 500 MPa
 Fracture Stress : 600 MPa
 Yield Strain : 0.0025
 Strain at Strain Hardening : 0.008
 Failure Strain : 0.080
 Elasticity Modulus : 200 000 MPa



$$K_{h,long} = \frac{EA}{L_{bar}} = \frac{200000 \times 29 \times \pi 20^2}{600} = 12147491.59 \frac{N}{mm} \text{ or } \frac{kN}{m}$$

Table 8.2 Gewi Bars 40 mm ST500/600 Material Properties

GEWI® Bar Diameter	Steel Grade Yield f _y /Tensile Strength f _t 1)	Ultimate Tensile Force F _t (k)	Yield Force F _y	Cross Sectional Area	Diameter over Threads	Bar Weight
[mm]	[N/mm ²]	[kN]	[kN]	[mm ²]	[mm]	[kg/m]
16	500/550	111	100	210	19	1.58
20	500/550	173	157	314	23	2.47
25	500/550	270	245	491	29	3.85
28	500/550	339	308	616	32	4.83
32	500/550	442	402	804	36	6.31
40	500/550	691	628	1257	45	9.87
50	500/550	1080	982	1963	56	15.40
63.5	555/700	2219	1758	3167	69	24.80

Gewi bars also meet the requirements according UK standard(500/600 N/mm) and Austrian standard (550/620 N/mm) .

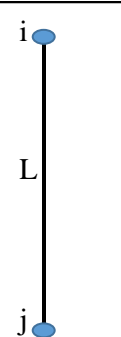
8.3 Nonlinear Static Analysis Under Non-Seismic Loads

The axial loads on the piers obtained from nonlinear static analysis are given in the Table 8.3. The nonlinear static analysis of the viaduct is performed for the following requirements :

- The axial loads due to gravity on each piers have to be determined for the moment-curvature analysis input data.
- To determine the initial deformed state of the structure due to the gravity loads before the starting dynamic analyses.
- To check the distribution of the loads on a structure and response of the structure under non-seismic loads.

Table 8.3. Axial Forces from the Nonlinear Static Analysis Results

Axis	Axial Forces from Nonlinear Static Analysis			
	P_i [kN]	P_j [kN]	P_{max} [kN]	Location
1	26,390.73	27,397.98	27,397.98	Top
1	28,405.23	29,412.48	29,412.48	Bottom
2	26,451.42	27,671.17	27,671.17	Top
2	32,550.17	33,769.92	33,769.92	Bottom
3	26,332.36	27,641.01	27,641.01	Top
3	36,810.53	38,110.17	38,110.17	Bottom
4	26,424.11	28,315.63	28,315.63	Top
4	42,634.54	44,254.99	44,254.99	Bottom
5	26,314.09	28,205.34	28,205.34	Top
5	45,528.34	47,495.03	47,495.03	Bottom
6	26,319.44	28,589.13	28,589.13	Top
6	46,230.03	48,370.57	48,370.57	Bottom
7	26,447.64	28,338.73	28,338.73	Top
7	44,055.94	46,143.20	46,143.20	Bottom
8	26,460.52	28,237.87	28,237.87	Top
8	33,569.02	35,347.27	35,347.27	Bottom



i : Top node of the frame element

j : Bottom node of the frame element

8.4 Modal Analysis

The purpose of the performing a modal analysis of the viaduct, was to try to understand the dynamic behavior of it. The results of modal analysis were given in Table 8.4. The natural frequencies and mode shapes can help to have a idea about how the structure responds when those modes are excited. Also, the modal analysis results are important because they provide means for validating the nonlinear model in SAP2000, and for required parameters to define the damping matrix needed in the Nonlinear Time History Analyses Cases.

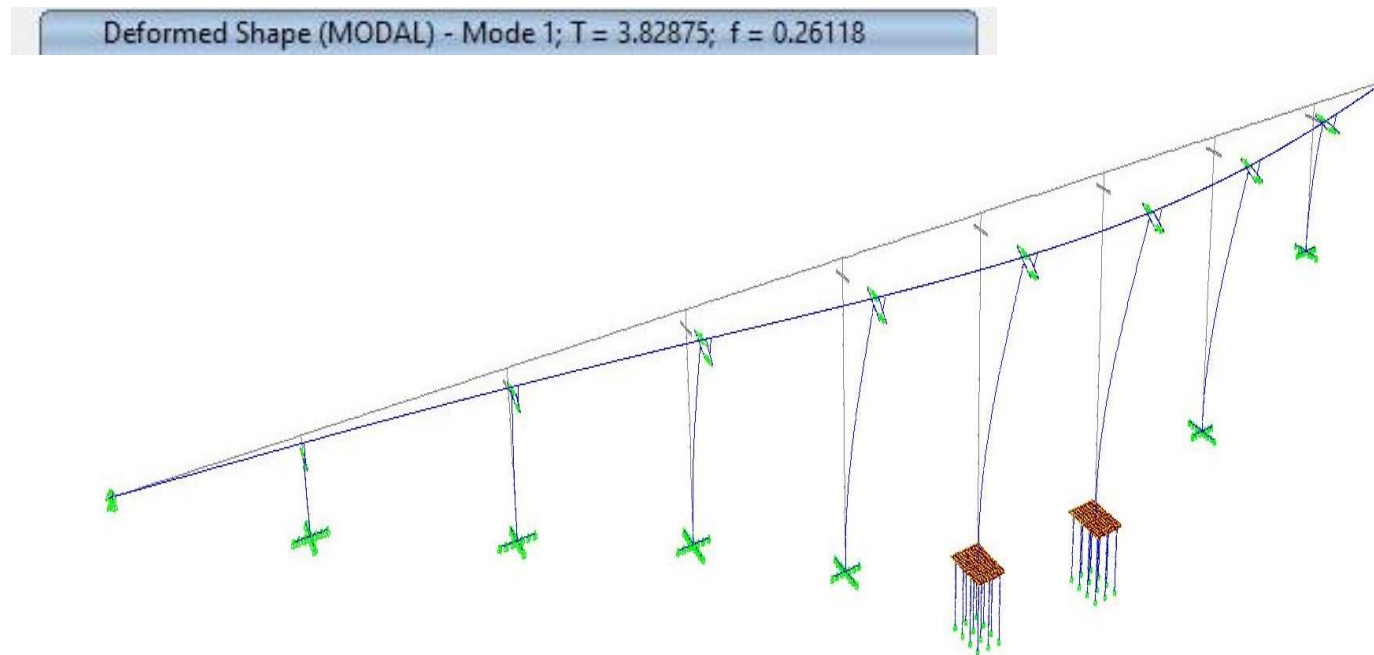


Figure 8.4. 1st Vibration Mode of the Viaduct in Transversal Direction ($T_1=3.82875$ sec.)

Deformed Shape (MODAL) - Mode 2; T = 1.92521; f = 0.51942

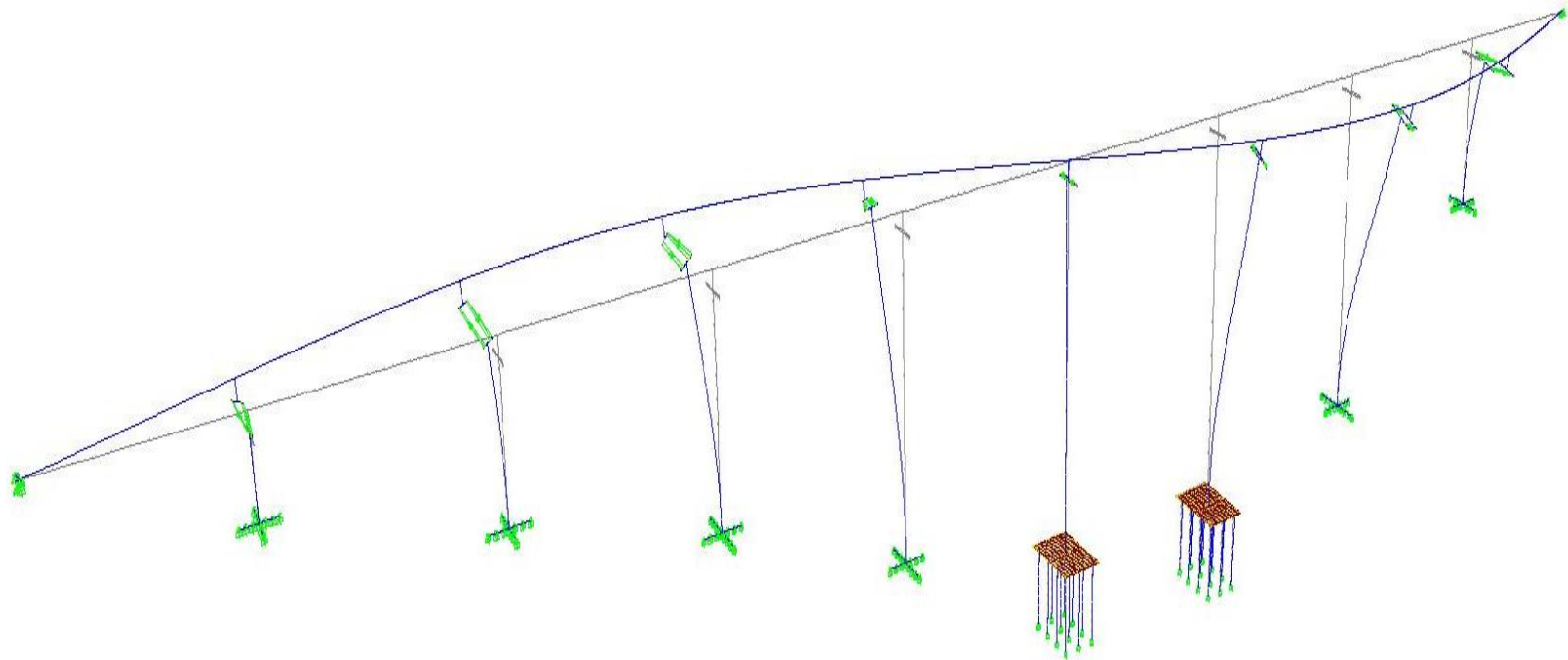


Figure 8.5. 2nd Vibration Mode of the Viaduct in Transversal Direction ($T_2=1.92521$ sec.)

Deformed Shape (MODAL) - Mode 3; T = 1.47649; f = 0.67728

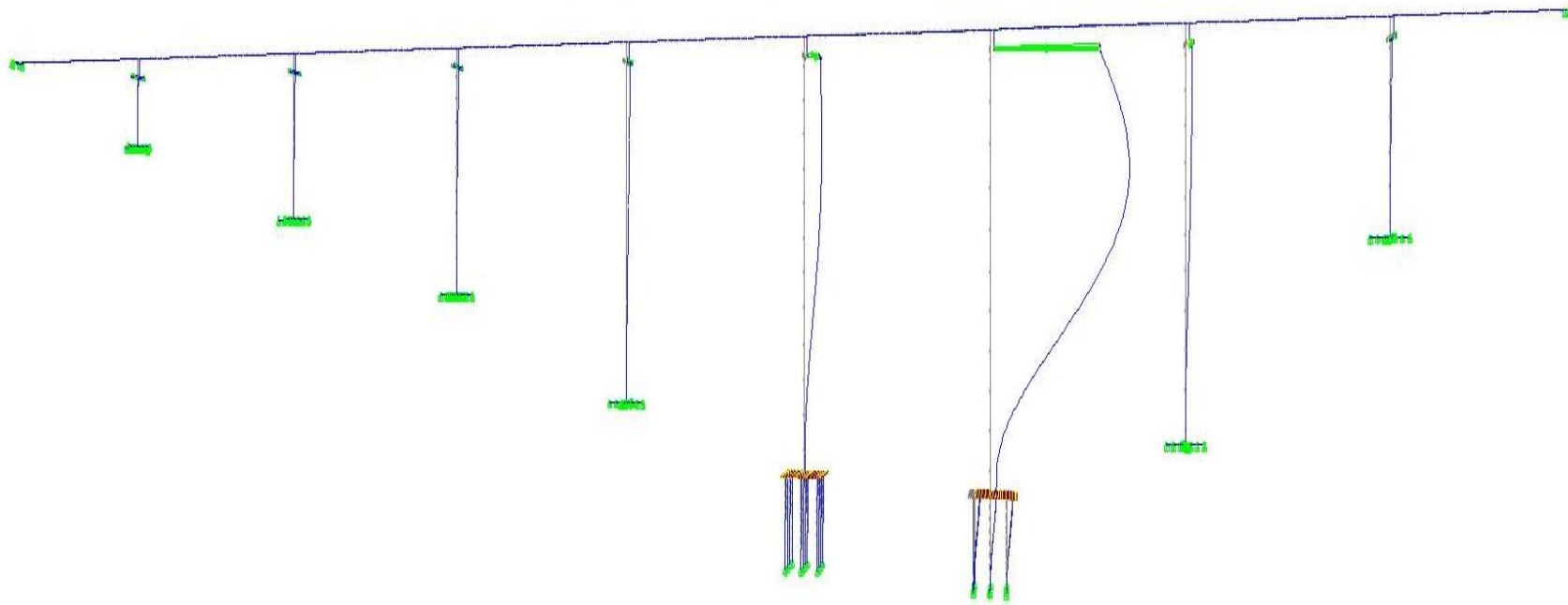


Figure 8.6. 3rd Vibration Mode of the Viaduct in Longitudinal Direction ($T_3=1.47649$ sec.)

8.4.1 Verification of Mass Participation

The required minimum mass participation 90% in both directions checked by displaying the Modal Participating Mass Ratios table for the “MODAL” load case it is found that the X-direction (longitudinal) reaches greater than 90% mass participation on the twentyfifth mode shape, while the Y-direction (transverse) reaches greater than 90% mass participation by the seventeenth mode shape. This implies that the minimum code requirements could be met by including only fourtyeighth mode shapes. The Modal Participating Mass Ratios table is shown in Figure 8.4.

8.4.2 Mass and Stifness Damping Proportional Coefficients

Mass proportional coefficients “ α ” and stifness proportional coefficient “ β ” were calculated using equation 8.1, by selecting equal damping value in two modes, $\xi_k = \xi_n = 0.05$.

$$\begin{Bmatrix} \alpha \\ \beta \end{Bmatrix} = 2 \frac{\omega_k - \omega_n}{\omega_n^2 - \omega_k^2} \begin{bmatrix} \omega_n & -\omega_k \\ -\frac{1}{\omega_n} & \frac{1}{\omega_k} \end{bmatrix} \begin{Bmatrix} \xi_k \\ \xi_n \end{Bmatrix} \quad (8.1)$$

$$C = \alpha M + \beta K \quad (8.2)$$

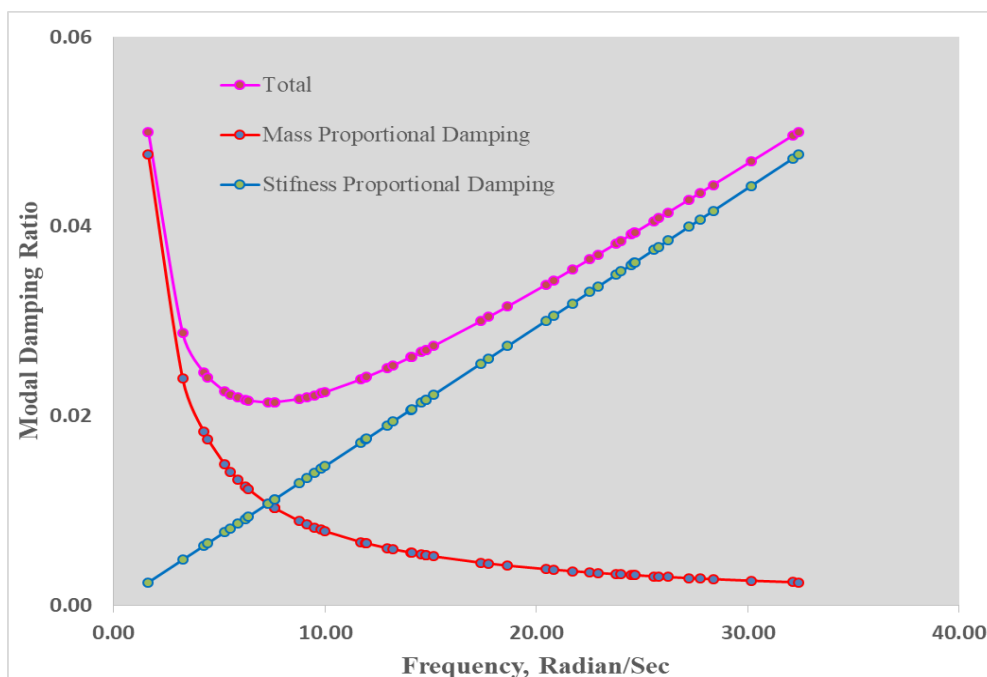


Figure 8.7 Rayleigh Proportional Damping

Table 8.4. Modal Analysis Results and Mass - Stiffness Proportional Coefficient

Mode	Period	UX	UY	UZ	SumUX	SumUY	SumUZ	Mass Proportional Coefficient	Stiffness Proportional Coefficient
	Sec	Unitless	Unitless	Unitless	Unitless	Unitless	Unitless	α	β
1	3.8288	0.0000	0.5479	0.0000	0.0000	0.5479	0.0000	0.109197	0.020389
2	1.9252	0.0000	0.0147	0.0000	0.0000	0.5627	0.0000	0.118433	0.016959
3	1.4765	0.1110	0.0000	0.0000	0.1110	0.5627	0.0000	0.119993	0.016380
4	1.4075	0.0662	0.0000	0.0000	0.1772	0.5627	0.0000	0.125079	0.014491
5	1.1946	0.0873	0.0000	0.0000	0.2645	0.5627	0.0000	0.126591	0.013930
6	1.1346	0.0000	0.0294	0.0000	0.2645	0.5920	0.0000	0.128322	0.013287
7	1.0677	0.0000	0.0065	0.0000	0.2645	0.5985	0.0000	0.129844	0.012722
8	1.0103	0.1072	0.0000	0.0000	0.3717	0.5985	0.0000	0.130460	0.012493
9	0.9874	0.0000	0.0726	0.0000	0.3717	0.6711	0.0000	0.133954	0.011196
10	0.8618	0.1299	0.0000	0.0000	0.5016	0.6711	0.0000	0.135011	0.010803

24	0.4456	0.0067	0.0000	0.0000	0.8966	0.8299	0.0000	0.147497	0.006167
25	0.4311	0.0053	0.0000	0.0000	0.9020	0.8299	0.0000	0.147695	0.006094
26	0.4254	0.0000	0.0000	0.0000	0.9020	0.8299	0.0000	0.147695	0.006093
27	0.4254	0.0000	0.0000	0.0000	0.9020	0.8299	0.0000	0.148070	0.005954
28	0.4146	0.0000	0.0308	0.0000	0.9020	0.8607	0.0000	0.149957	0.005254
29	0.3612	0.0000	0.0000	0.0000	0.9020	0.8607	0.0000	0.150219	0.005156

37	0.2643	0.0116	0.0000	0.0000	0.9152	0.8684	0.0019	0.153605	0.003899
38	0.2617	0.0000	0.0001	0.0000	0.9152	0.8685	0.0019	0.153798	0.003827
39	0.2566	0.0132	0.0000	0.0005	0.9284	0.8685	0.0024	0.153853	0.003807
40	0.2551	0.0032	0.0000	0.0008	0.9316	0.8685	0.0031	0.153870	0.003800
41	0.2547	0.0008	0.0000	0.0058	0.9324	0.8685	0.0089	0.154204	0.003677
42	0.2458	0.0000	0.0135	0.0000	0.9324	0.8820	0.0089	0.154283	0.003647
43	0.2438	0.0000	0.0000	0.1425	0.9324	0.8820	0.1515	0.154443	0.003588
44	0.2395	0.0000	0.0040	0.0000	0.9324	0.8861	0.1515	0.154779	0.003463
45	0.2307	0.0036	0.0000	0.0000	0.9361	0.8861	0.1515	0.154944	0.003402
46	0.2264	0.0000	0.0100	0.0000	0.9361	0.8961	0.1515	0.155130	0.003333
47	0.2215	0.0000	0.0000	0.1385	0.9361	0.8961	0.2900	0.155636	0.003145
48	0.2084	0.0000	0.0108	0.0000	0.9361	0.9069	0.2900	0.156136	0.002959
49	0.1954	0.0000	0.0000	0.0981	0.9361	0.9069	0.3881	0.156200	0.002935
50	0.1938	0.0027	0.0000	0.0000	0.9387	0.9069	0.3881	0	0.0609365

8.5 Response Spectrum Analysis

The response spectrums for ground motion level DD1 and DD2a are defined using informations that are given in Chapter 5.(Figure 8.8&8.9)

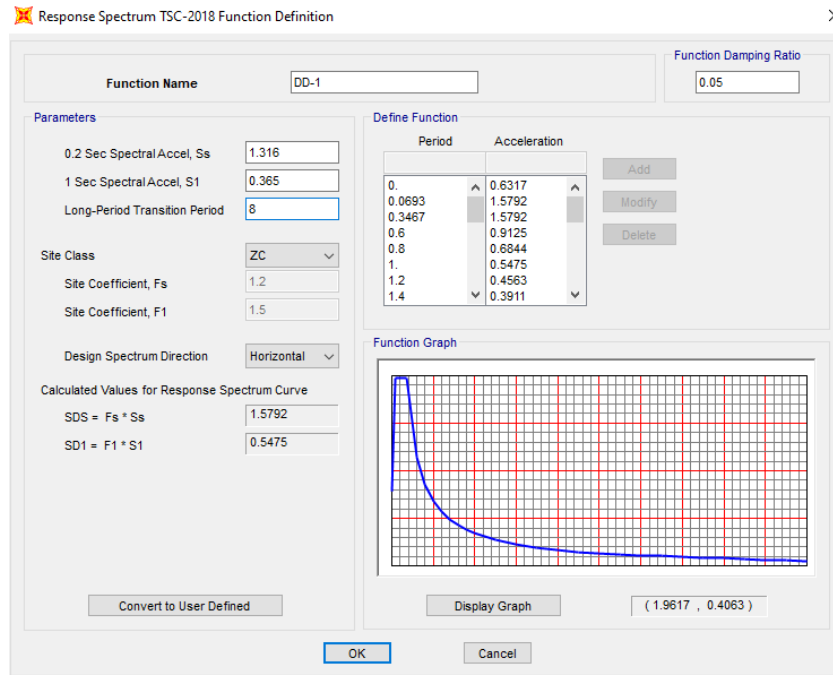


Figure 8.8 RS Definition – DD1 Earthquake Ground Motion Level

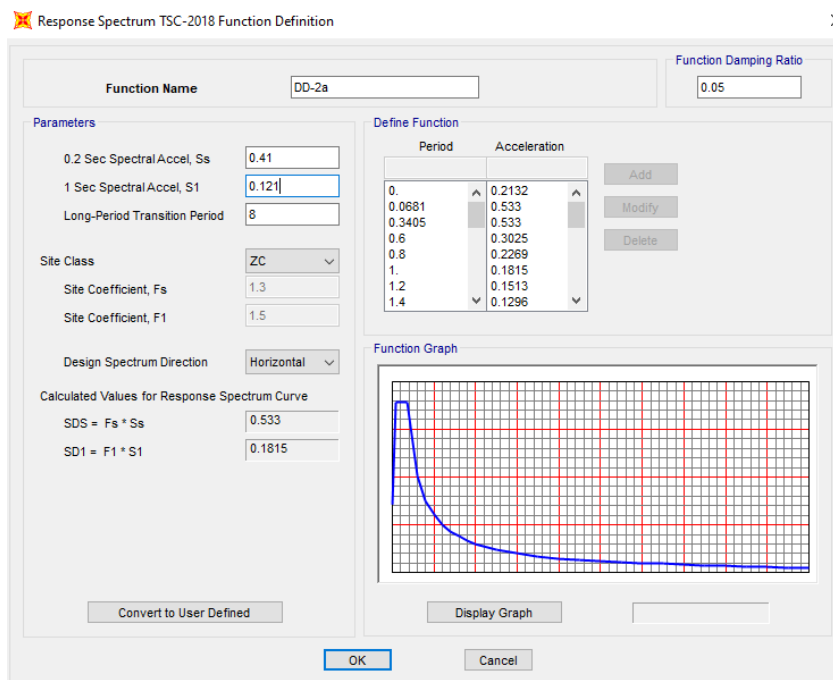


Figure 8.9 RS Definition – DD2a Earthquake Ground Motion Level

8.6 Nonlinear Time History Analysis

Nonlinear Time History analysis was carried out in SAP2000 using the Hilbert-Hughes-Taylor integration scheme with a time steps equal to the each one of the selected earthquake records time step. PEER NGA database(PEER 2013) is used to choose ground motion records that are compatible with design spectrum.

Viscous damping in the system was specified by entering the calculated mass proportional and stiffness proportional coefficients as $\alpha=0.1562$ and $\beta =0.002935$. (Figure 8.10)

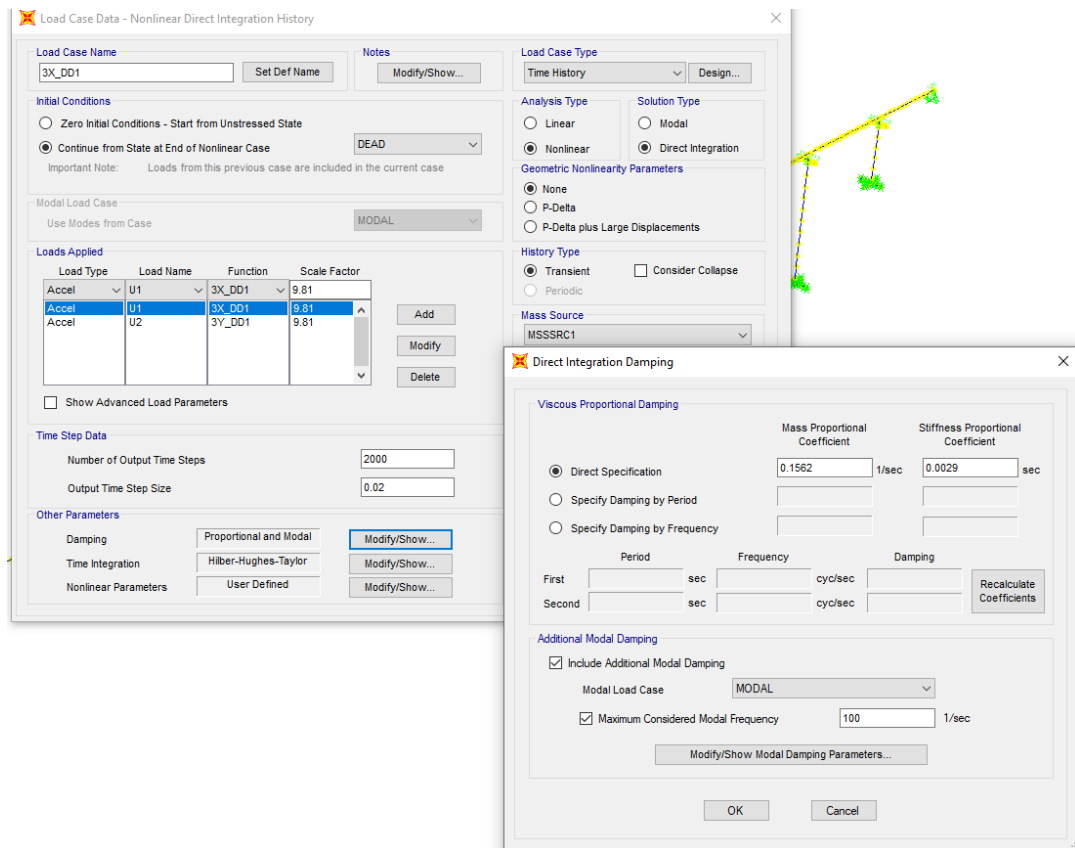


Figure 8.10. NLTH Load Case and Modal Proportional Damping Definition

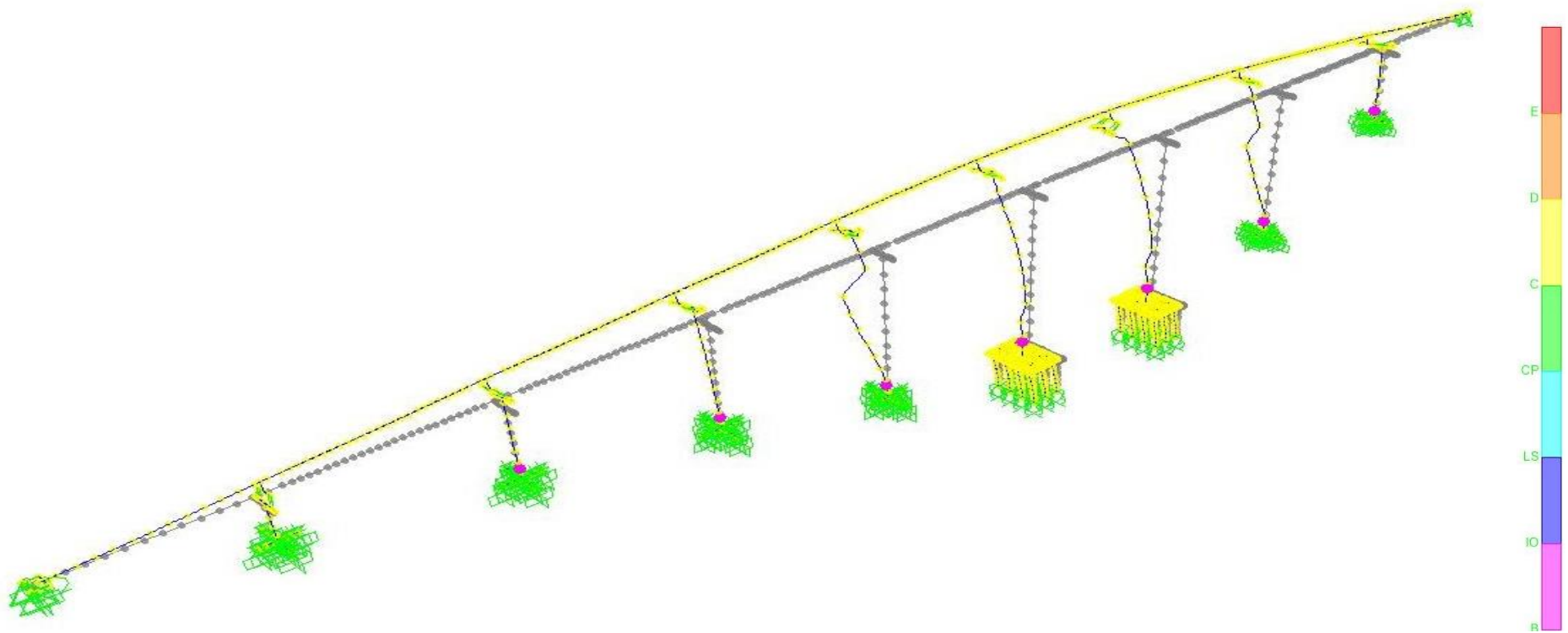


Figure 8.11 Nonlinear Time History Analysis – Deformed Shape (RSN1762_HECTOR_ABY360 Time History)

8.6.1 Deformation of the Elastomeric Bearings

In the first stage of analysis and evaluation, the elastomeric bearing shear deformation shall not exceed 2/3 ($\gamma \leq 2/3$) according to TBEC-2020 section 4.3.5.2b.

$$\frac{\text{Elastomeric bearing relative displacement}}{\text{Total thickness of elastomer layers except steel shims}} = \frac{\Delta_s}{h_{rt}} = \gamma_s \leq \frac{2}{3}$$

The elastomeric bearing shear deformations shall not exceed 2 ($\gamma \leq 2$) according to TBEC-2020 section 5.4.5.1. In the second stage, if the elastomeric bearing shear deformations exceed the $\gamma=1$ limit, the elastomeric bearings must be bolted to the relevant bridge load carrying (structural) system components (pier or girder) from the top and bottom. (TBEC-2020 section 5.4.5.2)

$$\frac{\text{Elastomeric bearing relative displacement}}{\text{Total thickness of elastomer layers except steel shims}} = \frac{\Delta_s}{h_{rt}} = \gamma_s \leq 2$$

The function and configuration of the bearings were given in Figure 4.11. The bearings on abutments restrained in transversal direction while free in longitudinal direction. The bearing of the Piers (P1-P2-P3-P4-P5-P6 and P7) are free in both transversal and longitudinal direction while the Pier 8 has longitudinally sliding bearing and free in transversal direction.

The calculated deformation of bearings from the results of performed fourteen Nonlinear Time History Load Cases Analyses were summarized and absolute average maximum values given in Table 8.5 and Table 8.6 for DD1 and DD2a earthquake ground motion levels. The results of the 90 ° degree counter-clockwise direction rotated DD1 earthquake level are given in Table 8.7.

Elastomeric bearings shear deformations are within the limits in the longitudinal and transversal direction for DD2a earthquake ground motion level while the shear deformations exceed the 2 in longitudinal and transversal direction for DD1 earthquake ground motion level.

Table 8.5. Elastomeric Bearing Shear deformations (DD1)

Axis	Longitudinal	Transversal	h_{rt}	Average Deformation / Thickness Ratio	
				Longitudinal	Transversal
0	122.07	Restrained	85	1.44	Restrained
1	120.12	114.97	85	1.41	1.35
2	76.29	165.50	85	0.90	1.95
3	118.13	177.22	85	1.39	2.08
4	215.93	190.52	101	2.14	1.89
5	386.71	371.04	165	2.34	2.25
6	397.24	227.09	165	2.41	1.38
7	277.89	139.1	125	2.22	1.11
8	Sliding	142.1	149	Sliding	0.95
9	Sliding	Restrained	85	Sliding	Restrained

Table 8.6. Elastomeric Bearing Shear deformations (DD2a –DD2a 90° Rotated)

Axis	DD2a		DD2a_90 °Rotated		h_{rt}	DD2a		DD2a 90° Rotated	
						Average Deformation / Thickness Ratio			
	Longitudinal	Transversal	Longitudinal	Transversal		Longitudinal	Transversal	Longitudinal	Transversal
0	21.46	Restrained	21.88	Restrained	85	0.25	Restrained	0.26	Restrained
1	19.81	37.83	20.24	38.21	85	0.23	0.45	0.24	0.45
2	19.47	58.36	19.75	58.25	85	0.23	0.69	0.23	0.69
3	51.27	62.84	49.09	63.22	85	0.60	0.74	0.58	0.74
4	72.20	62.36	71.04	62.75	101	0.71	0.62	0.70	0.62
5	118.79	124.86	117.30	123.68	165	0.72	0.76	0.71	0.75
6	125.49	76.63	124.62	74.08	165	0.76	0.46	0.76	0.45
7	93.19	47.98	92.82	45.35	125	0.75	0.38	0.74	0.36
8	Sliding	49.44	Sliding	51.29	149	Sliding	0.33	Sliding	0.34
9	Sliding	Restrained	Sliding	Restrained	85	Sliding	Restrained	Sliding	Restrained

Table 8.7. Elastomeric Bearing Shear deformations (DD1 and DD1_Rotated 90 °)

Axis	DD1		DD1 90° Rotated		h_{rt}	DD1		DD1 90° Rotated	
	Longitudinal	Transversal	Longitudinal	Transversal		Average Deformation / Thickness Ratio			
						Longitudinal	Transversal	Longitudinal	Transversal
0	122.07	Restrained	156.74	Restrained	85	1.44	Restrained	1.84	Restrained
1	120.12	114.97	128.55	116.70	85	1.41	1.35	1.51	1.37
2	76.29	165.50	78.15	166.01	85	0.90	1.95	0.92	1.95
3	118.13	177.22	130.11	171.56	85	1.39	2.08	1.53	2.02
4	215.93	190.52	203.60	203.99	101	2.14	1.89	2.02	2.02
5	386.71	371.04	374.72	347.89	165	2.34	2.25	2.27	2.11
6	397.24	227.09	375.21	222.14	165	2.41	1.38	2.27	1.35
7	277.89	139.1	293.93	147.82	125	2.22	1.11	2.35	1.18
8	Sliding	142.1	Sliding	138.62	149	Sliding	0.95	Sliding	0.93
9	Sliding	Restrained	Sliding	Restrained	85	Sliding	Restrained	Sliding	Restrained

8.6.2 Hinge States and Plastic Deformation

The viaduct was analyzed in 2 stages(DD-1 and DD2a) according to the level of earthquake ground motion. Controlled Damage performance target for DD-1 earthquake ground motion level and Limited Damage performance target for DD2a earthquake ground motion level were considered in the analysis.

The concrete and reinforcing steel strain capacities given below were used according to TBEC-2020 section 5.6.1.4 and 9.1.3.3 , since the pier columns of the molla gürani viaduct lapped reinforcement joints are not made far enough from the plastic hinge impact zone.

$$\begin{aligned}
 \varepsilon_c^{(LD)} &= 0.003 ; & \varepsilon_s^{(LD)} &= 0.015 & \text{DD} - 2a \text{ Earthquake Level} \\
 \varepsilon_c^{(CD)} &= 0.004 ; & \varepsilon_s^{(CD)} &= 0.04 & \text{DD} - 1 \text{ Earhquake Level}
 \end{aligned}
 \tag{8.3}$$

The plastic rotation capacity of columns for Controlled Damage Performance Level calculated using equation 8.4. The detailed calculation example given in the section 7.4.4

$$\theta_p^{(CD)} = (\phi^{(CD)} - \phi_Y) L_p \quad (8.4)$$

At the DD1 earthquake ground motion level, plastic rotations occurred in the hinges defined at the lower ends of the columns (just above the raft or cap-beam) in the longitudinal and transverse directions while at DD2a were not occurred. Deformations in concrete and steel materials are below the limits.

Table 8.8. Plastic Hinge Rotation Capacity in Longitudinal Direction (DD1)

Pier	L_p	Longitudinal Direction			
	[m]	Elastic Curvature ϕ_{el}	Plastic Curvature ϕ_{pl}	Total Curvature $\Sigma\phi$	Plastic Rotation [rad]
P1-B	1.166	1.16E-03	3.65E-03	4.81E-03	4.26E-03
P2-B	2.244	1.17E-03	4.26E-04	1.60E-03	9.56E-04
P3-B	3.363	1.19E-03	0.00E+00	1.19E-03	0.00E+00
P4-B	4.882	1.23E-03	2.35E-04	1.46E-03	1.15E-03
P5-B	5.723	1.24E-03	8.11E-04	2.05E-03	4.64E-03
P6-B	5.942	1.24E-03	7.62E-04	2.01E-03	4.53E-03
P7-B	5.35	1.24E-03	9.39E-04	2.17E-03	5.02E-03
P8-B	2.558	1.18E-03	1.93E-03	3.10E-03	4.93E-03

Table 8.9. Plastic Hinge Rotation Capacity in Transversal Direction (DD1)

Pier	L_p	Transversal Direction			
	[m]	Elastic Curvature ϕ_{el}	Plastic Curvature ϕ_{pl}	Total Curvature $\Sigma\phi$	Plastic Rotation [rad]
P1-B	1.166	5.23E-04	0.00E+00	5.23E-04	0.00E+00
P2-B	2.244	5.30E-04	6.77E-04	1.21E-03	1.52E-03
P3-B	3.363	5.38E-04	1.90E-03	2.44E-03	6.39E-03
P4-B	4.882	5.76E-04	1.12E-03	1.70E-03	5.46E-03
P5-B	5.723	5.83E-04	6.92E-04	1.27E-03	3.96E-03
P6-B	5.942	5.85E-04	2.37E-04	8.21E-04	1.41E-03
P7-B	5.35	5.80E-04	2.33E-04	8.13E-04	1.25E-03
P8-B	2.558	5.33E-04	2.55E-04	7.88E-04	6.53E-04

8.6.3 Tie Bar Deformations

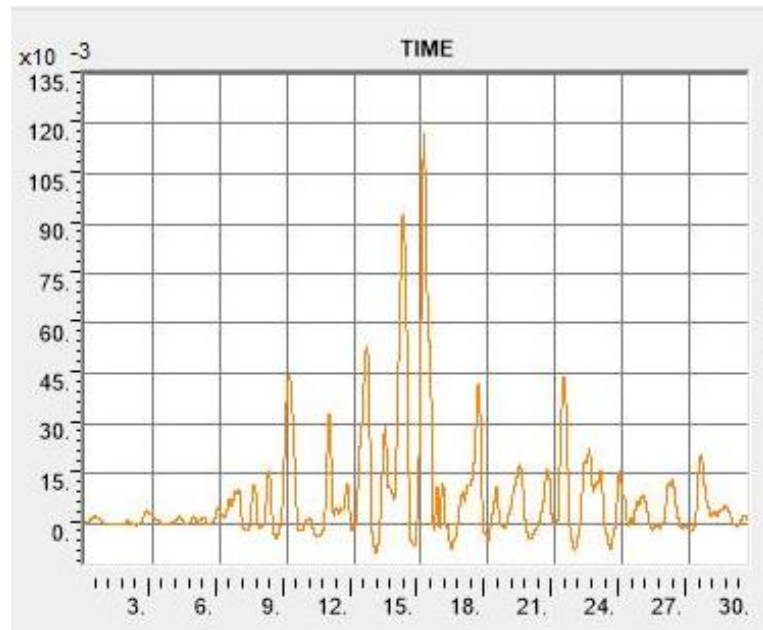


Figure 8.12. Tie Bar Axial Deformation- RNS1166 Kocaeli Earthquake (DD1)

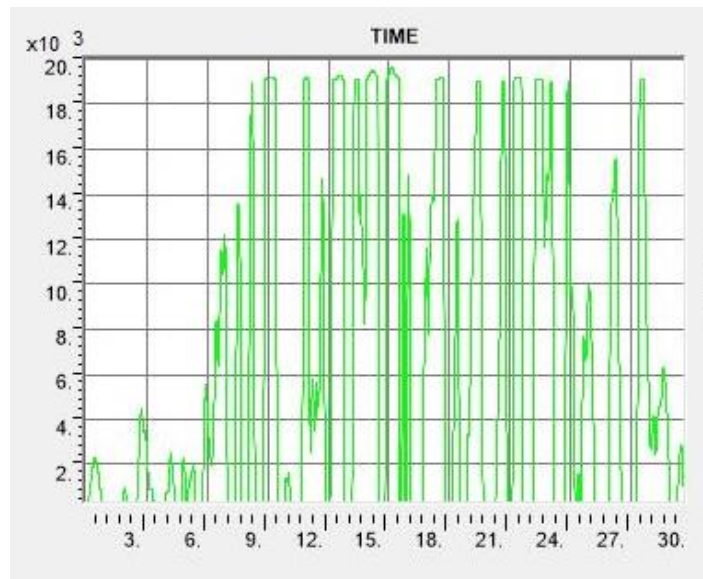


Figure 8.13. Tie Bar End Axial Forces - RNS1166 Kocaeli Earthquake (DD1)

Maximum axial force in tie bars is :

Max Axial Load

N : 1.965e+04 kN (SAP2000)

Time

t : 15.13 sec

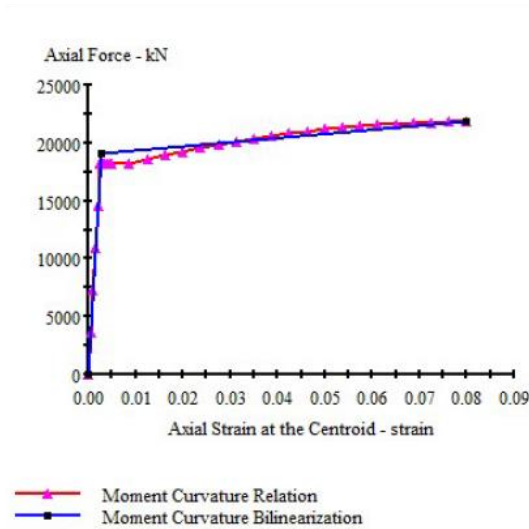


Figure 8.14. Tie Bar Force-Displacement Relation

L_{bar} : 6 m

Yield strain ϵ_{sy} : Yield Strain: 0.00262 1/m (Tension)

Failure strain ϵ_{su} : 0.08 1/m

Effective Yield Axial Force : 19.05E+03 kN

Ultimate Axial Force : 21.81E+3 kN

Table 8.10. Tie Bar Deformations (DD1)

	Tie Bar Deformations -DD1 Earthquake Ground Motion Level						
	RSN15	RSN731	RSN838	RSN1166	RSN1206	RSN1762	RSN3747
DD1_X	9.28E-02	8.13E-02	1.60E-01	1.17E-01	2.55E-01	1.18E-01	7.39E-02
DD1_Y	1.20E-01	1.55E-01	1.09E-01	3.59E-01	3.98E-02	7.12E-02	1.26E-01
Avarage	1.06E-01	1.18E-01	1.35E-01	2.38E-01	1.47E-01	9.46E-02	9.97E-02
Δ_{avg}	134.07 mm						

Yield unit deformation : $0.00262 \times 6 = 0.01572$ m

Ultimate unit deformation : $0.08 \times 6 = 0.48$ m

Unit deformation : $0.13407/6 = 0.022345$ (DD1 Level SAP 2000 Analysis)

$$\epsilon_s = 0.022345 > \epsilon_{sy} = 0.00262$$

$$\epsilon_s = 0.022345 < \epsilon_{su} = 0.08$$

Tie bars will have plastic deformation under the DD1 Earthquake Ground Motion Level.

Table 8.11. Tie Bar Deformations (DD2a)

	Tie Bar Deformations -DD2a Earthquake Ground Motion Level						
	RSN15	RSN731	RSN838	RSN1166	RSN1206	RSN1762	RSN3747
DD2a_X	2.57E-02	1.21E-02	1.73E-02	1.14E-02	2.55E-02	7.39E-02	1.30E-02
DD2a_Y	1.51E-02	1.56E-02	3.31E-02	2.78E-02	3.98E-02	1.26E-01	1.53E-02
Avarage	2.04E-02	1.39E-02	2.52E-02	1.96E-02	3.27E-02	9.97E-02	1.42E-02
Δ_{avg}	35.24 mm						

Unit deformation : 0.03524/6 = 0.00587 (DD2a Level SAP 2000 Analysis)

$$\epsilon_s = 0.00587 > \epsilon_{sy} = 0.00262$$

$$\epsilon_s = 0.00587 < \epsilon_{su} = 0.08$$

Tie bars will have plastic deformation under the DD2a Earthquake Ground Motion Level.

Table 8.12. Tie Bar Deformations (90 ° Rotated DD1)

	Tie Bar Deformations -90° Rotated DD1 Earthquake Ground Motion Level						
	RSN15	RSN731	RSN838	RSN1166	RSN1206	RSN1762	RSN3747
DD1_X_90°	1.84E-01	2.41E-01	1.46E-01	3.60E-01	3.65E-02	8.65E-02	1.57E-01
DD1_Y_90°	8.96E-02	7.51E-02	1.59E-01	1.35E-01	2.47E-01	1.04E-01	6.47E-02
Avarage	1.37E-01	1.58E-01	1.53E-01	2.47E-01	1.42E-01	9.50E-02	1.11E-01
Δ_{avg}	148.91 mm						

Unit deformation : 0.14891/6 = 0.0248 (90° Rotated DD1a Level SAP 2000 Analysis)

$$\epsilon_s = 0.0248 > \epsilon_{sy} = 0.00262$$

$$\epsilon_s = 0.0248 < \epsilon_{su} = 0.08$$

Tie bars will have plastic deformation under the Rotated 90° DD1 Earthquake Ground Motion Level.

8.6.4 Pounding Effect

There is a gap of 1.50 m between the superstructures of the viaduct. High shear deformations in elastomeric bearings can cause the superstructure to collide. We used the results of twenty-eight Time Domain Analysis results to control the transverse displacement of the superstructure. The highest transverse displacements are obtained at the DD1 earthquake ground motion level. A summary of the results is provided in Table 8.13 below.

Since the viaducts have the same material, structural and geometrical properties we can multiply the transversal displacement by 2 if we accept the transversal displacements of the viaducts will be in opposite direction (towards each other) to each other at exact same excitation time .

Table 8.13. Transversal Deformations of Superstructure (DD1)

	Transversal Deformations -DD1 Earthquake Ground Motion Level						
	RSN15	RSN731	RSN838	RSN1166	RSN1206	RSN1762	RSN3747
DD1_X	4.88E-01	7.41E-01	1.39E+00	7.37E-01	5.92E-01	8.92E-01	5.16E-01
DD1_Y	4.15E-01	8.80E-01	7.00E-01	4.60E-01	5.39E-01	1.26E+00	9.33E-01
Average	4.52E-01	8.10E-01	1.05E+00	5.99E-01	5.66E-01	1.07E+00	7.24E-01
δ_{avg}	0.753 m						

$$2 \times \delta_{avg} = 2 \times 0.753 = 1.506 \text{ m} > 1.50 \text{ m} = \text{Gap between superstructures is not enough.}$$

Additionally, it should also be taken into account that high Pier columns can increase the lateral deformations that will occur under the effect of earthquake ground motion, even if the probability of making the same transverse deformation at the same time seems low.

8.6.5. Shear Strength of the Pier Columns

There are different formulas proposed by many researchers to calculate the shear strength of bridge columns. The formulas given in TBEC-2020 section 5.6.5 are compatible with the formulas given in Caltrans 2013 chapter 3.

The nominal shear capacity V_n is the sum of the shear capacity V_c of the concrete and the shear capacity V_s of the transverse reinforcement.

$$V_n = V_c + V_s \leq 0.8 A_c \sqrt{f_{ck}} \quad (8.5)$$

Shear force capacity of concrete can be determined by the following equation according to TBEC 5.6.6.1.

$$V_c = 0.8 k_c A_c \sqrt{f_{ck}} \quad ; \quad k_c \leq 0.33 \quad (8.6)$$

The coefficient k_c in Eq.(8.6) shall be defined as follows, different inside and outside the plastic hinge impact zone defined in paragraph (c) below. The coefficient k_c to be defined for the outside of the plastic hinge effect zone will also be used for all capacity preserved elements.

(a) Inside the plastic hinge zone;

$$k_c = k_{c1} k_{c2} \leq 0.33 \quad (8.7)$$

(b) Outside the plastic hinge zone;

$$k_c = 0.25 k_{c2} \leq 0.33 \quad (8.8)$$

(c) The length of the impact zone of the plastic hinge shall be taken as the greater of 1.5 times the maximum cross-sectional dimension and the length of the plastic hinge defined by Eq.(8.9).

$$L_p = 0.08 L_k + 0.022 f_{ye} d_{bl} \geq 0.044 f_{ye} d_{bl} \quad (8.9)$$

k_{c1} and k_{c2} defined by Eq.8.10:

$$\begin{aligned} k_{c1} &= \alpha + 0.305 - 0.083 \mu_d \quad ; \quad 0.025 \leq k_{c1} \leq 0.25 \\ k_{c2} &= 1 + 0.073 \frac{N_k}{A_c} \quad ; \quad k_{c2} \leq 1.5 \end{aligned} \quad (8.10)$$

In the rectangular section, the coefficient α , depending on the direction considered:

$$\alpha = 0.16\rho_x f_{ywk} \leq 0.193 \quad \left(\rho_x = \frac{A_{swx}}{h_o s} \right) \quad (8.11)$$

$$\alpha = 0.16\rho_y f_{ywk} \leq 0.193 \quad \left(\rho_y = \frac{A_{swy}}{b_o s} \right) \quad (8.12)$$

Here, A_{swx} and A_{swy} show the total transverse reinforcement area in the x and y directions, the dimensions of the b_o and h_o rectangular section in the direction perpendicular to the shear force direction, and the s transverse reinforcement spacing.

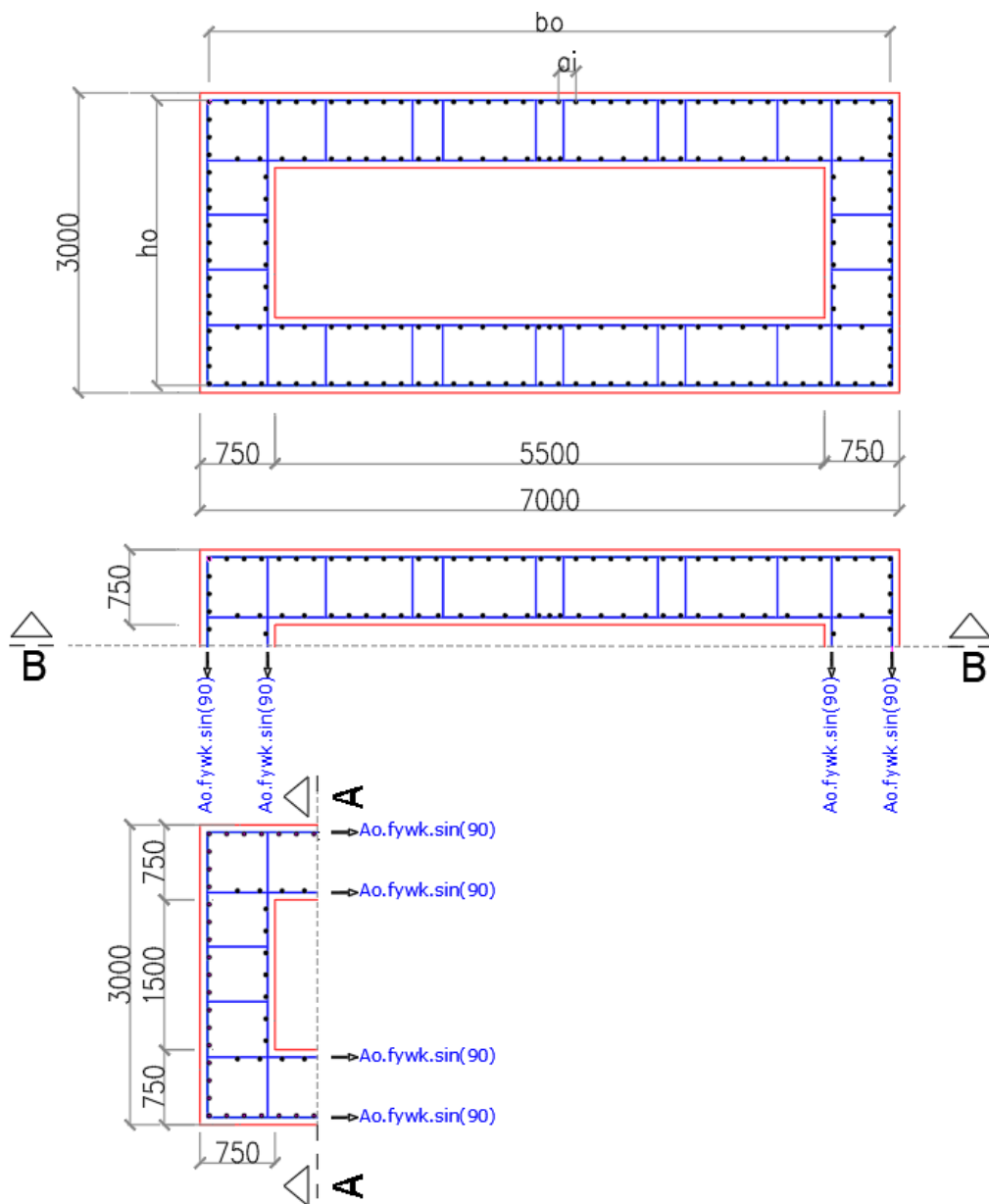


Figure 8.15. Molla Gürani Pier Column Shear Capacity Calculation

μ_d in Eq.(8.10) represents the displacement ductility ratio demand for the relevant plastic hinge:

$$\mu_d = \frac{u_{dj}}{u_{ij}} \quad (8.13)$$

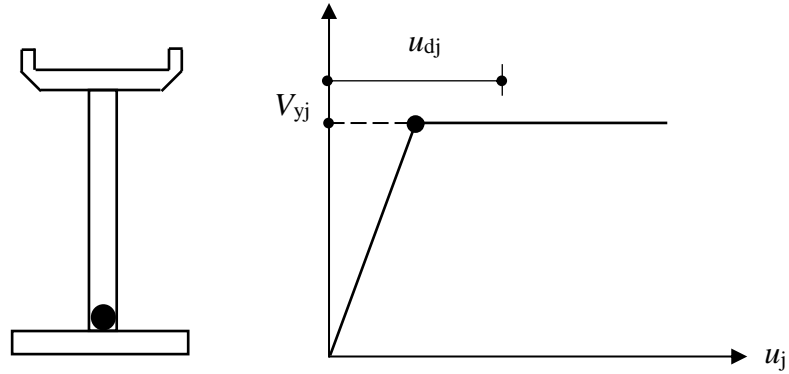


Figure 8.16. Single Column Cantilever Bridge Pier

8.6.6. Shear Strength of Transverse Reinforcement

The equation 8.14 is given in TBEC-2020 section 5.67 for calculation of shear strength of the transverse reinforcement of the rectangular column. The upper limit of the shear strength capacity of the transverse reinforcement is defined by Equation (8.15).

$$V_s = \frac{A_{sw} f_{yw} d}{s} \quad (8.14)$$

$$V_s = 0.8 k_s A_c \sqrt{f_{ck}} \quad ; \quad k_s \leq 0.67 \quad (8.15)$$

The shear strength capacities of the Molla Gürani Viaduct columns are calculated by using equations that are given above. The calculated capacities were checked if they can resist without any structural failure to the shear forces obtained from NLTH analyses.

Table 8.14. Column Shear Force Capacity in Longitudinal Direction (DD1)

Axis	A _c [mm ²]	φ _s	d	d'	h ₀ [mm]	n	s [mm]	ρ	α	N _k [kN]	μ _d	k _{c1}	k _{c2}	k _c	A _{sp} [mm ²]	A _{swx} [mm ²]	V _c [kN]	V _s [kN]	V _{s,max} [kN]	V _n [kN]	V _{n,max} [kN]	V _d [kN]	V _d /V _n ≤ 2/3		Check	
																							0.25	≤ 0.66		
1	1.28E+07	16	2918	50	2884	4	300	0.09%	0.06	27398	1.5	0.240	1.16	0.28	201	804	14188	3286	34170	17473.15	51000	4404	0.25	≤	0.66	OK !!!
2	1.28E+07	16	2918	50	2884	4	300	0.09%	0.06	33770	1.1	0.250	1.19	0.30	201	804	15215	3286	34170	18500.72	51000	3584	0.19	≤	0.66	OK !!!
3	1.28E+07	16	2918	50	2884	4	300	0.09%	0.06	38110	1.0	0.250	1.22	0.30	201	804	15532	3286	34170	18817.56	51000	4826	0.26	≤	0.66	OK !!!
4	1.28E+07	16	2918	50	2884	4	300	0.09%	0.06	44255	1.1	0.250	1.25	0.31	201	804	15981	3286	34170	19266.13	51000	7220	0.37	≤	0.66	OK !!!
5	1.28E+07	16	2918	50	2884	4	300	0.09%	0.06	47495	1.5	0.244	1.27	0.31	201	804	15841	3286	34170	19126.57	51000	7930	0.41	≤	0.66	OK !!!
6	1.28E+07	16	2918	50	2884	4	300	0.09%	0.06	48371	1.5	0.244	1.28	0.31	201	804	15893	3286	34170	19178.20	51000	8177	0.43	≤	0.66	OK !!!
7	1.28E+07	16	2918	50	2884	4	300	0.09%	0.06	46143	1.3	0.250	1.26	0.32	201	804	16118	3286	34170	19403.97	51000	8160	0.42	≤	0.66	OK !!!
8	1.28E+07	16	2918	50	2884	4	300	0.09%	0.06	35347	1.5	0.238	1.20	0.29	201	804	14624	3286	34170	17909.16	51000	4082	0.23	≤	0.66	OK !!!

Table 8.15. Column Shear Force Capacity in Transversal Direction (DD1)

Axis	A _c [mm ²]	φ _s	d	d'	h ₀ [mm]	n	s [mm]	ρ	α	N _k [kN]	μ _d	k _{c1}	k _{c2}	k _c	A _{sp} [mm ²]	A _{swx} [mm ²]	V _c [kN]	V _s [kN]	V _{s,max} [kN]	V _n [kN]	V _{n,max} [kN]	V _d [kN]	V _d /V _n ≤ 2/3			Check
																							0.17	≤	0.66	
1	1.28E+07	16	6918	50	6884	4	300	0.18%	0.12	27398	1.0	0.25	1.16	0.29	201.06	804.25	14750.05	7789.30	34170	22539.35	51000	3808	0.17	≤	0.66	OK !!!
2	1.28E+07	16	6918	50	6884	4	300	0.18%	0.12	33770	1.3	0.25	1.19	0.30	201.06	804.25	15215.20	7789.30	34170	23004.5	51000	6326	0.28	≤	0.66	OK !!!
3	1.28E+07	16	6918	50	6884	4	300	0.18%	0.12	38110	1.9	0.25	1.22	0.30	201.06	804.25	15532.04	7789.30	34170	23321.3	51000	7131	0.31	≤	0.66	OK !!!
4	1.28E+07	16	6918	50	6884	4	300	0.18%	0.12	44255	1.3	0.25	1.25	0.31	201.06	804.25	15980.61	7789.30	34170	23769.9	51000	8496	0.36	≤	0.66	OK !!!
5	1.28E+07	16	6918	50	6884	4	300	0.18%	0.12	47495	1.3	0.25	1.27	0.32	201.06	804.25	16217.14	7789.30	34170	24006.4	51000	10329	0.43	≤	0.66	OK !!!
6	1.28E+07	16	6918	50	6884	4	300	0.18%	0.12	48371	1.1	0.25	1.28	0.32	201.06	804.25	16281.05	7789.30	34170	24070.4	51000	6736	0.28	≤	0.66	OK !!!
7	1.28E+07	16	6918	50	6884	4	300	0.18%	0.12	46143	1.0	0.25	1.26	0.32	201.06	804.25	16118.45	7789.30	34170	23907.8	51000	5962	0.25	≤	0.66	OK !!!
8	1.28E+07	16	6918	50	6884	4	300	0.18%	0.12	35347	1.1	0.25	1.20	0.30	201.06	804.25	15330.35	7789.30	34170	23119.7	51000	5959	0.26	≤	0.66	OK !!!

Table 8.16. Column Shear Force Capacity in Longitudinal Direction (DD2a)

Axis	A_c [mm ²]	ϕ_s	d	d'	h_0 [mm]	n	s [mm]	ρ	α	N_k [kN]	μ_d	k_{c1}	k_{c2}	k_c	A_{sp} [mm ²]	A_{swx} [mm ²]	V_c [kN]	V_s [kN]	$V_{s,max}$ [kN]	V_n [kN]	$V_{n,max}$ [kN]	V_d [kN]	$V_d/V_n \leq 2/3$			Check
1	1.28E+07	16	2918	50	2884	4	300	0.09%	0.06	27398	1.0	0.25	1.16	0.29	201.06	804.25	14750.05	3285.51	34170	18035.57	51000	960.84	0.05	≤	0.66	OK !!!
2	1.28E+07	16	2918	50	2884	4	300	0.09%	0.06	33770	1.0	0.25	1.19	0.30	201.06	804.25	15215.20	3285.51	34170	18500.7	51000	1063.8	0.06	≤	0.66	OK !!!
3	1.28E+07	16	2918	50	2884	4	300	0.09%	0.06	38110	1.0	0.25	1.22	0.30	201.06	804.25	15532.04	3285.51	34170	18817.6	51000	1829.9	0.10	≤	0.66	OK !!!
4	1.28E+07	16	2918	50	2884	4	300	0.09%	0.06	44255	1.0	0.25	1.25	0.31	201.06	804.25	15980.61	3285.51	34170	19266.1	51000	2515.5	0.13	≤	0.66	OK !!!
5	1.28E+07	16	2918	50	2884	4	300	0.09%	0.06	47495	1.0	0.25	1.27	0.32	201.06	804.25	16217.14	3285.51	34170	19502.6	51000	2616.4	0.13	≤	0.66	OK !!!
6	1.28E+07	16	2918	50	2884	4	300	0.09%	0.06	48371	1.0	0.25	1.28	0.32	201.06	804.25	16281.05	3285.51	34170	19566.6	51000	2952.3	0.15	≤	0.66	OK !!!
7	1.28E+07	16	2918	50	2884	4	300	0.09%	0.06	46143	1.0	0.25	1.26	0.32	201.06	804.25	16118.45	3285.51	34170	19404	51000	1909.7	0.10	≤	0.66	OK !!!
8	1.28E+07	16	2918	50	2884	4	300	0.09%	0.06	35347	1.0	0.25	1.20	0.30	201.06	804.25	15330.35	3285.51	34170	18615.9	51000	2777.1	0.15	≤	0.66	OK !!!

Table 8.17. Column Shear Force Capacity in Transversal Direction (DD2a)

Axis	A _c [mm ²]	φ _s	d	d'	h ₀ [mm]	n	s [mm]	ρ	α	N _k [kN]	μ _d	k _{c1}	k _{c2}	k _c	A _{sp} [mm ²]	A _{swx} [mm ²]	V _c [kN]	V _s [kN]	V _{s,max} [kN]	V _n [kN]	V _{n,max} [kN]	V _d [kN]	V _d /V _n ≤ 2/3			Check
																							0.06	≤	0.66	
1	1.28E+07	16	6918	50	6884	4	300	0.18%	0.12	27398	1.0	0.25	1.16	0.29	201	804	14750	7789	34170	22539	51000	1355	0.06	≤	0.66	OK !!!
2	1.28E+07	16	6918	50	6884	4	300	0.18%	0.12	33770	1.0	0.25	1.19	0.30	201	804	15215	7789	34170	23005	51000	2283	0.10	≤	0.66	OK !!!
3	1.28E+07	16	6918	50	6884	4	300	0.18%	0.12	38110	1.0	0.25	1.22	0.30	201	804	15532	7789	34170	23321	51000	2682	0.12	≤	0.66	OK !!!
4	1.28E+07	16	6918	50	6884	4	300	0.18%	0.12	44255	1.0	0.25	1.25	0.31	201	804	15981	7789	34170	23770	51000	2950	0.12	≤	0.66	OK !!!
5	1.28E+07	16	6918	50	6884	4	300	0.18%	0.12	47495	1.0	0.25	1.27	0.32	201	804	16217	7789	34170	24006	51000	3652	0.15	≤	0.66	OK !!!
6	1.28E+07	16	6918	50	6884	4	300	0.18%	0.12	48371	1.0	0.25	1.28	0.32	201	804	16281	7789	34170	24070	51000	2059	0.09	≤	0.66	OK !!!
7	1.28E+07	16	6918	50	6884	4	300	0.18%	0.12	46143	1.0	0.25	1.26	0.32	201	804	16118	7789	34170	23908	51000	1980	0.08	≤	0.66	OK !!!
8	1.28E+07	16	6918	50	6884	4	300	0.18%	0.12	35347	1.0	0.25	1.20	0.30	201	804	15330	7789	34170	23120	51000	2389	0.10	≤	0.66	OK !!!

8.6.7. Longitudinal and Transversal Reinforcement Requirement for Columns

The minimum longitudinal reinforcement ratio in bridge columns is defined by Equation (8.16) in TBEC-2020 Section 8.3.1.1.

$$A_s \geq 0.01A_c \quad (8.16)$$

The area of longitudinal reinforcement of Pier-3 is calculated in Section 4, Table 4.1 and Table 4.2.

$$A_s = 1463.73 \text{ cm}^2 \geq 0.01A_s = 0.01 \times 127500 \text{ cm}^2 = 1275 \text{ cm}^2$$

$$A_s = 932.93 \text{ cm}^2 \leq 0.01A_s = 0.01 \times 127500 \text{ cm}^2 = 1275 \text{ cm}^2$$

The Pier-3 column longitudinal reinforcement is not satisfy the minimum longitudinal reinforcement requirement of TBEC-2020 8.3.2.2b(Eq.8.17)

In TBEC-2020, the requirement for rectangular column transverse reinforcement is given as:

$$\frac{A_{swx}}{h_0s} \geq 0.30 \frac{f_{ck}}{f_{ywk}} \left(\frac{A_c}{A_{ck}} - 1 \right) \quad ; \quad \frac{A_{swy}}{b_0s} \geq 0.30 \frac{f_{ck}}{f_{ywk}} \left(\frac{A_c}{A_{ck}} - 1 \right) \quad (8.17)$$

TBEC-2020 - 8.3.2

$$A_{swx} = 0.30h_0s \frac{f_{ck}}{f_{ywk}} \left(\frac{A_c}{A_{ck}} - 1 \right)$$

Longitudinal

s	=	300	mm	Vertical spacing of hoops -stirrups
h _o	=	2884	mm	Length of column core area
f _{ck}	=	25	Mpa	Compressive Strength of Concrete
f _{ywk}	=	420	mm ²	Yield strength of transverse reinforcement
A _c	=	1E+07	mm ²	Gross area of column
A _{ck}	=	1E+07	mm ²	Area of column core
A _{swx}	≥	<u>2826.81</u>	mm ²	Exist 4Ø16 = 804 mm ² NOT O.K

Transverse

s	=	300	mm	Vertical spacing of hoops -stirrups
h _o	=	6884	mm	Length of column core area
f _{ck}	=	25	Mpa	Compressive Strength of Concrete
f _{ywk}	=	420	mm ²	Yield strength of transverse reinforcement
A _c	=	1E+07	mm ²	Gross area of column
A _{ck}	=	1E+07	mm ²	Area of column core

$A_{swx} \geq \underline{6747.50} \text{ mm}^2$ Exist 4Ø16 = 804 mm² **NOT O.K**

Molla Gürani Viaduct column reinforcements do not meet the minimum longitudinal and transverse reinforcement requirements specified in the TBEC-2020.

8.6.8. Shear Force Strength of Transverse Reinforcement



Figure 8.17. Shear Forces on Shear Key at Abutments

Table 8.18. Shear Forces on Shear Keys (DD1)

	Shear Forces on Shear Keys -DD1 Earthquake Ground Motion Level						
	RSN15	RSN731	RSN838	RSN1166	RSN1206	RSN1762	RSN3747
DD1_X	10660	12530	9922	15710	7905	7889	9215
DD1_Y	7907	9656	9146	7051	9931	11320	7208
Avarage	9284	11093	9534	11381	8918	9605	8212
V=	9718. kN						

Table 8.19. Shear Forces on Shear Keys (90° Rotated DD1)

Axis	Shear Forces on Shear Keys -90° Rotated DD1-Earthquake Ground Motion Level						
	RSN15	RSN731	RSN838	RSN1166	RSN1206	RSN1762	RSN3747
DD1_X	7676	9549	8278	16570	9409	11920	8331
DD1_Y	10660	12530	9977	7042	7970	7852	9238
Avarage	9168	11040	9128	11806	8690	9886	8785
V=	9953. kN						



Figure 8.18. Shear Deformations at Shear Keys of Molla Gürani Viaduct

The interface shear resistance is given in AASHTO LRFD Equation 5.8.4.1-3 as:

$$V_{ni} = cA_{cv} + \mu[A_{vf}f_y + P_c] \quad \text{AASHTO LRFD Eq. 5.8.4.1 - 3}$$

where :

- V_{ni} : Nominal shear resistance (kN)
- c : Cohesion factor (MPa)
- A_{cv} : Area of concrete engaged in shear transfer (mm^2)
- μ : Friction factor
- A_{vf} : Area of shear reinforcement crossing the shear plane (mm^2)
- f_y : Yield strength of reinforcement (ksi)
- P_c : Permanent net compressive force normal to the shear plane; if force is tensile, $P_c = 0.0$ (kip)

The values given in AASHTO LRFD Article 5.8.4.3 for the cohesion and friction factors are dependent upon how the two different concretes are placed (see Table 8.20).

Table 8.20. Cohesion and Friction Factors

Description	c (ksi)	μ	K1	K2 (ksi)
For normal weight concrete placed monolithically	0.4	1.4	0.25	1.5
For cast-in-place concrete slab on clean concrete girder surfaces, free of laitance with surface roughened to an amplitude of 0.25 in.				
For normal weight concrete	0.28	1	0.3	1.8
For lightweight concrete	0.28	1	0.3	1.3
For concrete placed against a clean concrete surface, free of laitance, but not intentionally roughened	0.075	0.6	0.2	0.8

- **DD1 Earthquake Level – Shear Resistance Capacity of Shear Keys**

$$V_{ui} = 9718 \text{ kN}$$

$$f_y = 420 \text{ MPa} \quad , \quad f_c = 35 \text{ Mpa} \quad , \quad c=0.28 \text{ ksi} = 1.92 \text{ MPa} \quad , \quad \mu=1 \quad , \quad P_c=0$$

$$A_{vf} = 18x \frac{25^2 x \pi}{4} + 9x \frac{16^2 x \pi}{4} = 10645.29 \text{ mm}^2 \quad (18\emptyset 25 + 9\emptyset 16)$$

$$A_{cv} = 600x1100 = 660000 \text{ mm}^2$$

$$V_{ni} = 1.92x660000 + 1[10645.29x420] = 5738221.8 \text{ N} = 5738.22 \text{ kN}$$

Upper limits on the strength are given in AASHTO LRFD Equations 5.8.4.1-4 and 5.8.4.1-5 as:

$$V_{ni} \leq K_1 f_c A_{cv} = 0.25 x 35 x 660000 = 5775 \text{ kN} \text{ or}$$

$$V_{ni} \leq K_2 A_{cv} = 10.34 x 660000 = 6824.4 \text{ kN}$$

$$V_{ri} = \Phi V_{ni} = 0.9x5738.22 = 5164.4 \text{ kN} < V_{ui} = 9718 \text{ kN}$$

$$V_{ri,max} = 5775 \text{ kN} < V_{ui} = 9718 \text{ kN}$$

As can be seen from the results, shear keys do not have sufficient strength to safely withstand the shear forces that will occur in DD1 earthquake level.

CHAPTER 9

9. CONCLUSION

9.1 Conclusion

Molla Gürani Viaduct has been serving for 35 years without interruption. During this period, viaduct elastomeric bearings were exposed to many external effects such as aging, seasonal temperature differences, friction-induced heating and so on. It has been verified as a result of performed Nonlinear Time History Analyses that elastomeric bearings will deform at a level that cannot fulfill their functions in a possible Istanbul earthquake. When the elastomeric bearings are torn and cannot fulfill their function, the superstructure will become free in the transverse direction and will come into contact with the support bases directly, causing undesirable deformations on both the pedestals and the lower part of the box girder. In addition, stresses will increase in shear keys that will try to prevent the movement of the superstructure in the transverse direction, and these elements, which already have insufficient strength, will be exposed to much larger deformations.

The transverse movement of the superstructure, which has become free in the piers, will be tried to be prevented by the shear keys at abutments in proportion to their capacities, while the longitudinal movement will be tried to be prevented by the tension rods(tie bars). The superstructure will deform in the transverse direction like a simple beam. The maximum deformation in the transverse direction will occur in a region close to the middle of the box girder. If the viaduct superstructures deform simultaneously and towards each other during an earthquake, there will be a possibility

of the superstructures colliding with each other. For all these reasons, first of all, deformations of elastomeric bearings have to be limited.

Shear keys that are found to have insufficient shear strength capacity have to be strengthened.

It has been understood by the analyzes that plastic deformation will occur in the tension rods(tie bars) in the event of an earthquake, and the levels of deformations that have occurred under service loads in the existing situation should be determined, and the necessary ones should be replaced or another device with the same function should be placed.

The superstructure displacement may not be alone a reason for the formation of high elastomer bearing displacement in longitudinal direction, also the movements of the columns themselves due to the column height possibly may considerable as one of the other reasons.

Since Molla Gürani Viaduct have continuous deck acts as a diaphragm in the longitudinal direction there is no possibility to fell down from the abutments.

The engineer who will take part in the evaluation of the earthquake performance of bridges and viaducts with structural irregularities such as the Molla Gürani Viaduct and the preparation of retrofitting projects should have sufficient knowledge and experience about how every change he will make on the analysis model and every choice he will make when choosing the input datas will affect the analysis results.

REFERENCES

- AASHTO. (1992). Standard Design Specifications for Highway Bridges. Washington, D.C: American Association of State Highway and Transportation Officials.
- Ady Aviram, Kevin R. Mackie, and Božidar Stojadinović. (August 2008). PEER 2008/03 Guidelines for Nonlinear Analysis of Bridge Structures in California. California: Pacific Earthquake Engineering Research Center (PEER).
- Arslanboğan, E. (2010). Seismic Evaluation and Retrofit of an Existing Reinforced Concrete School Building in Hadjidimovo. Unpublished Master Thesis, University of Architecture, Civil Engineering and Geodesy, Structural Engineering, Sofia.
- Chopra, A. K. (1995). Dynamics of Structures : Theory and Applications to Earthquake Engineering.
- Institute, A. P. (December, 2005). API Recommended Practice 2A-WSD Planning, Designing, and Constructing Fixed Offshore Platforms—Working Stress Design (21 th b.). Washington, D.C.: American Petroleum Institute.
- J. B. Mander, M. J. N. Priestley, and R. Park, Fellow, ASCE. (1988, August). Theoretical Stress-Strain Model. Journal of Structural Engineering, 1-23.
- M. J. N. Priestly, F. Sieble, G. M. Calvi. (1996). Seismic Design and Retrofit of Bridges. New York: John Wiley & Sons, Inc.
- (TBEC- 2020). Turkey Bridge Earthquake Code. Ankara: Disaster and Emergency Management Presidency , AFAD.
- (TBDY-2018). Turkish Earthquake Code (Specification For Structures To Be Built in Disaster Areas). Ankara: Disaster and Emergency Management Presidency, AFAD .

APPENDICES

APPENDIX A : EARTHQUAKE RECORDS

In this appendix ;

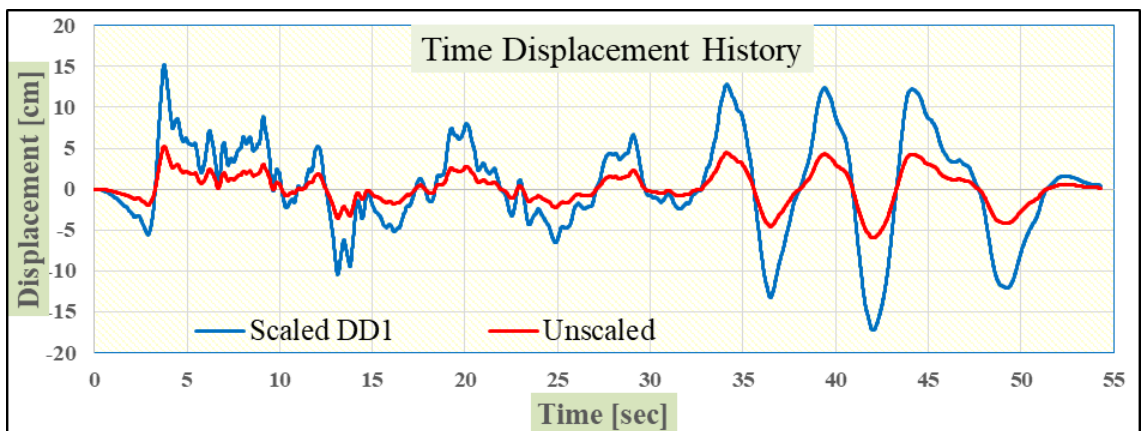
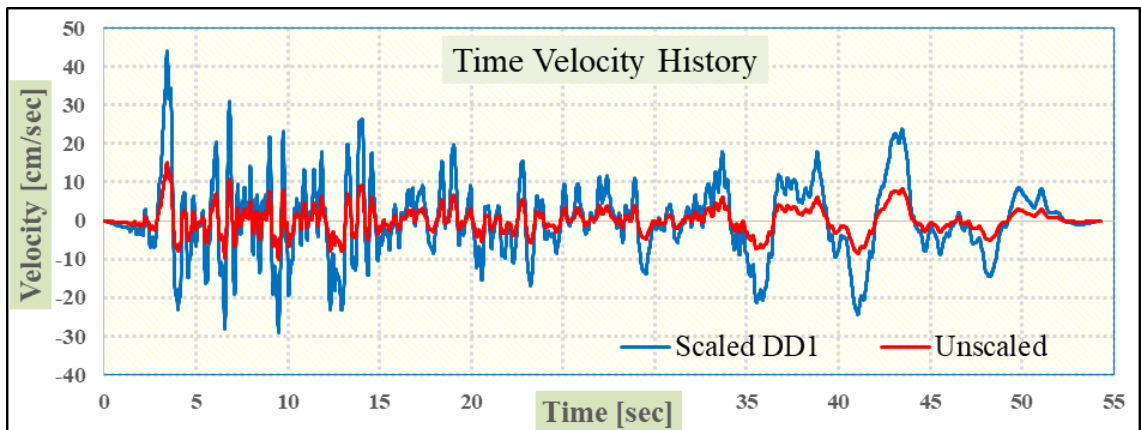
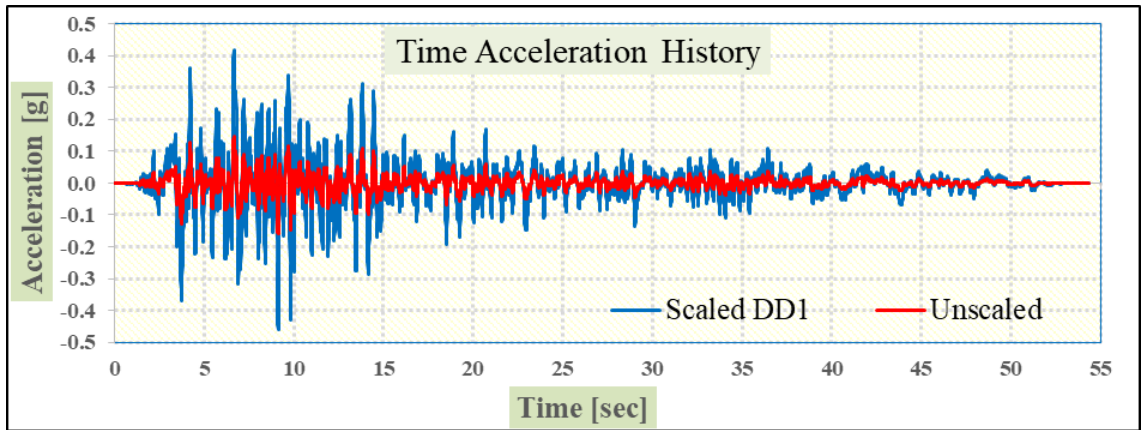
- Earthquake ground motion records time series
- Scaled earthquake ground motion records time series
- Response Spectrums
- Scaled Response Spectrums
- Avarage of SRSS Response Spectrums

of the Earthquake Ground Motion sets used in Nonliner Time History Analysis were given.

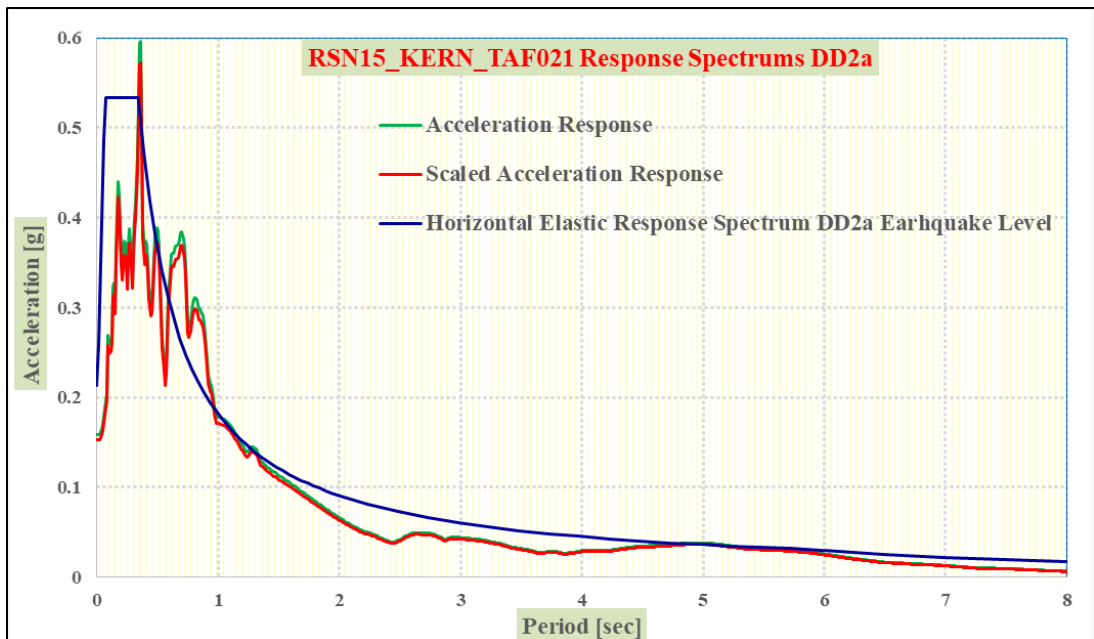
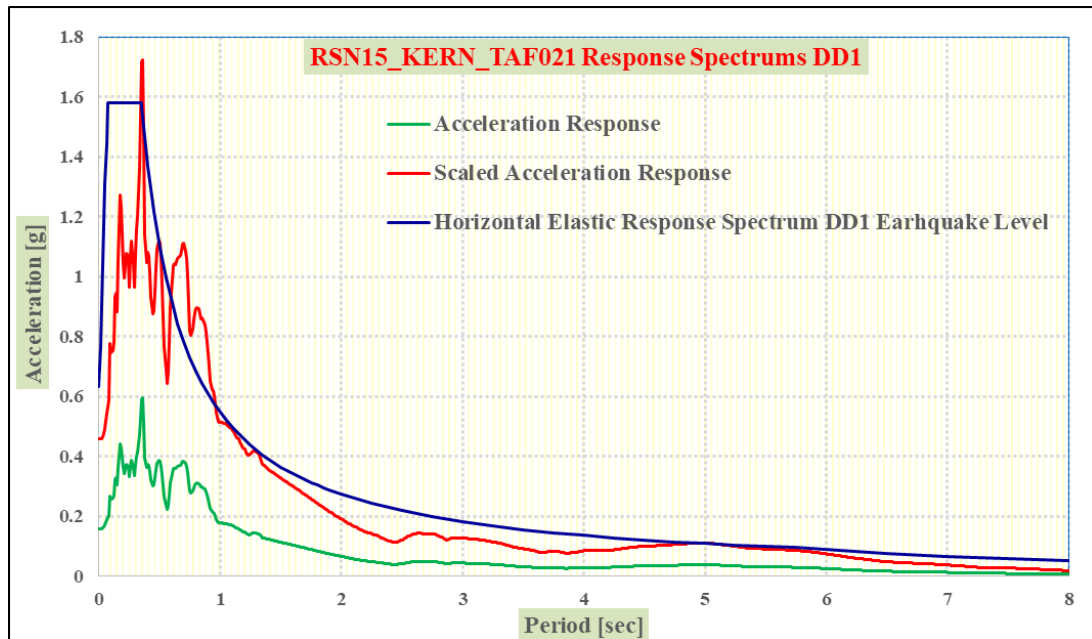
RNS	Earthquake Name	Year	Moment Magnitude	Mechanism	Epicentral Distance	Closest Distance
15	Kern County	1952	7.36	Reverse	38.42	38.89
731	Loma Prieta	1989	6.93	Reverse Oblique	27.47	41.88
838	Landers	1992	7.28	Strike Slip	41.71	34.86
1166	Kocaeli_Turkey	1999	7.51	Strike Slip	29.22	30.73
1206	Chi-Chi_Taiwan	1999	7.62	Reverse Oblique	41.81	28.17
1762	Hector Mine	1999	7.13	Strike Slip	34.86	43.05
3747	Cape Mendocino	1992	7.01	Reverse	30.73	31.46

A1. KERN COUNTY EARTHQUAKE

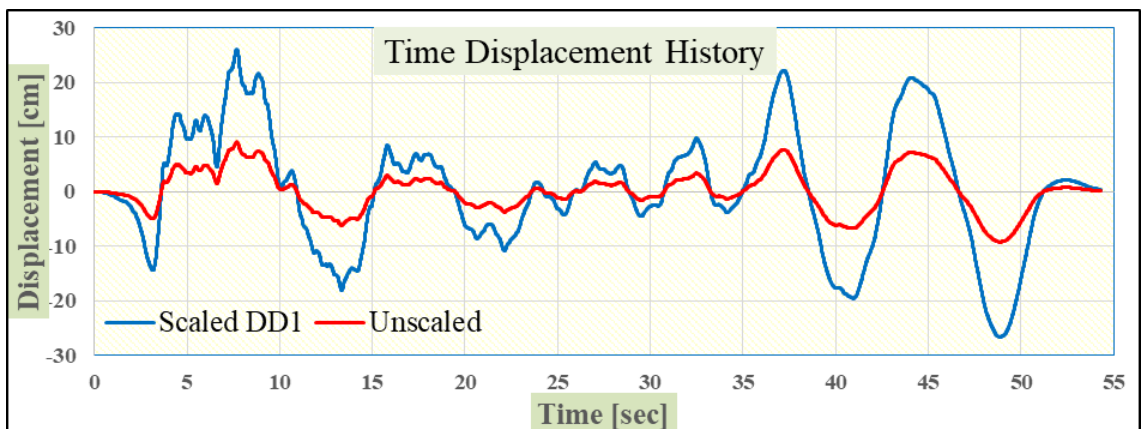
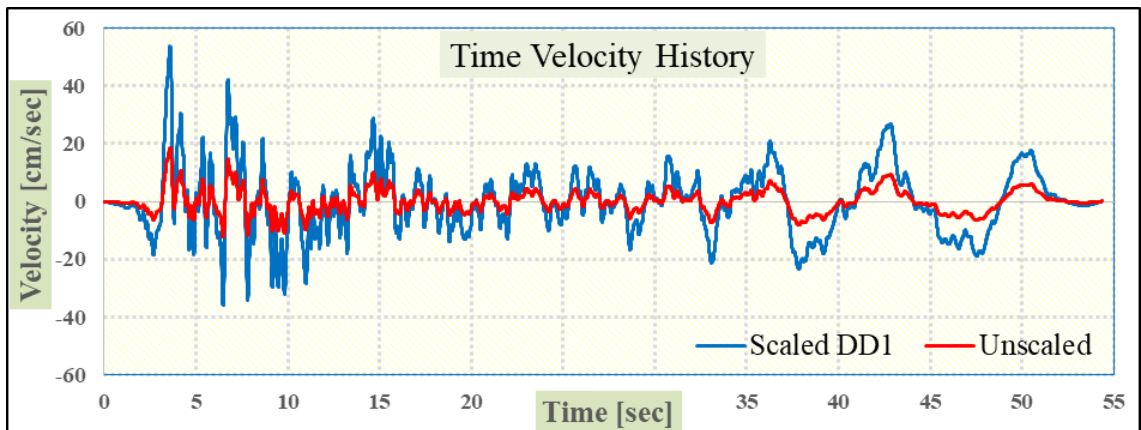
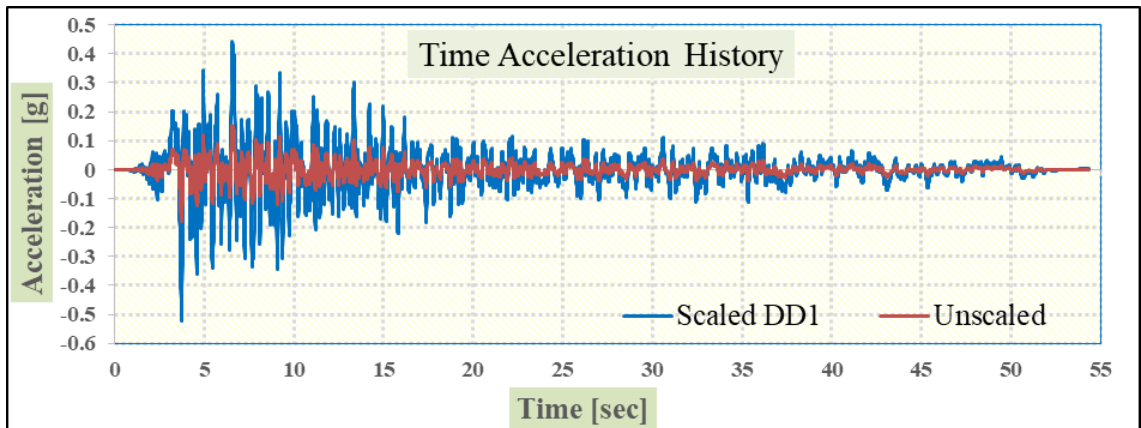
A1.1 RSN15_KERN_TAF021 Time Series



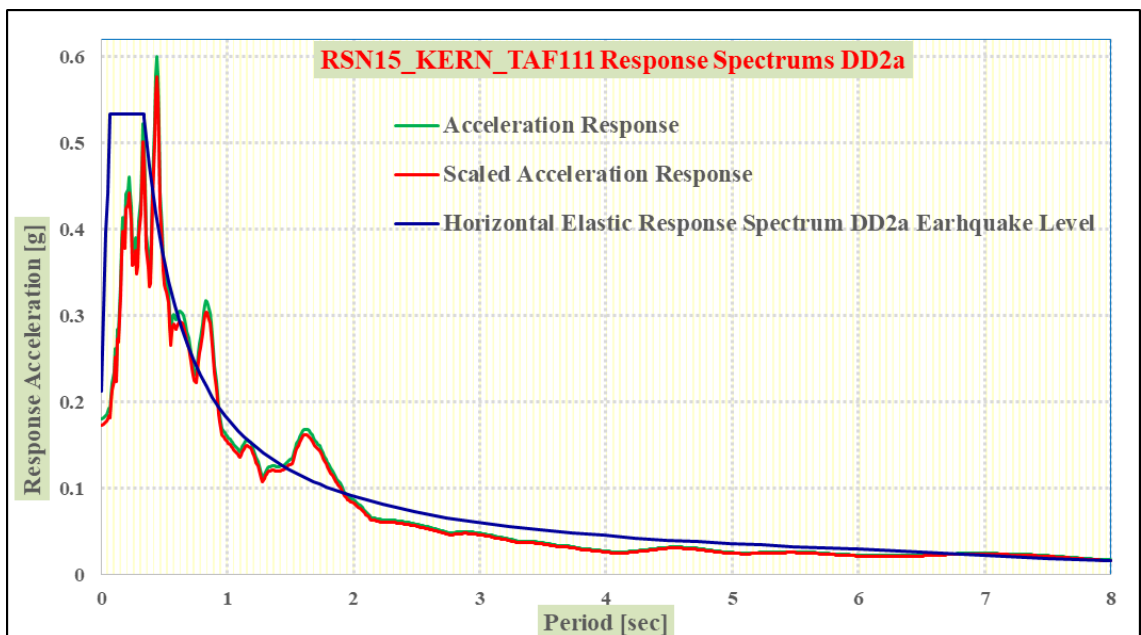
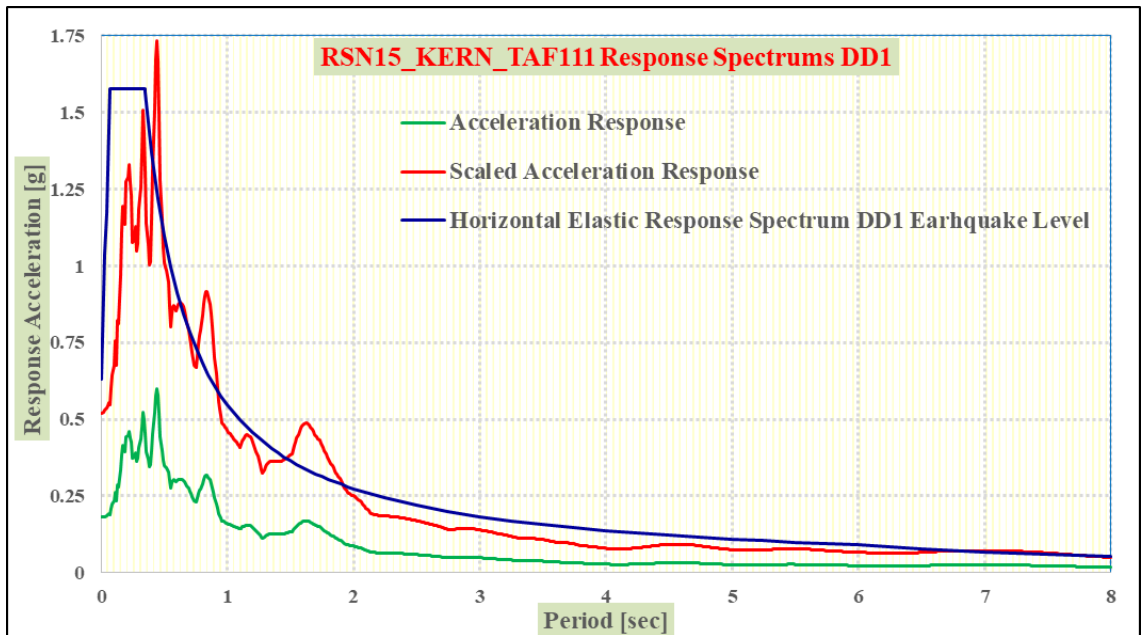
A1.2 RSN15_KERN_TAF021 Response Spectrums



A1.3 RSN15_KERN_TAF0111 Time Series

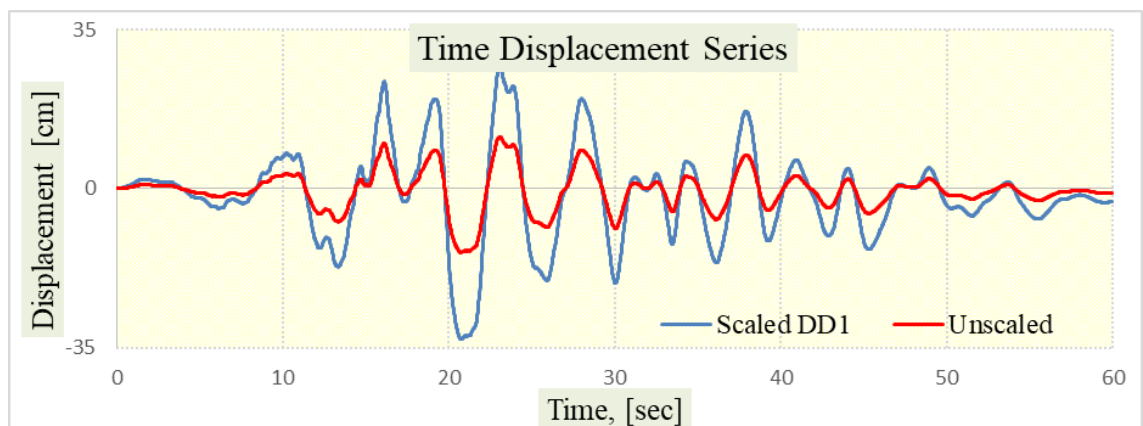
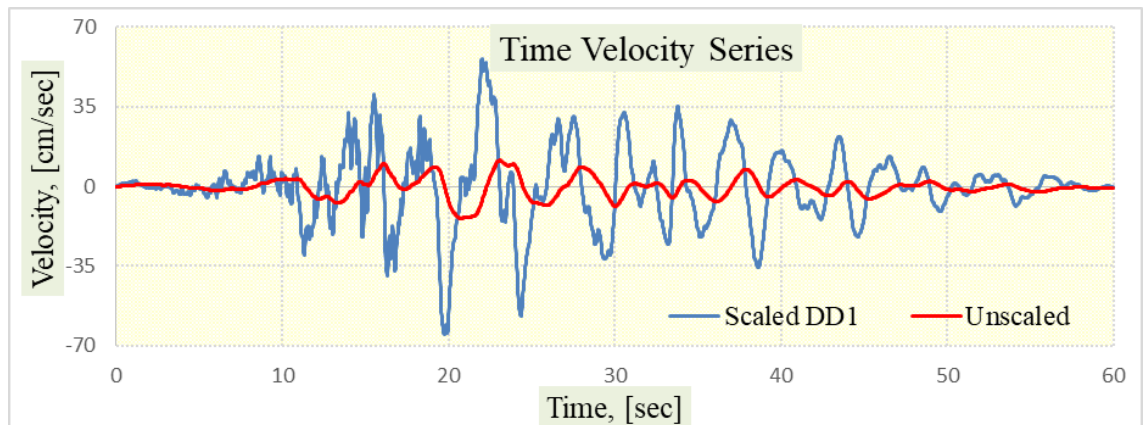
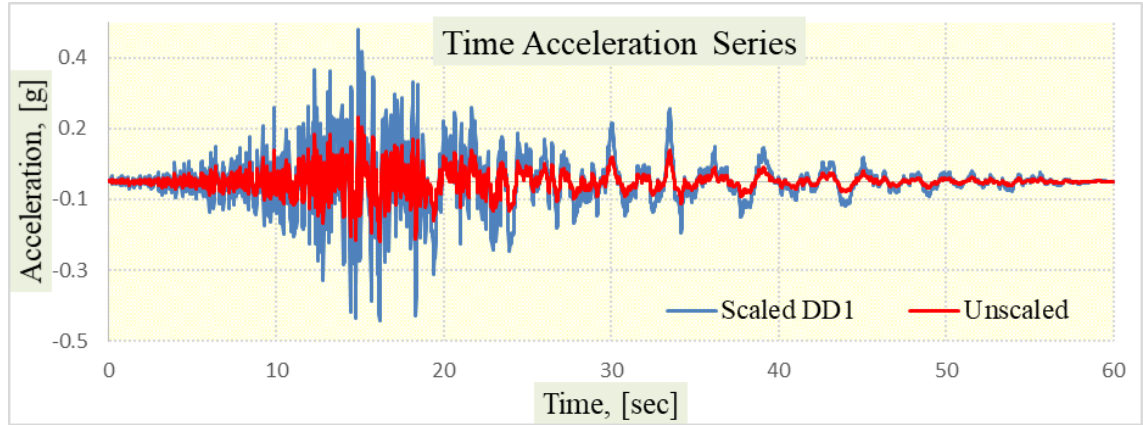


A1.4 RSN15_KERN_TAF0111 Response Spectrums

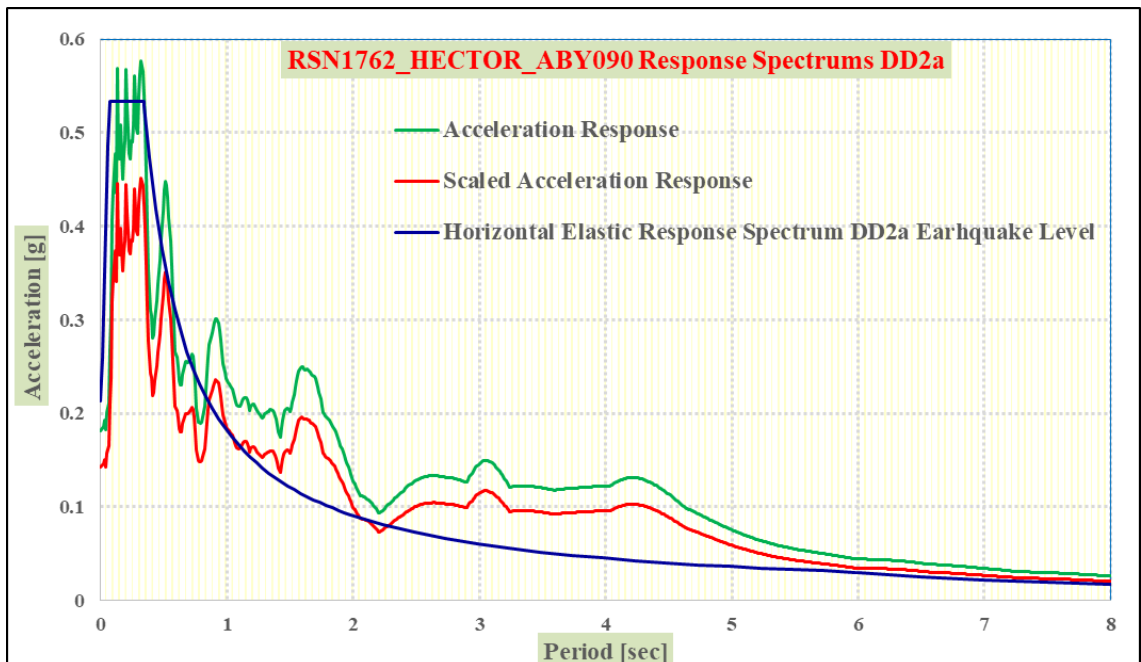
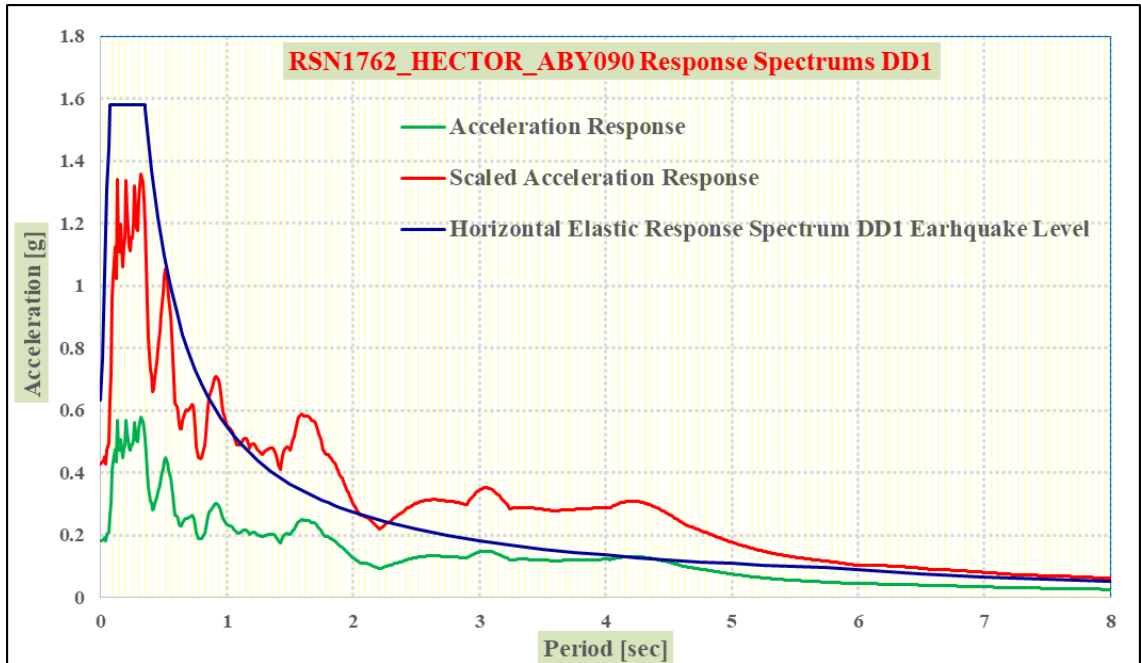


A2. HECTOR MINE EARTHQUAKE

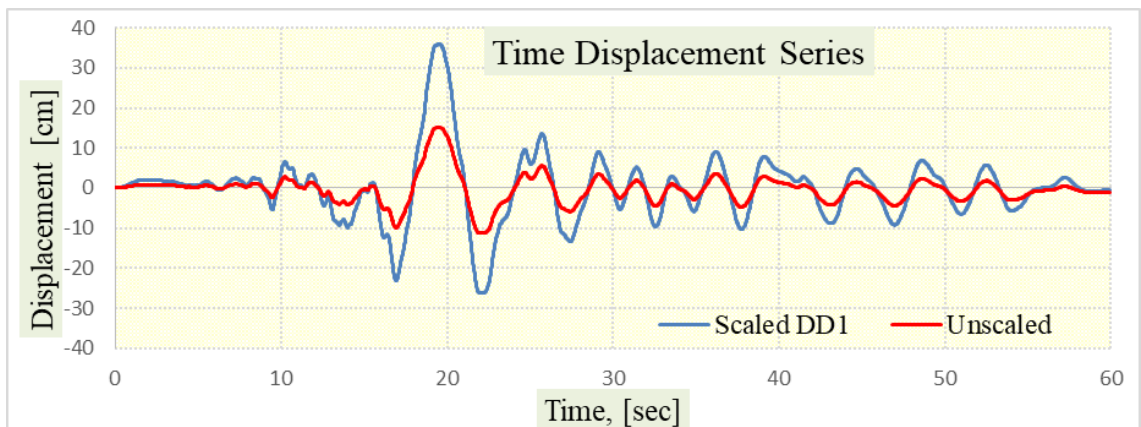
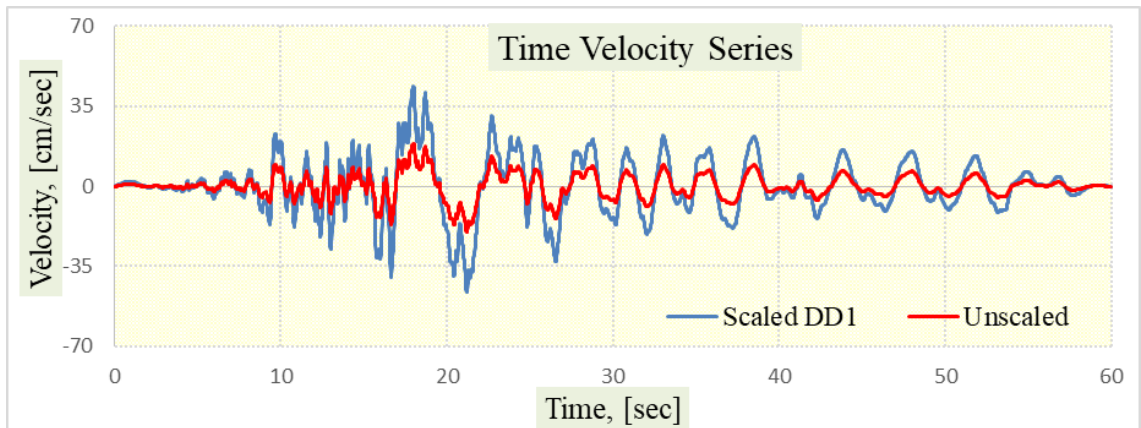
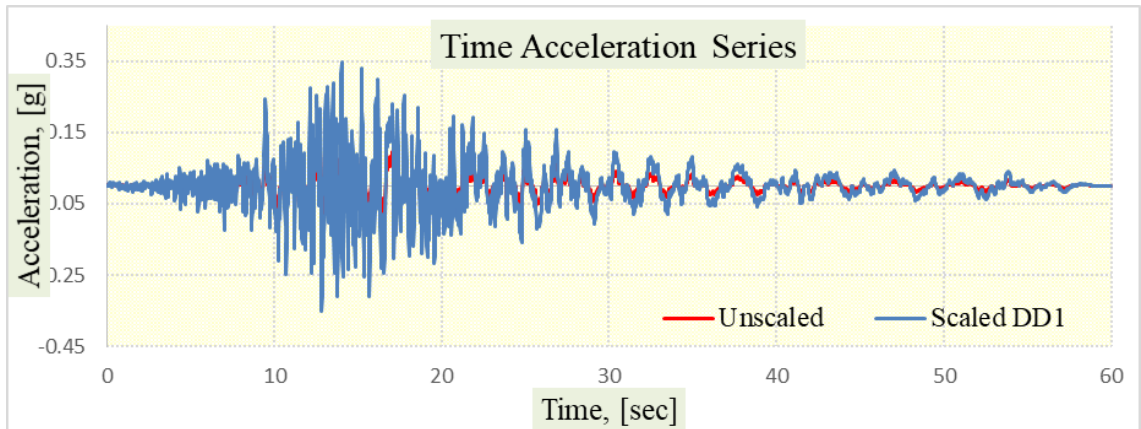
A2.1 RSN1762_HECTOR_ABY090 Time Series



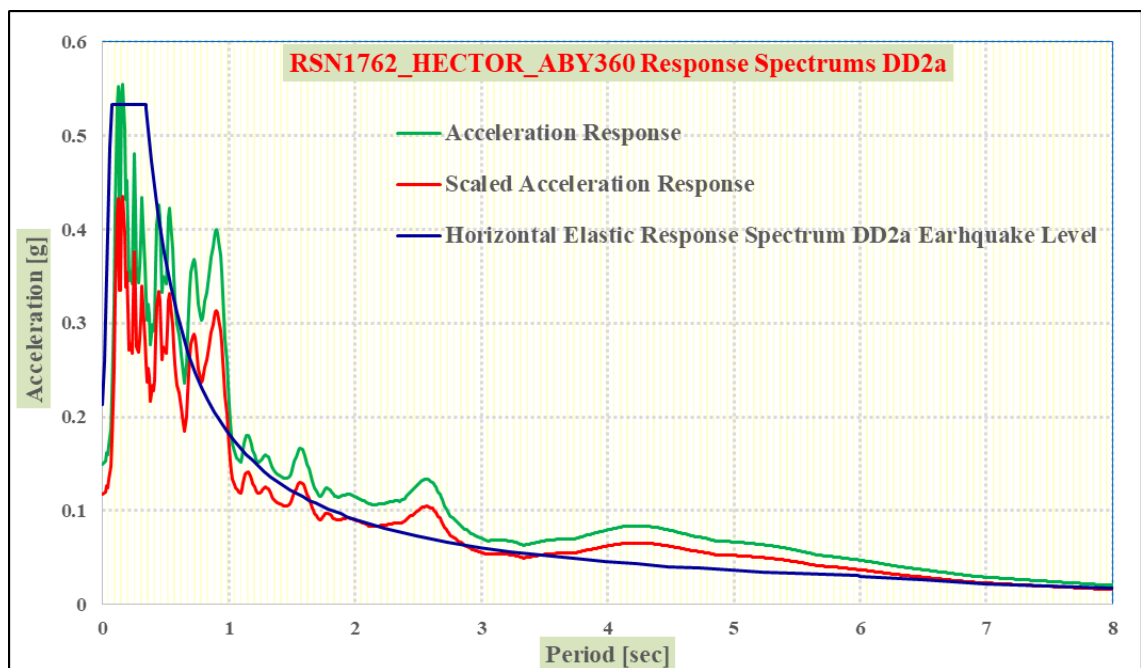
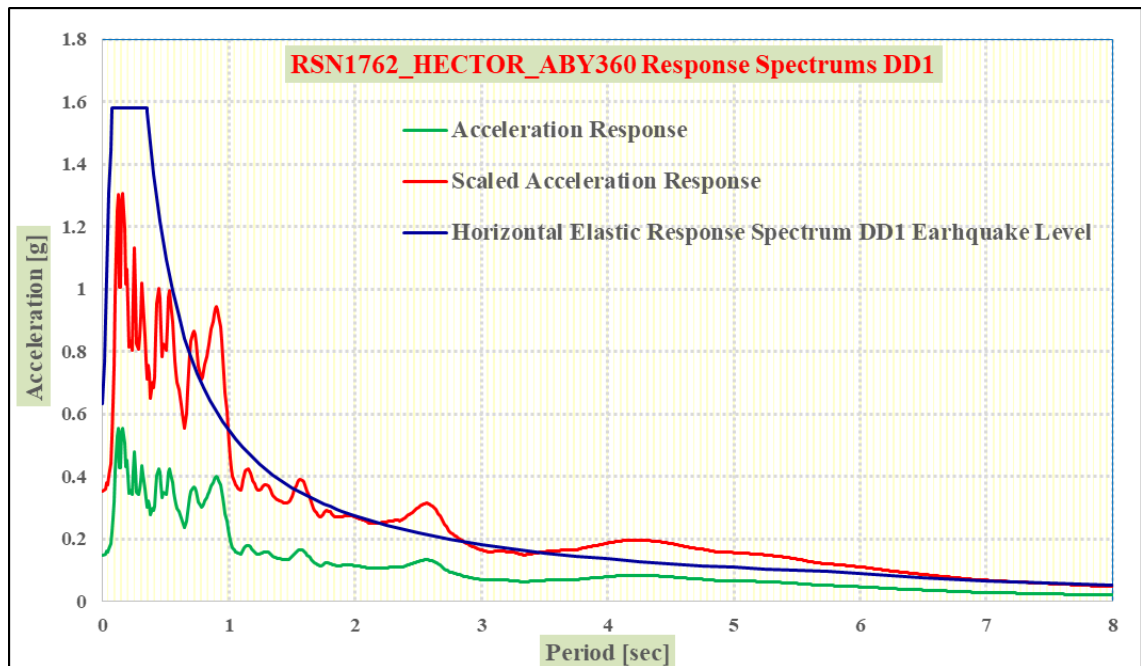
A2.2 RSN1762_HECTOR_ABY090 Response Spectrums



A2.3 RSN1762_HECTOR_ABY360 Time Series

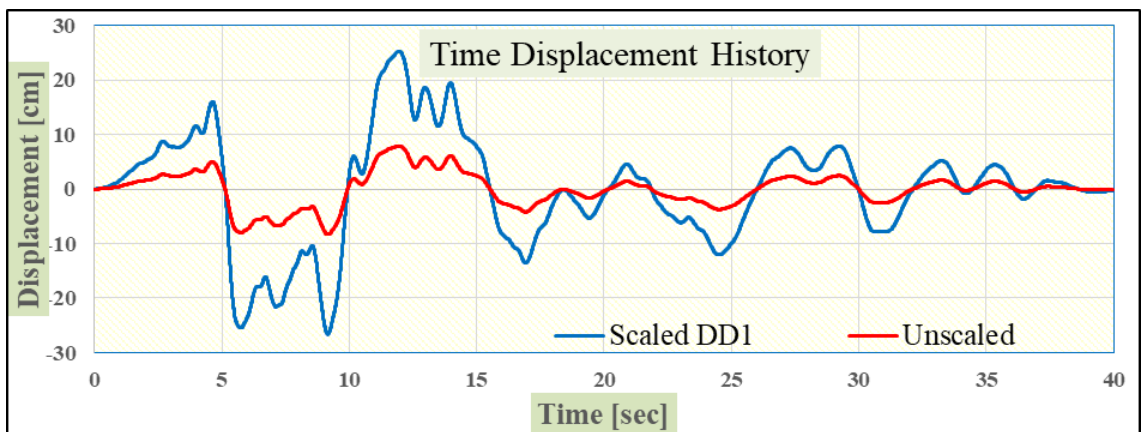
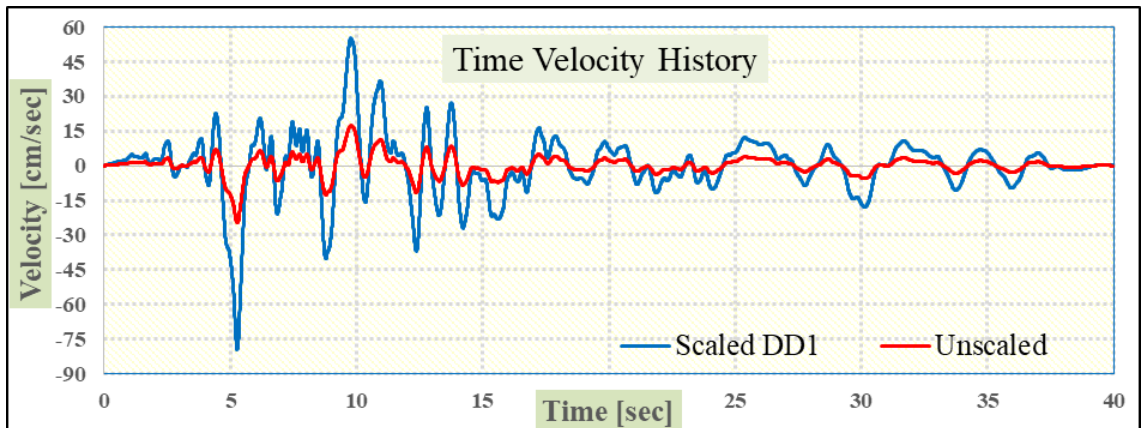
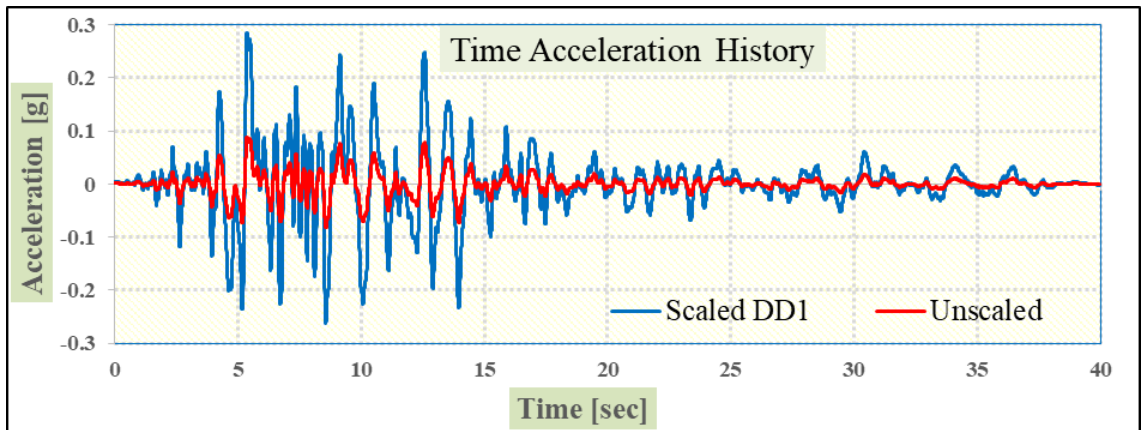


A2.4 RSN1762_HECTOR_ABY360 Response Spectrums

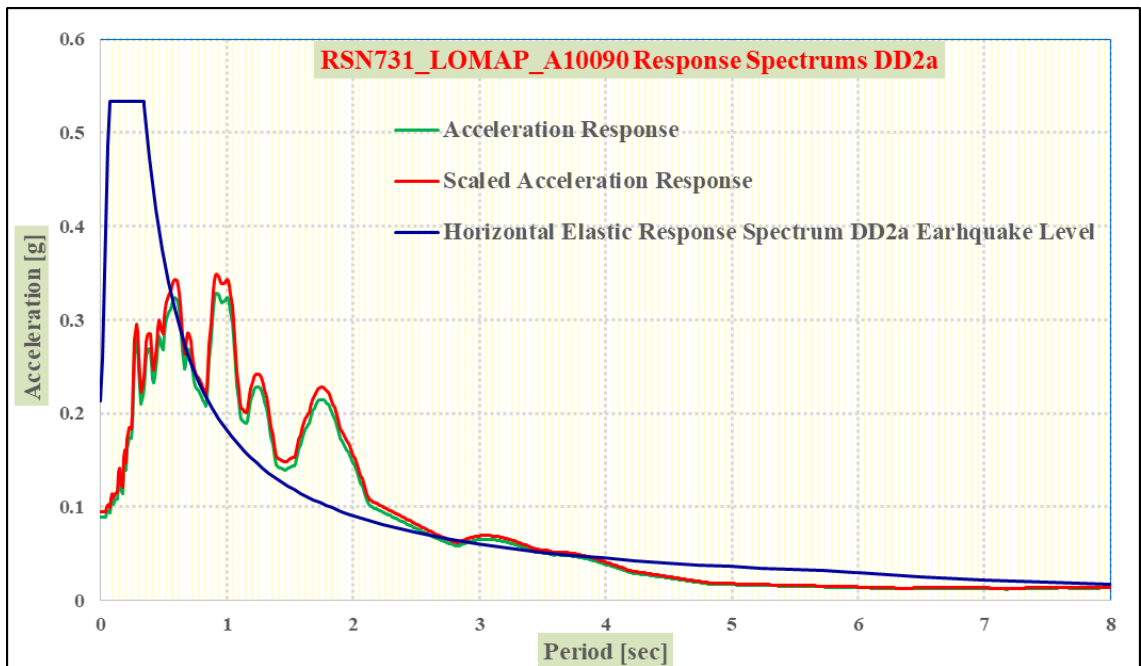
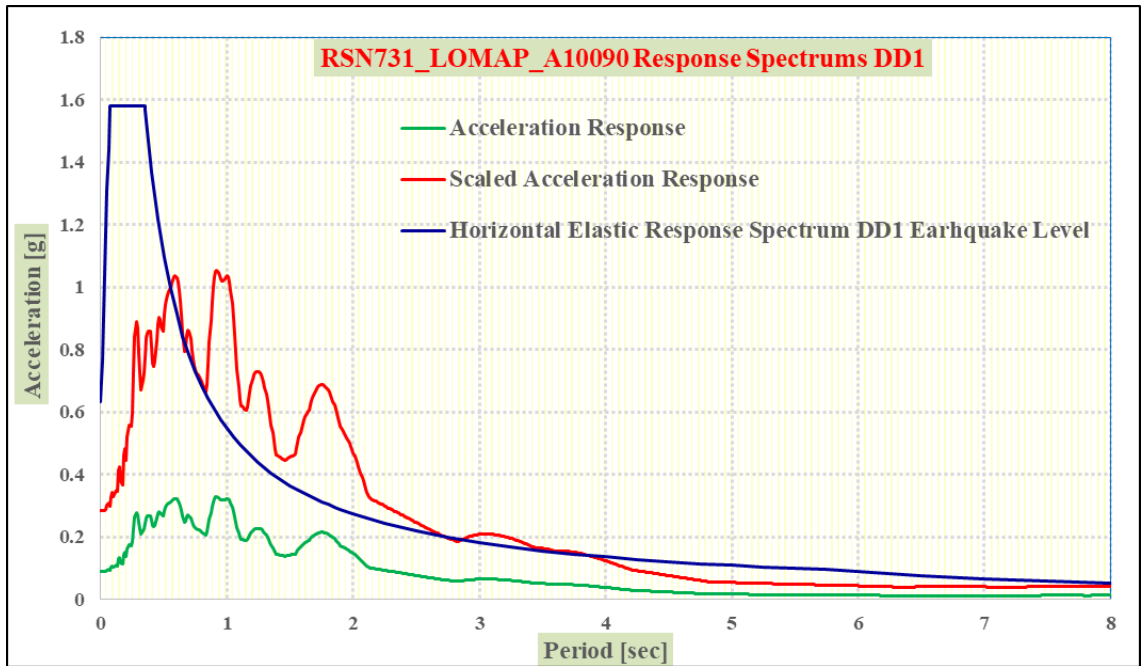


A3. LOMA PRIETO EARTHQUAKE

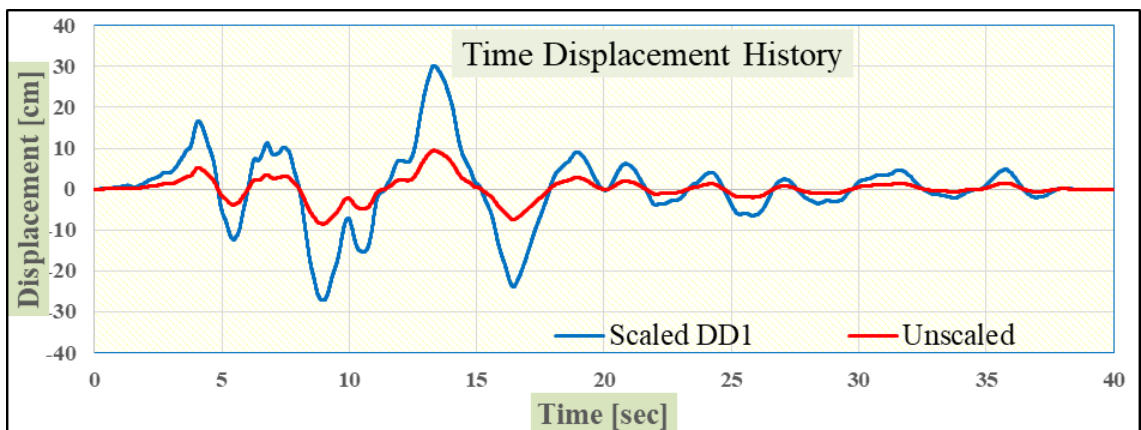
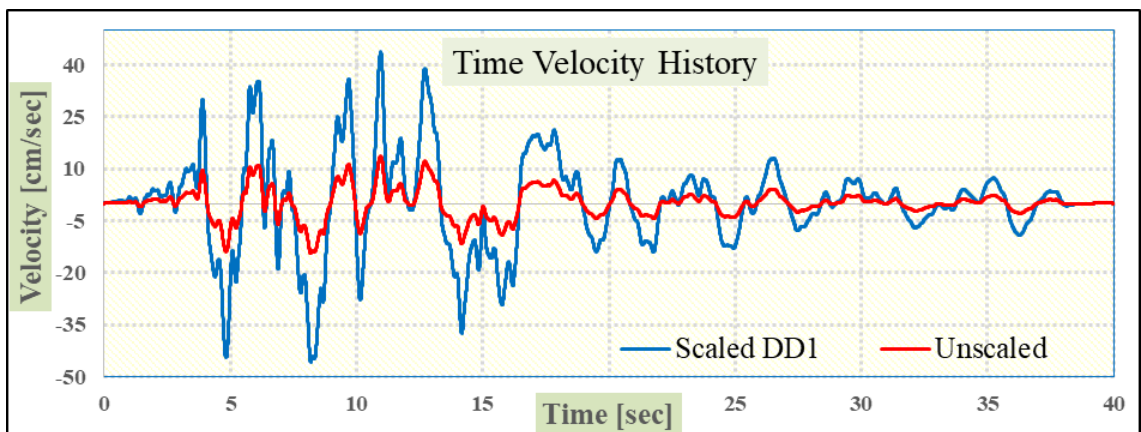
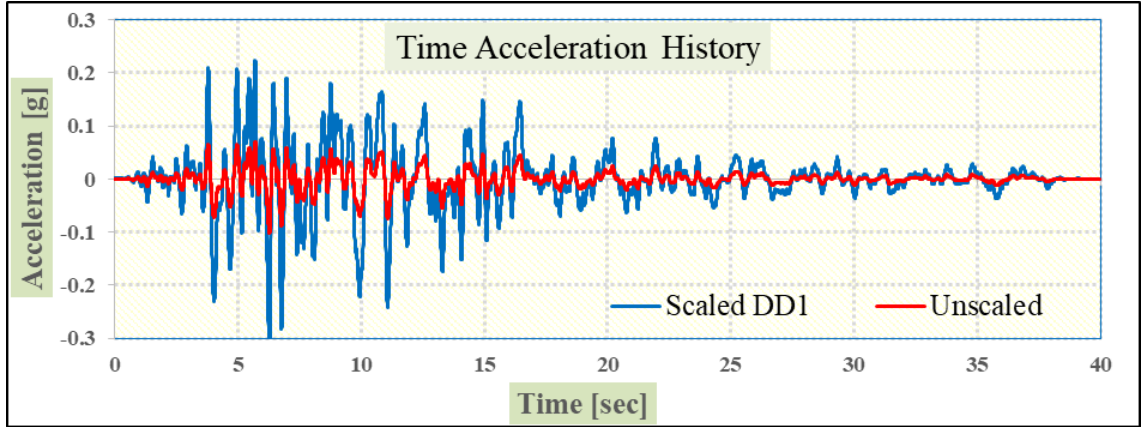
A3.1 RSN731_LOMAP_A10090 Time Series



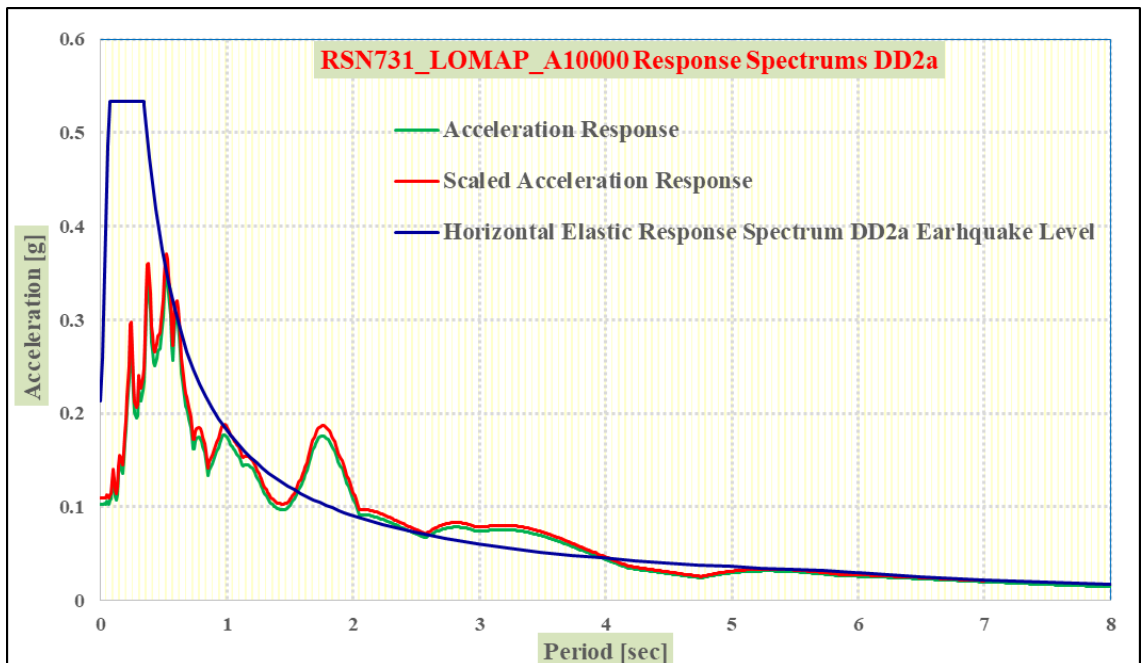
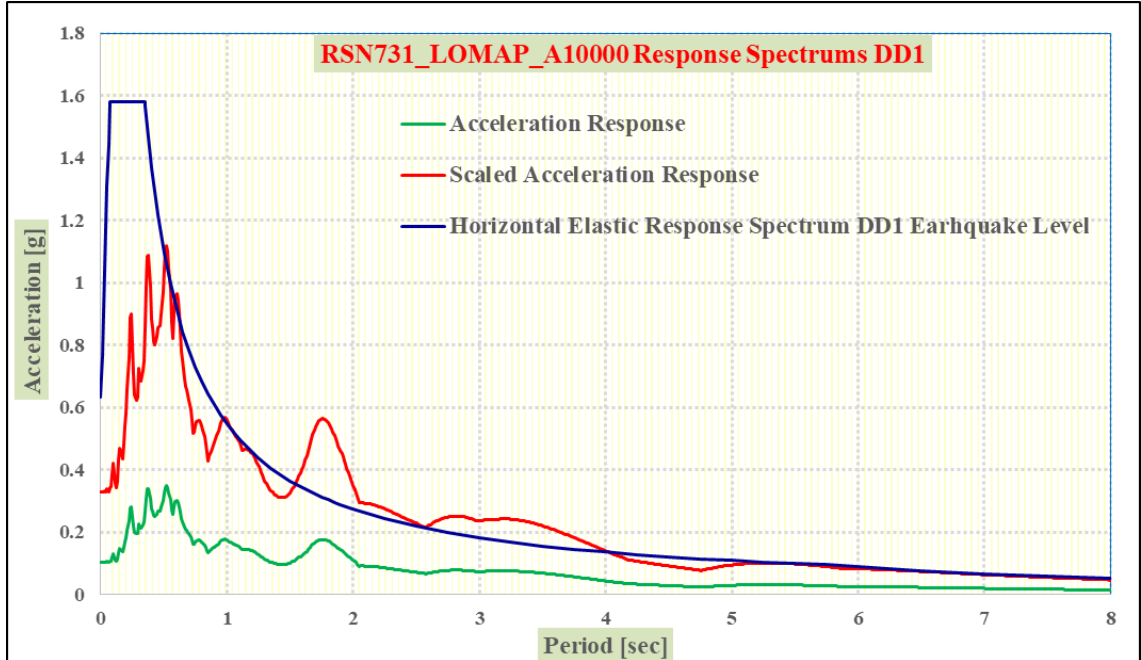
A3.2 RSN731_LOMAP_A10090 Response Spectrums



A3.3 RSN731_LOMAP_A10000 Time Series

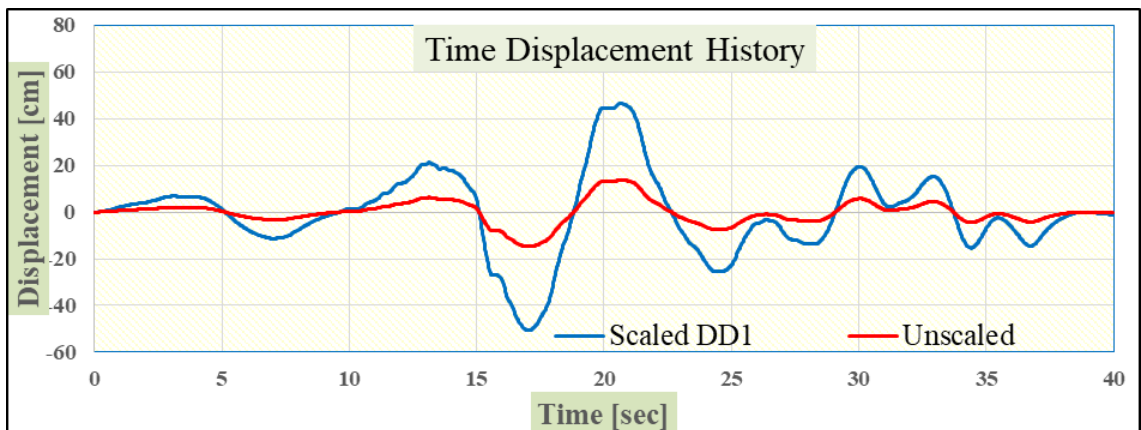
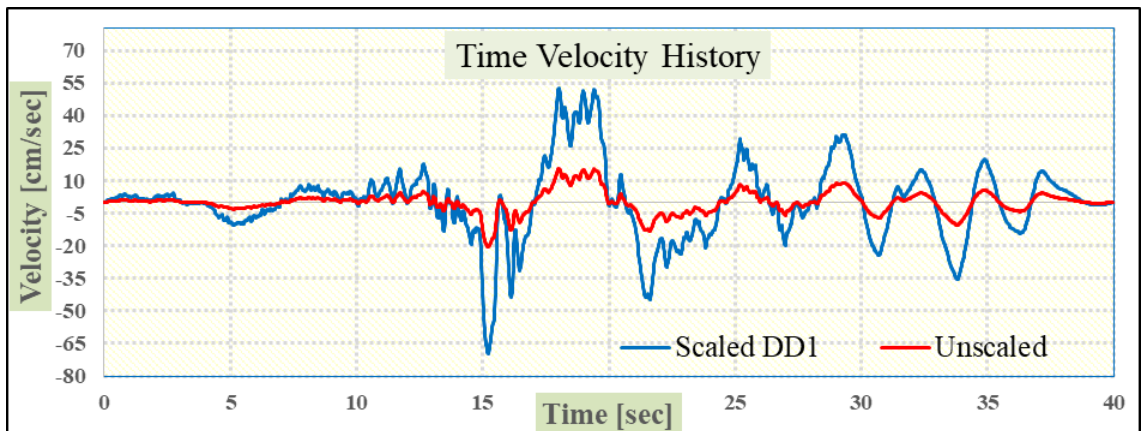
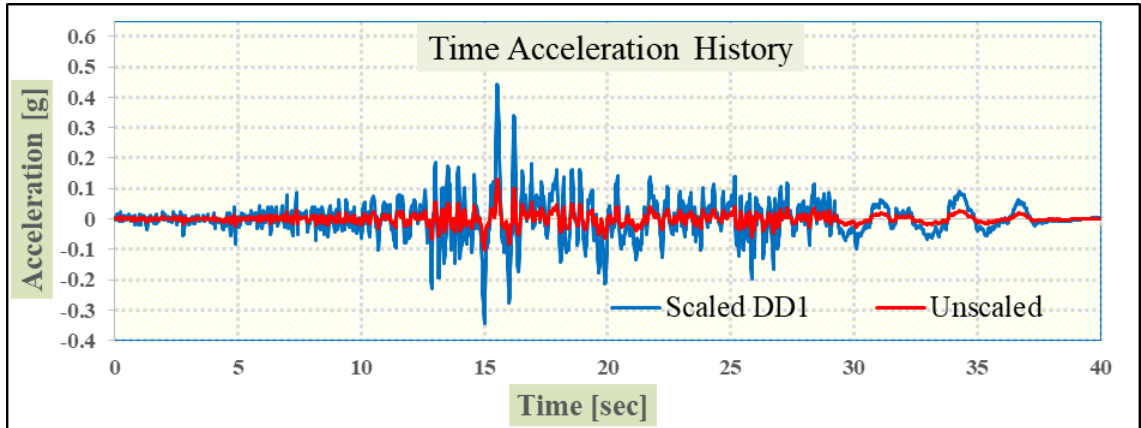


A3.4 RSN731_LOMAP_A10090 Response Spectrums

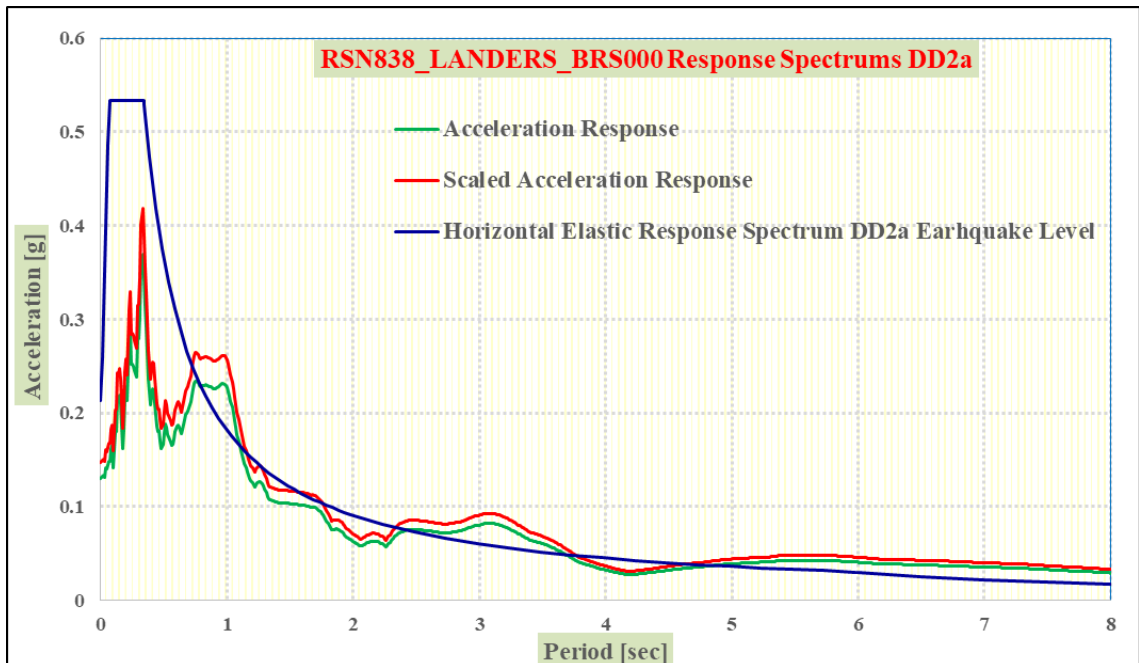
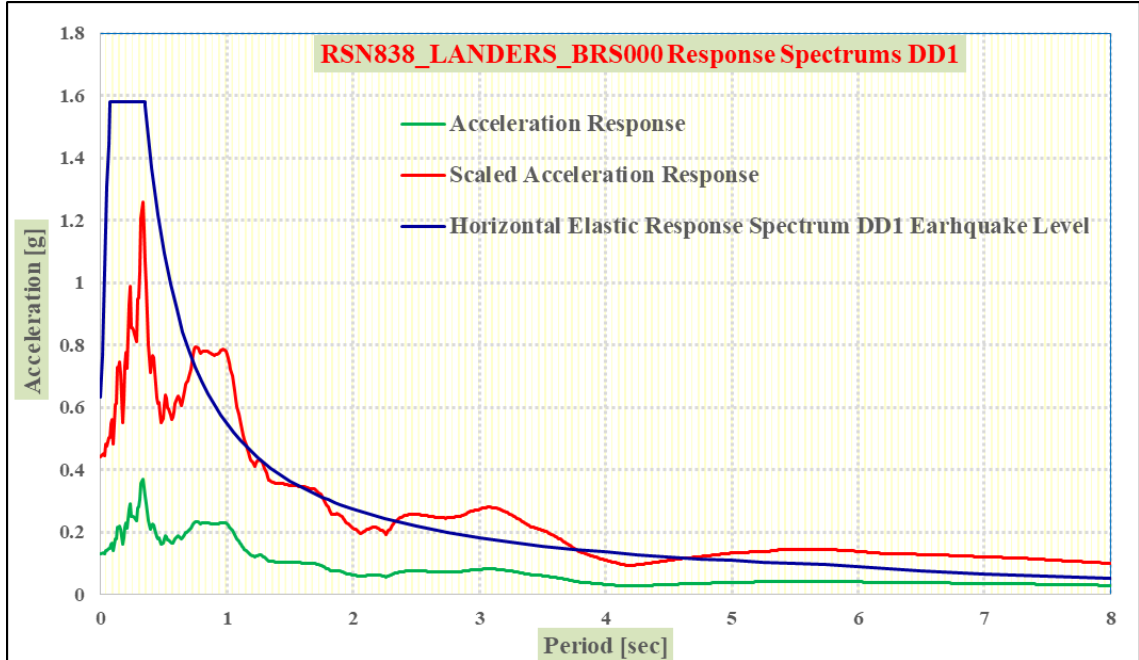


A4. LANDERS EARTHQUAKE

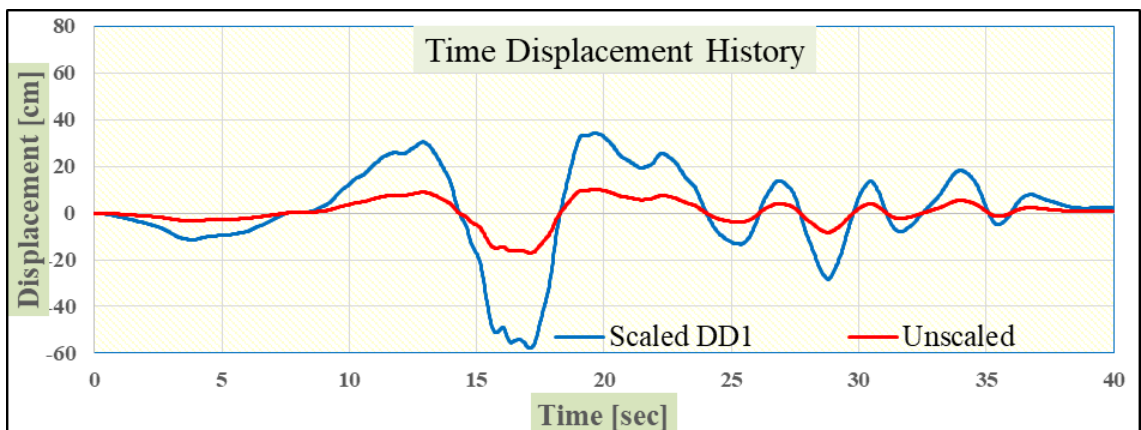
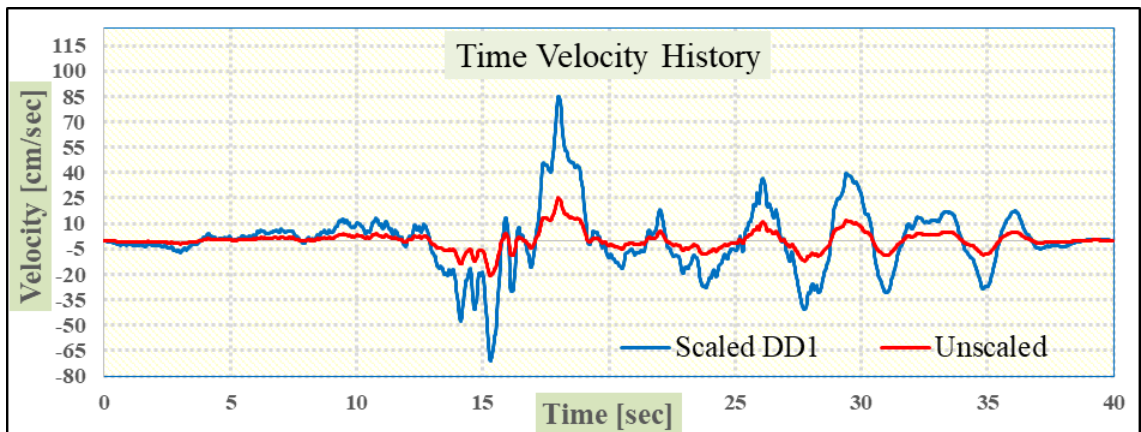
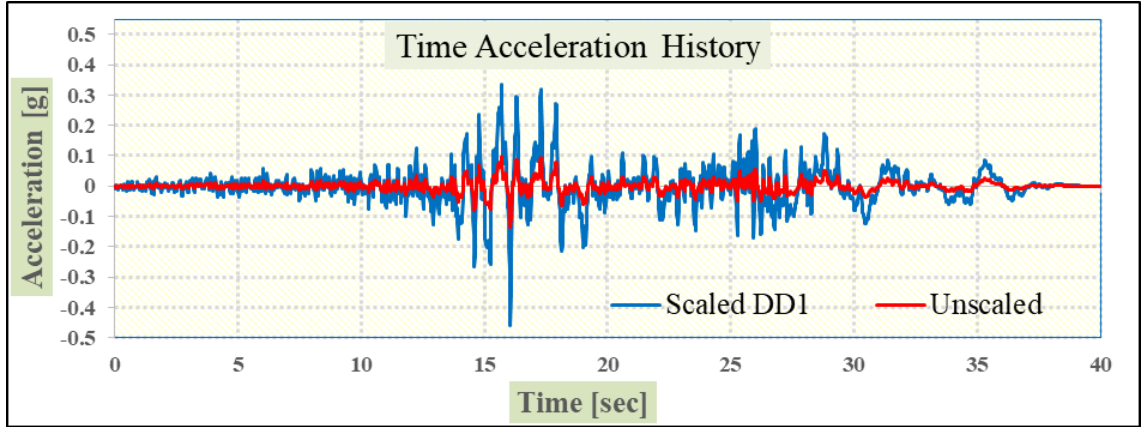
A4.1 RSN838_LANDERS_BRS000 Time Series



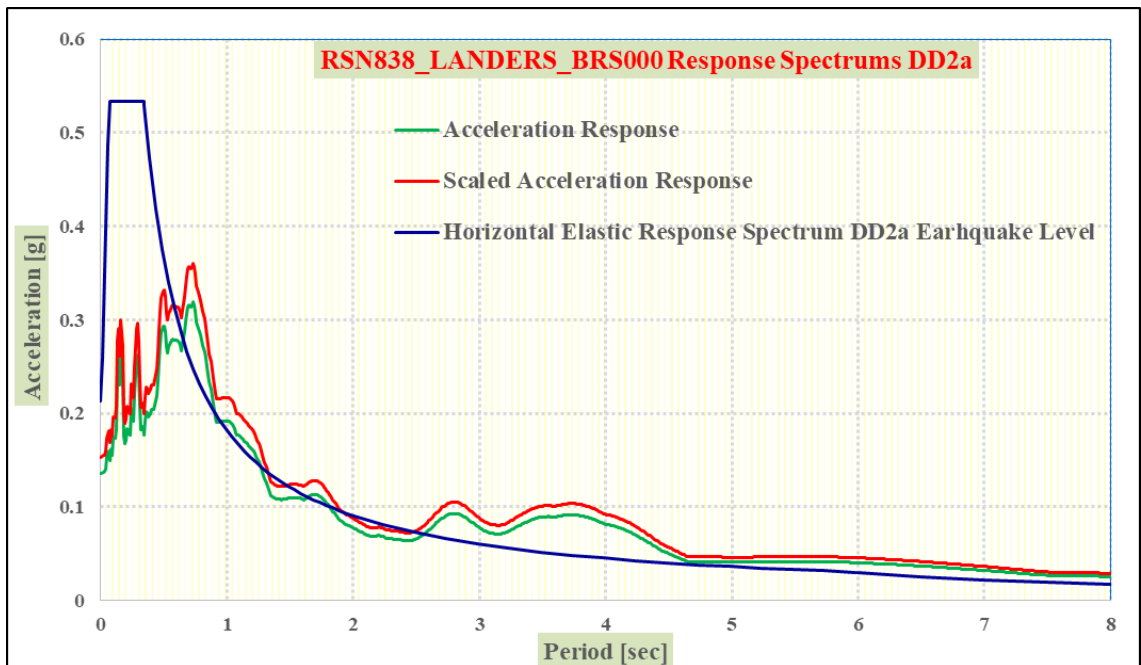
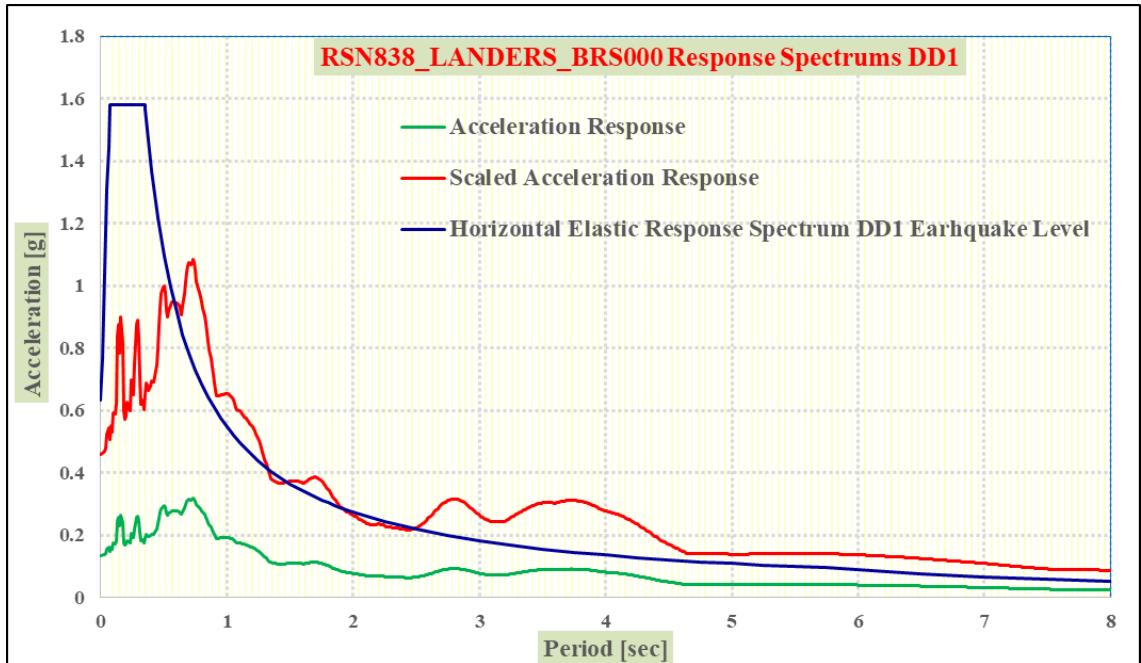
A4.2 RSN838_LANDERS_BRS000 Response Spectrums



A4.3 RSN838_LANDERS_BRS090 Time Series

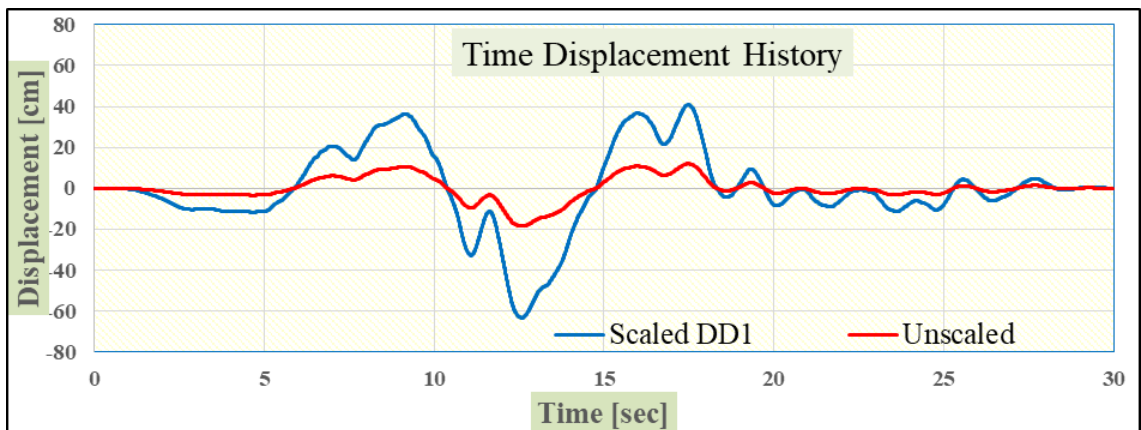
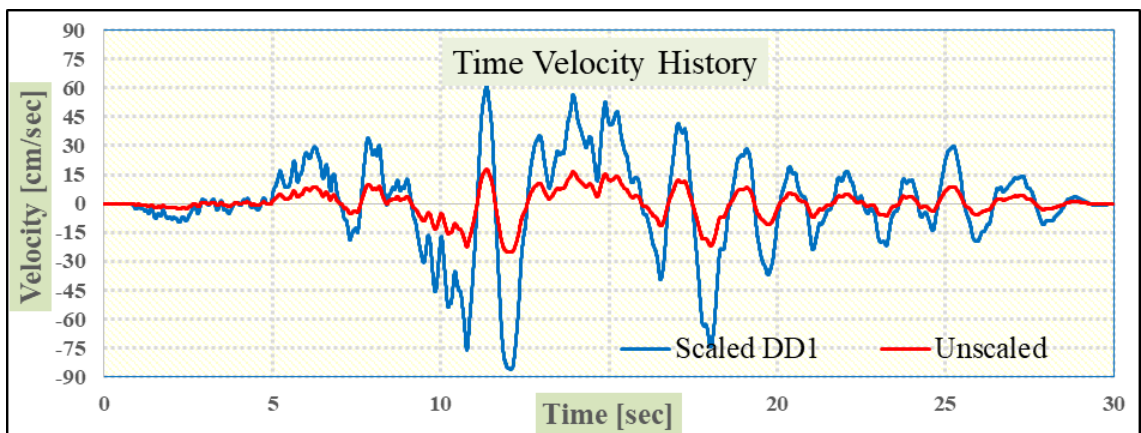
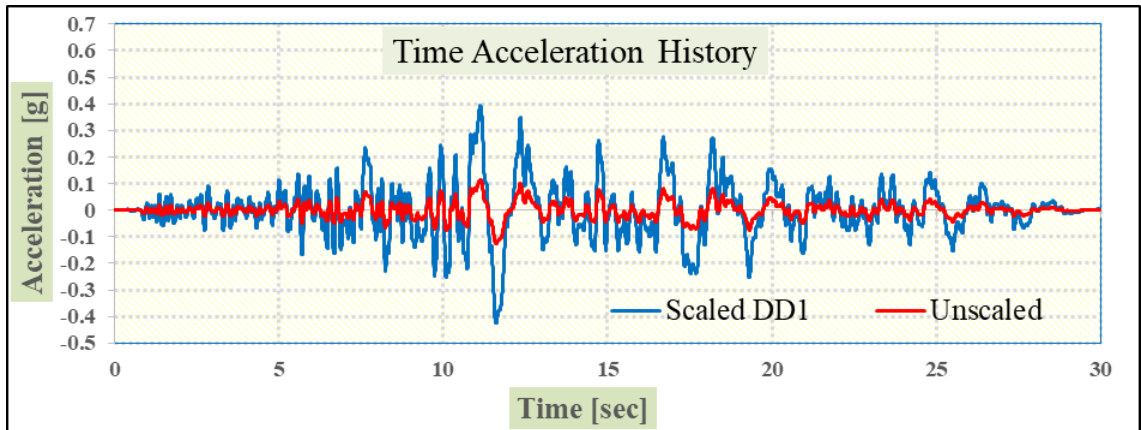


A4.4 RSN838_LANDERS_BRS000 Response Spectrums

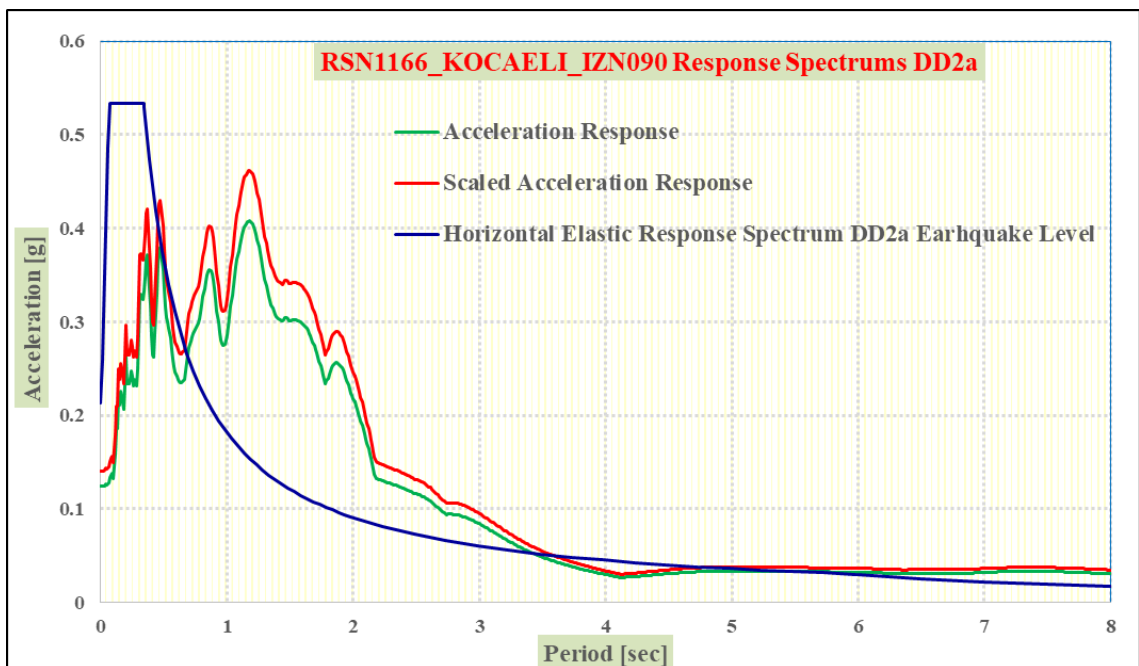
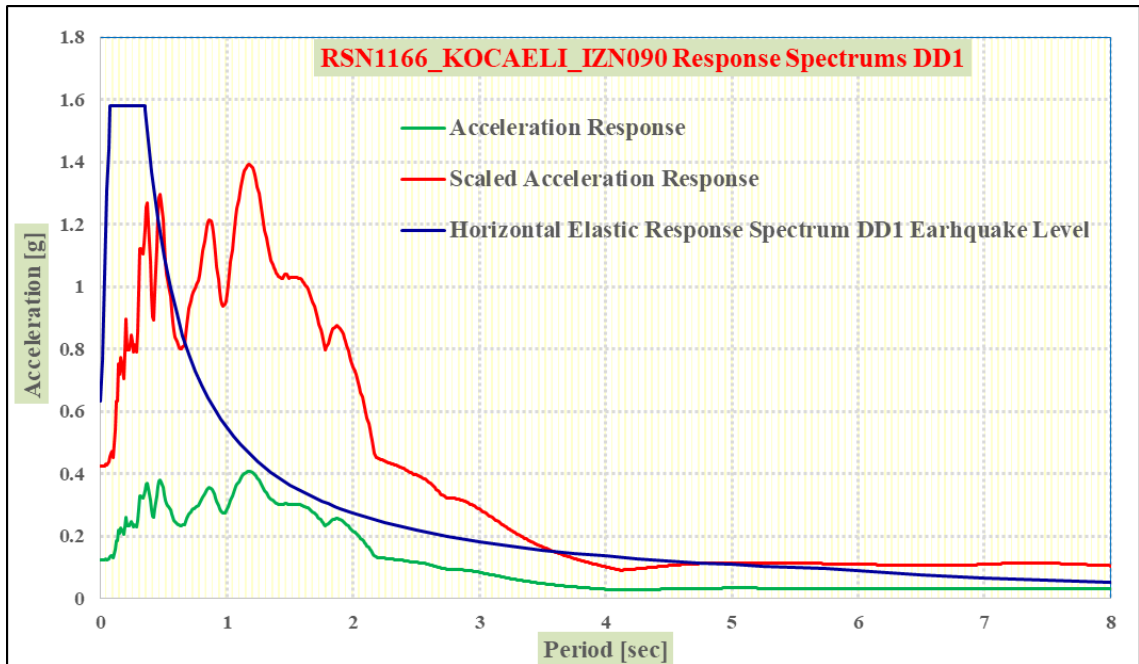


A5. KOCAELI EARTHQUAKE

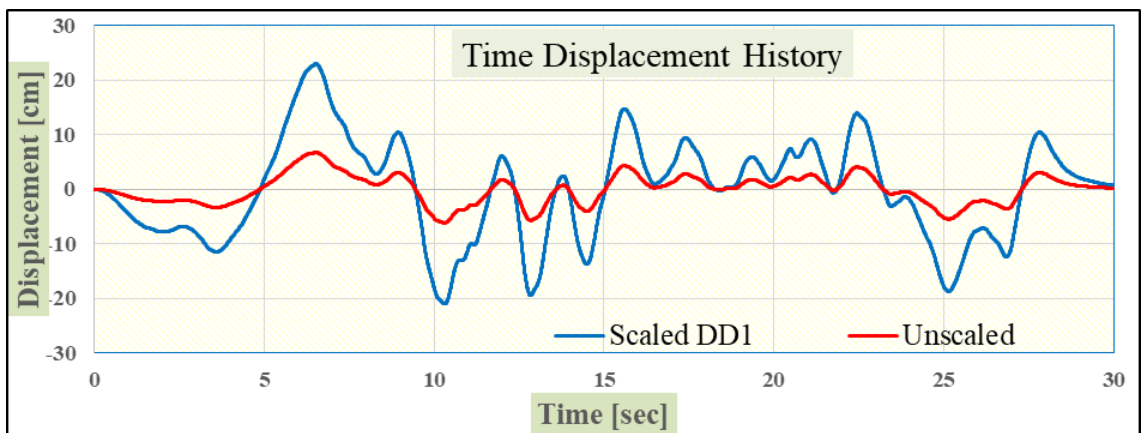
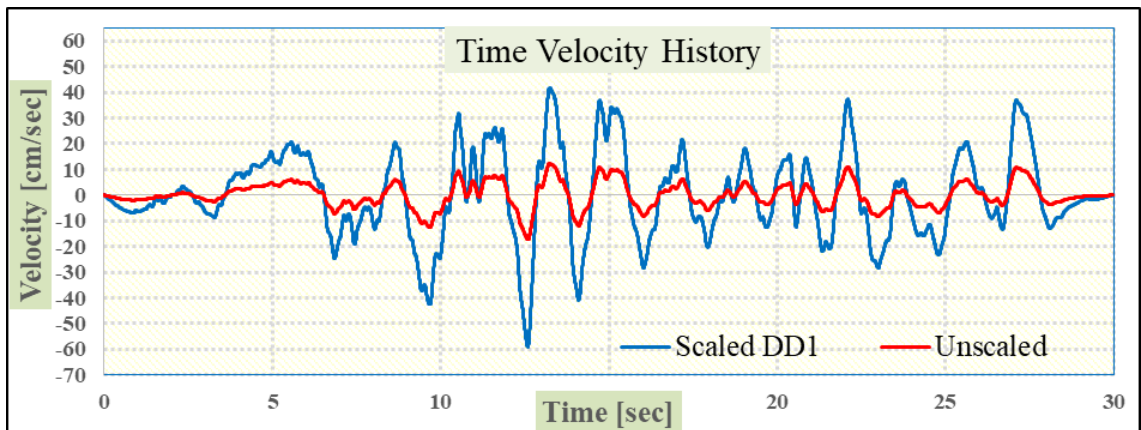
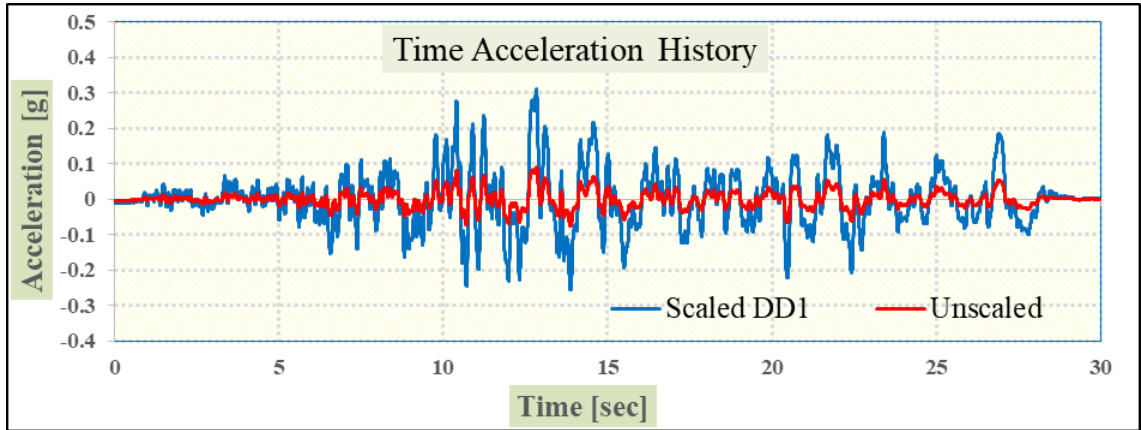
A5.1 RSN1166_KOCAELI_IZN090 Time Series



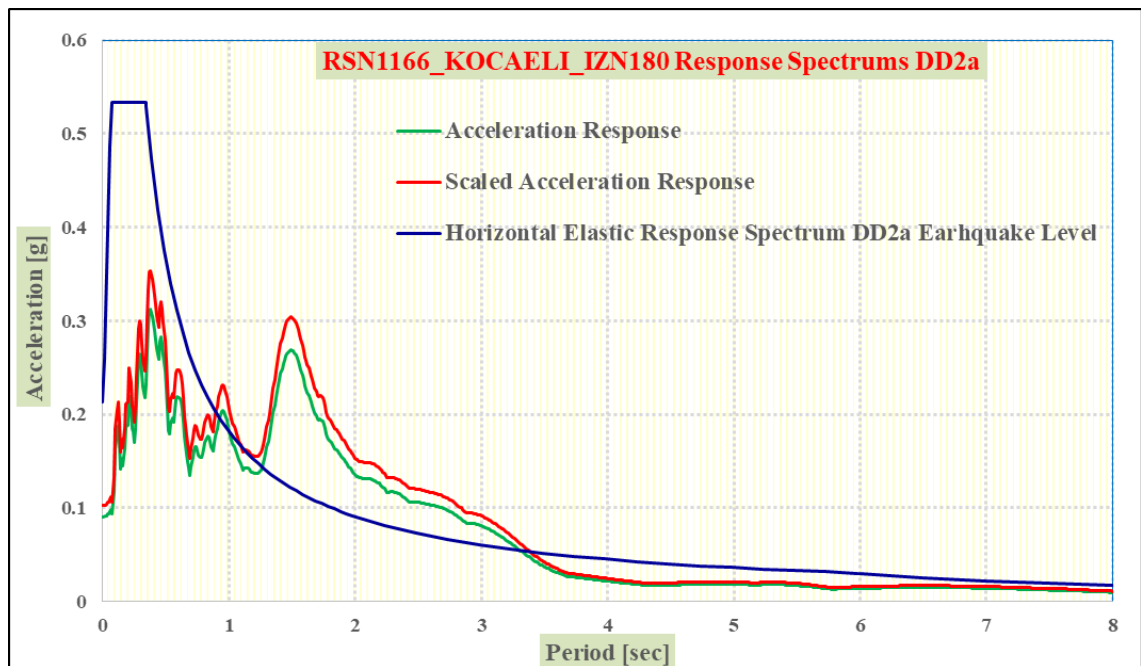
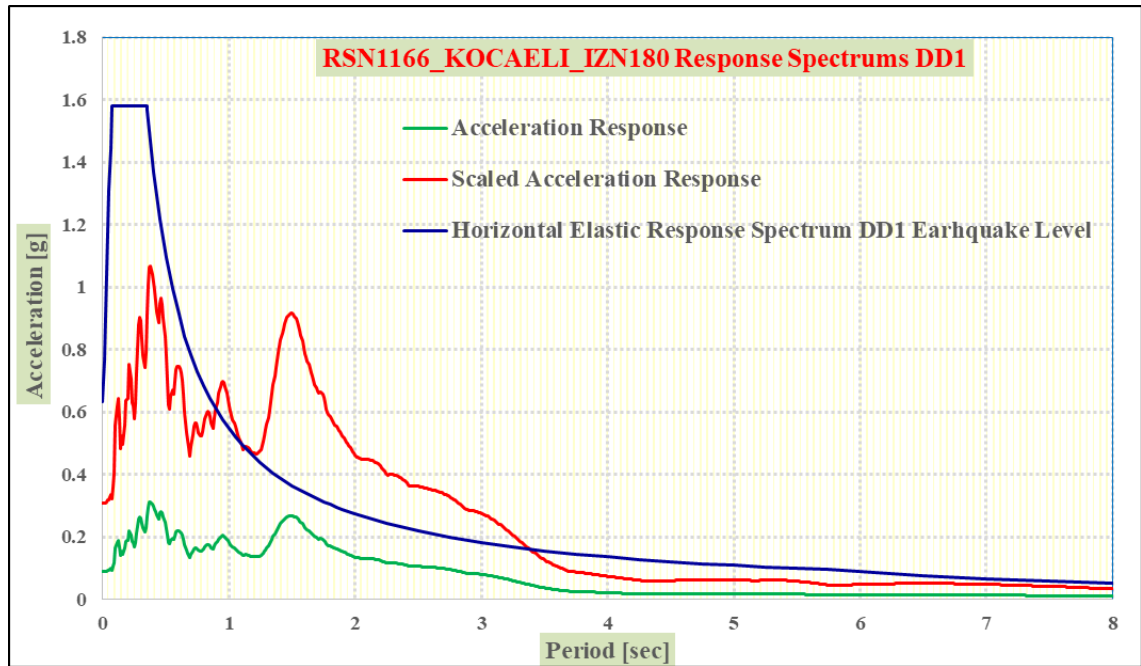
A5.2 RSN1166_KOCAELI_IZN090 Response Spectrums



A5.3 RSN1166_KOCAELI_IZN180 Time Series

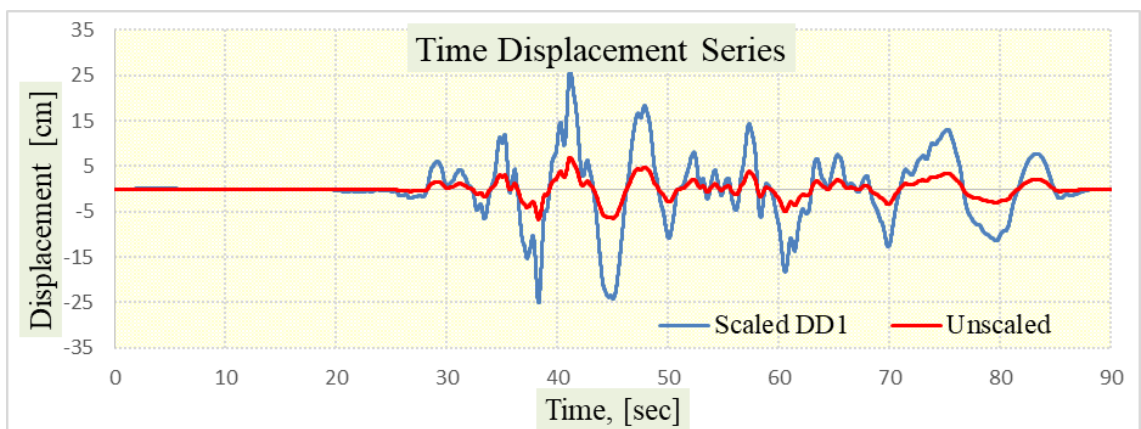
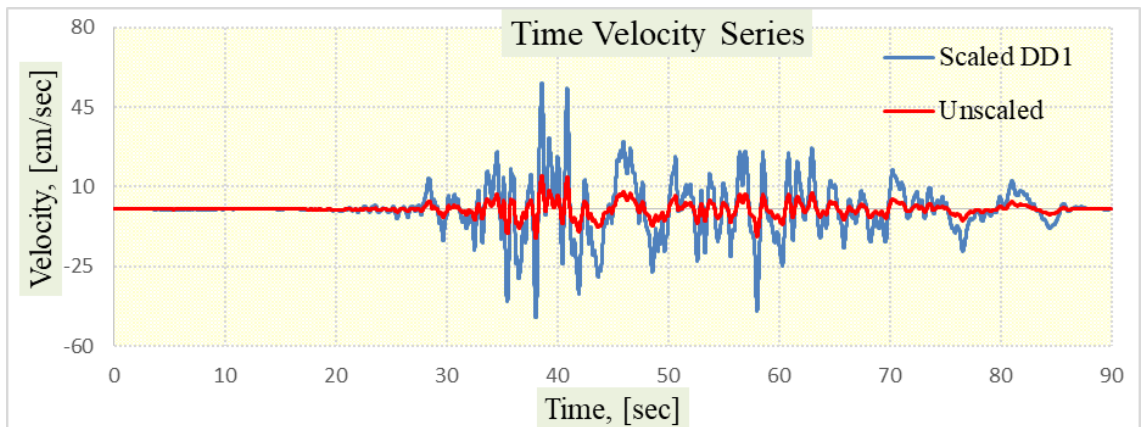
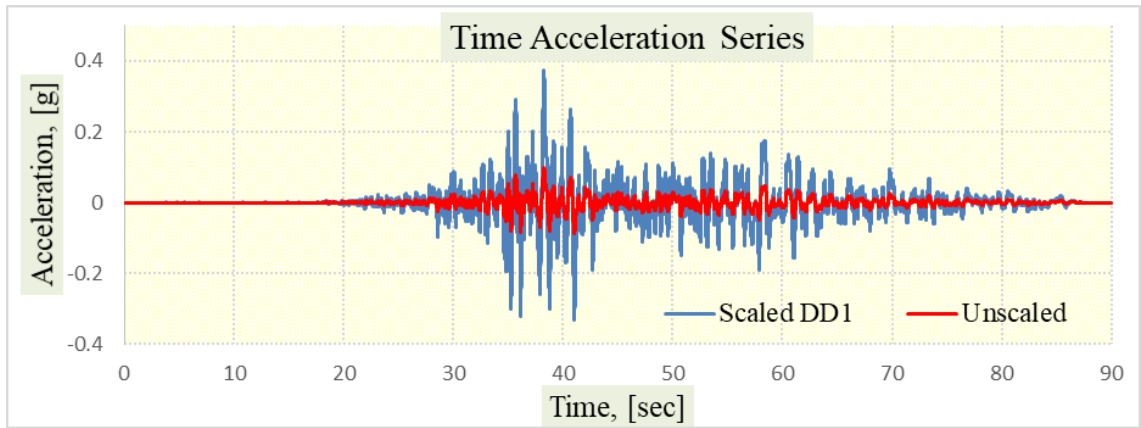


A5.4 RSN1166_KOCAELI_IZN180 Response Spectrums

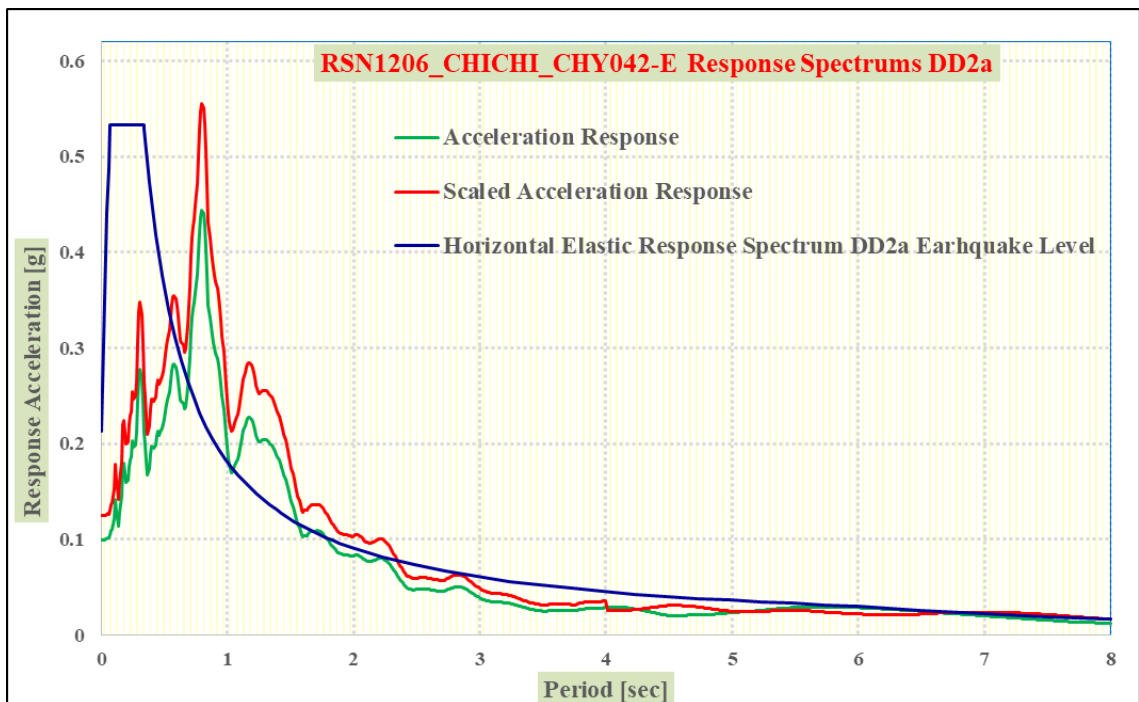
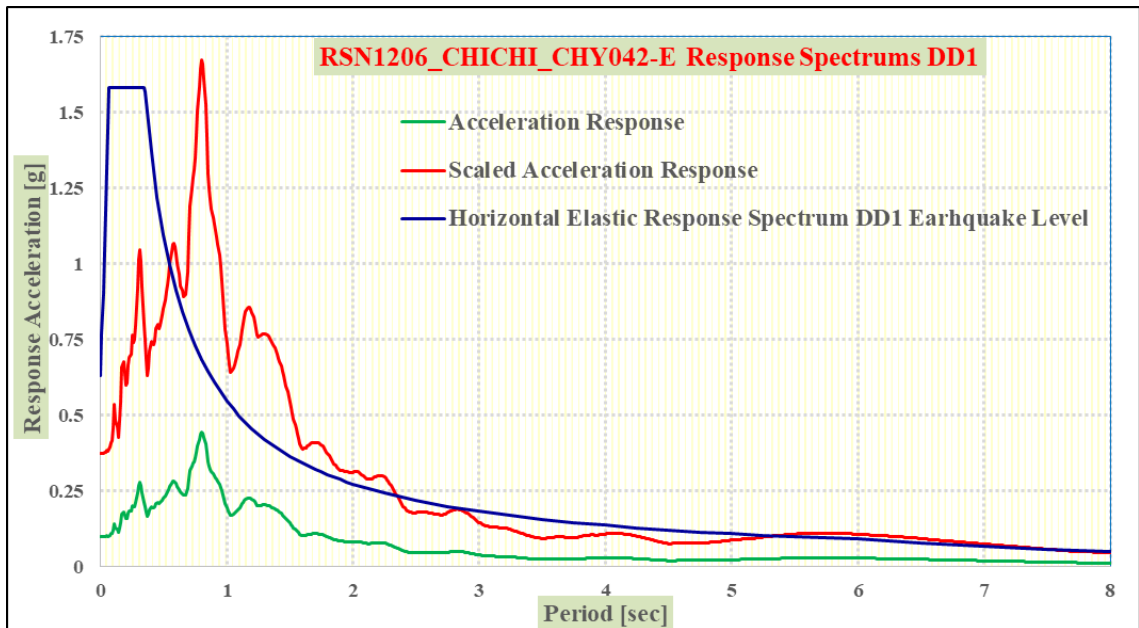


A6. CHICHI EARTHQUAKE

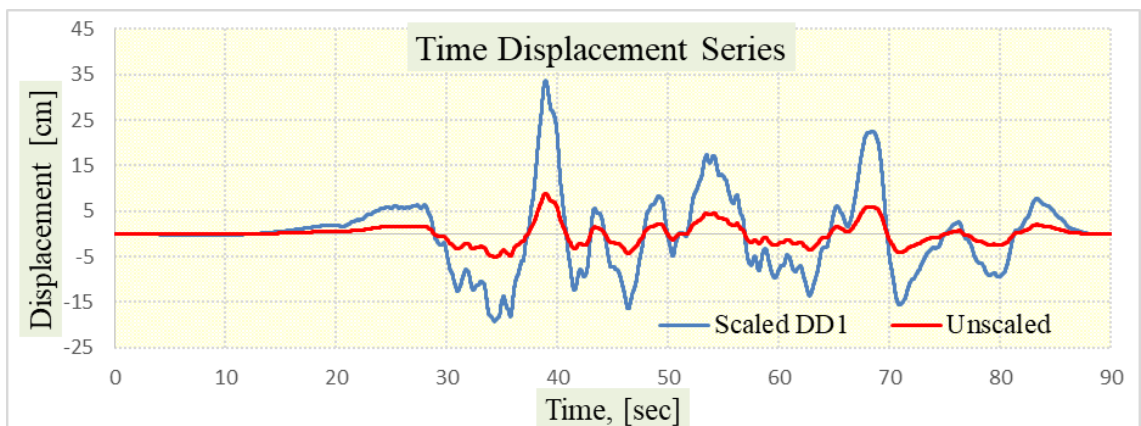
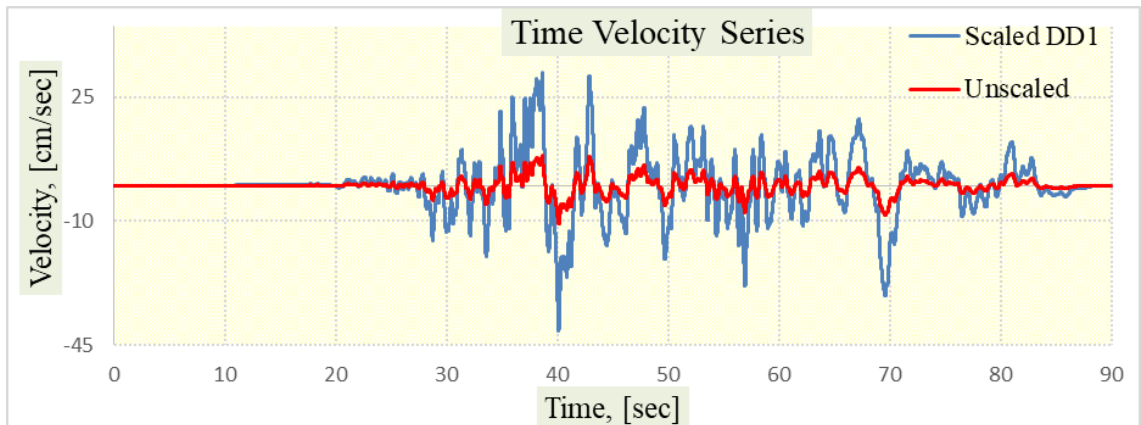
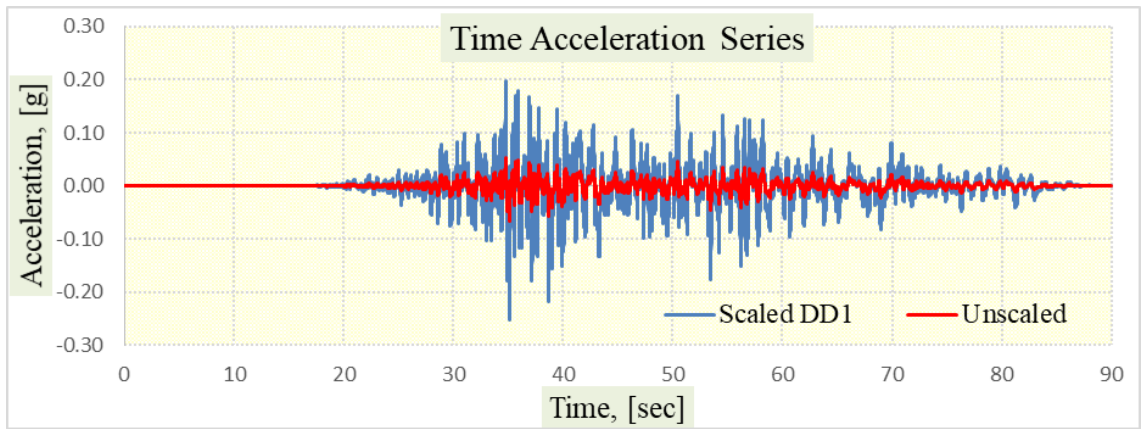
A6.1 RSN1206_CHICHI_CHY042-E Time Series



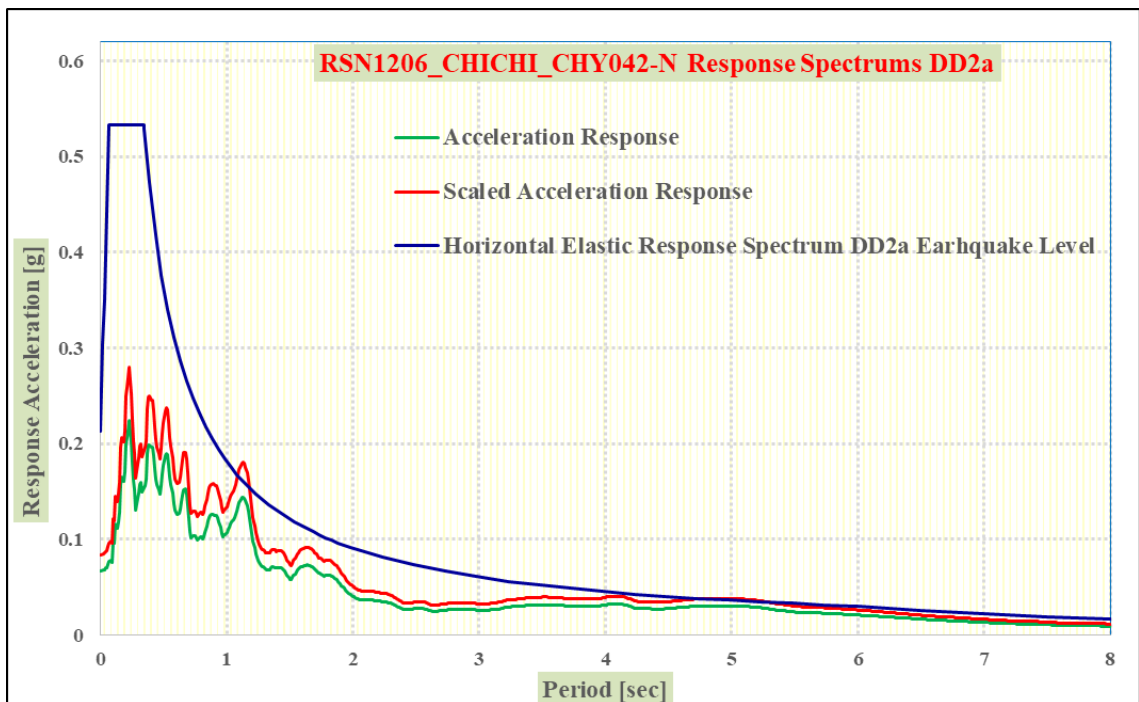
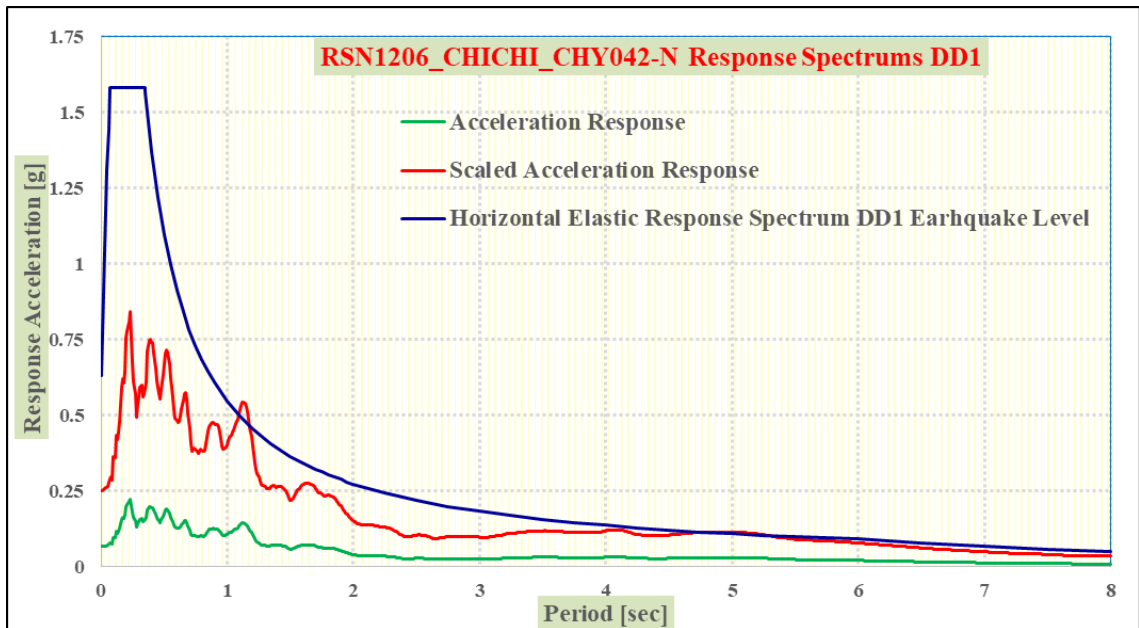
A6.2 RSN1206_CHICHI_CHY042-E Response Spectrums



A6.3 RSN1206_CHICHI_CHY042-N Time Series

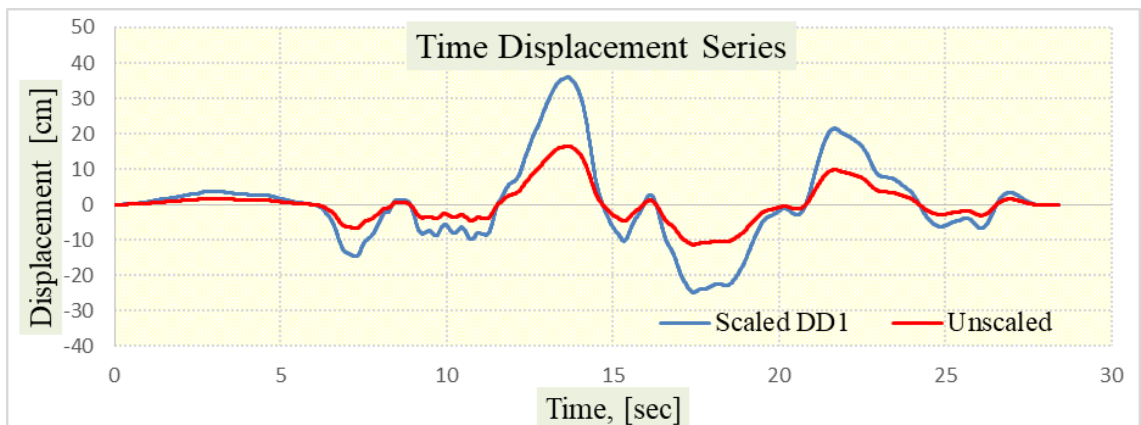
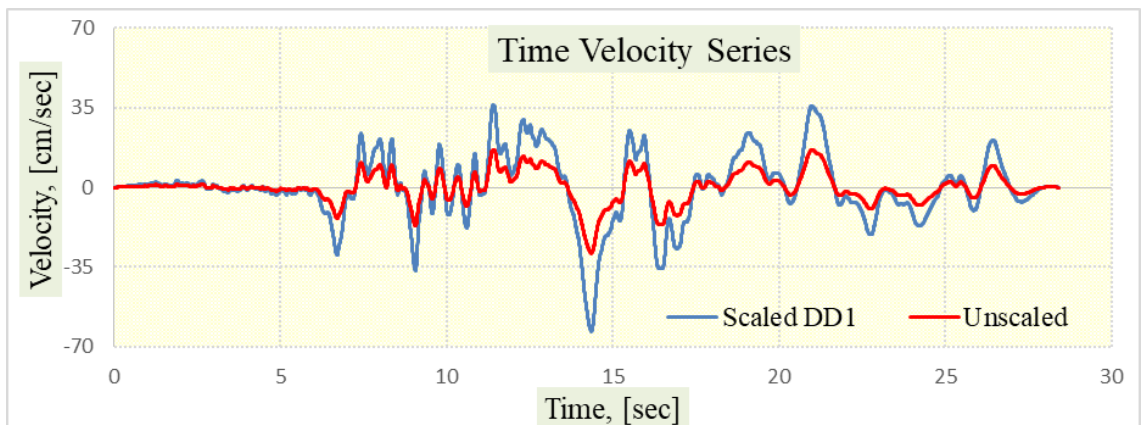
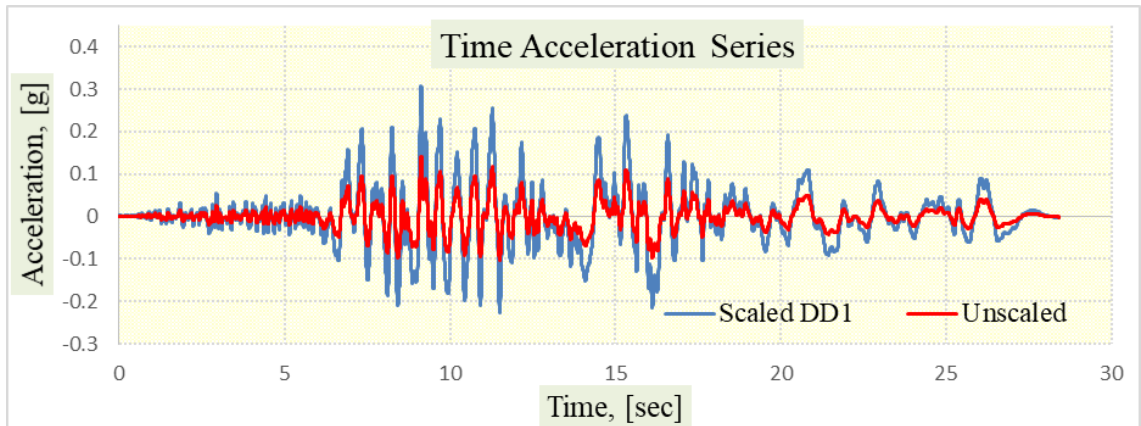


A6.4 RSN1206_CHICHI_CHY042-N Response Spectrums

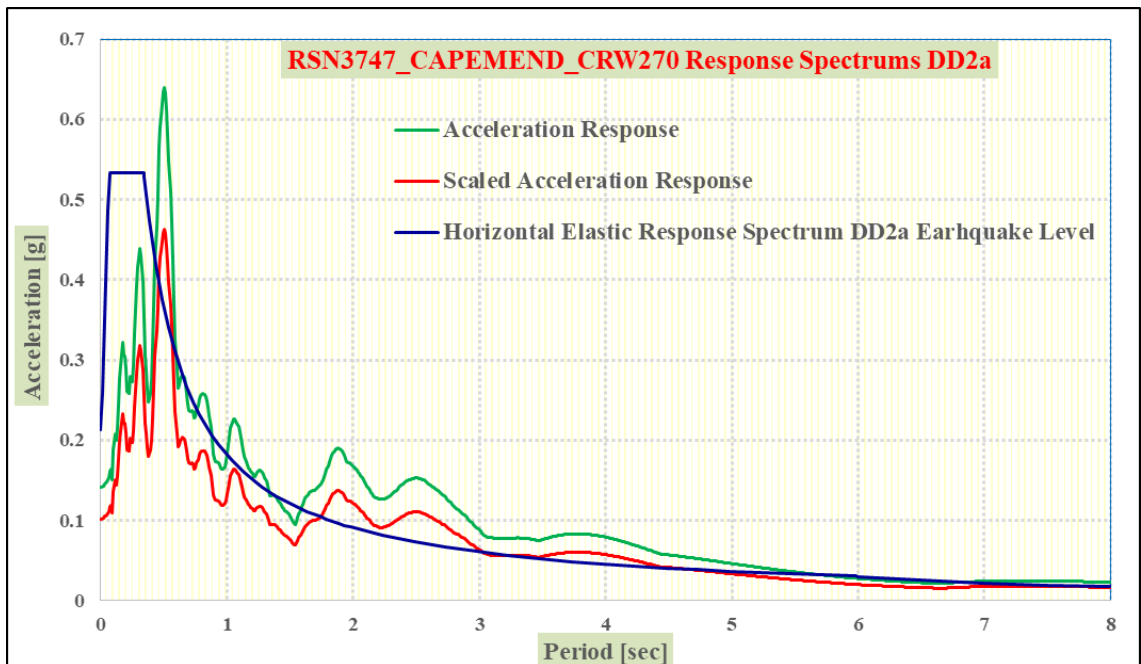
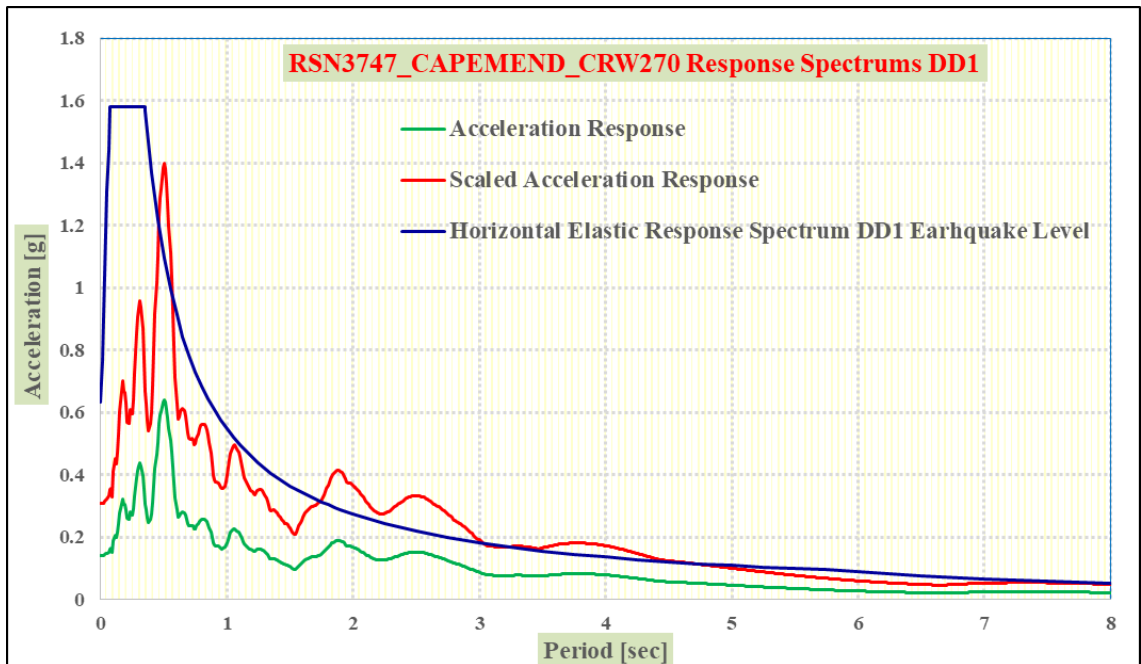


A7. CAPE MENDOCINO EARTHQUAKE

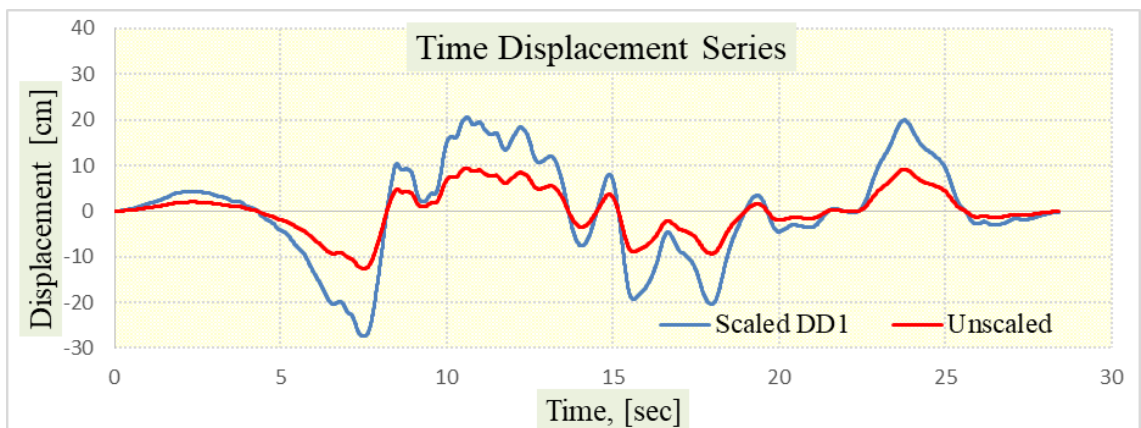
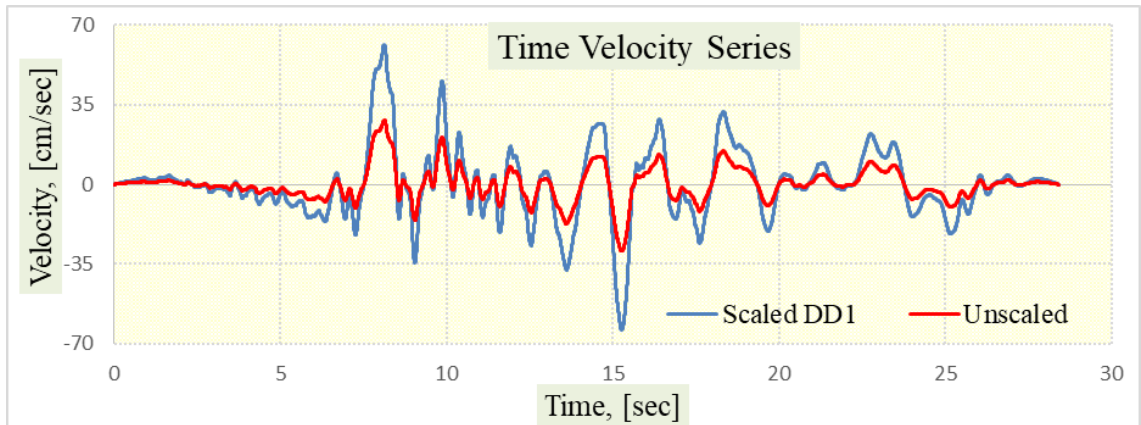
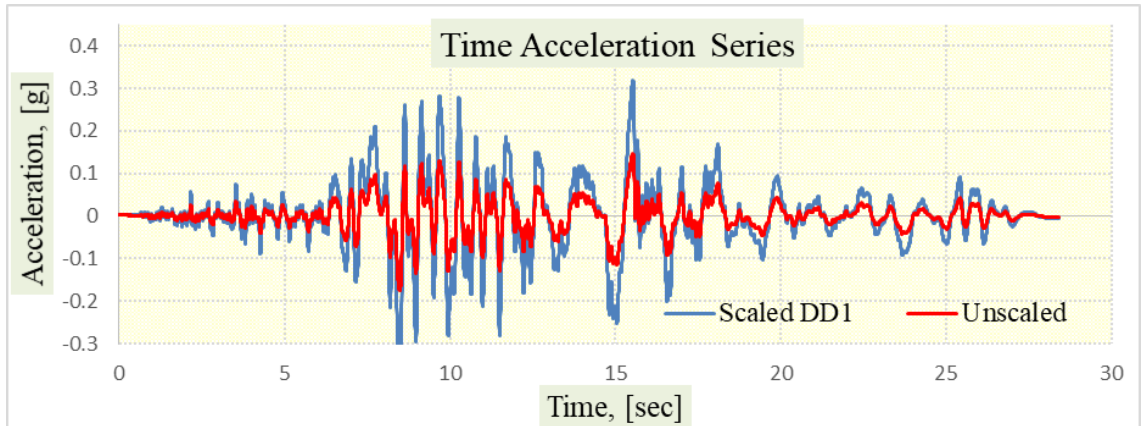
A7.1 RSN3747_CAPEMEND_CRW270 Time Series



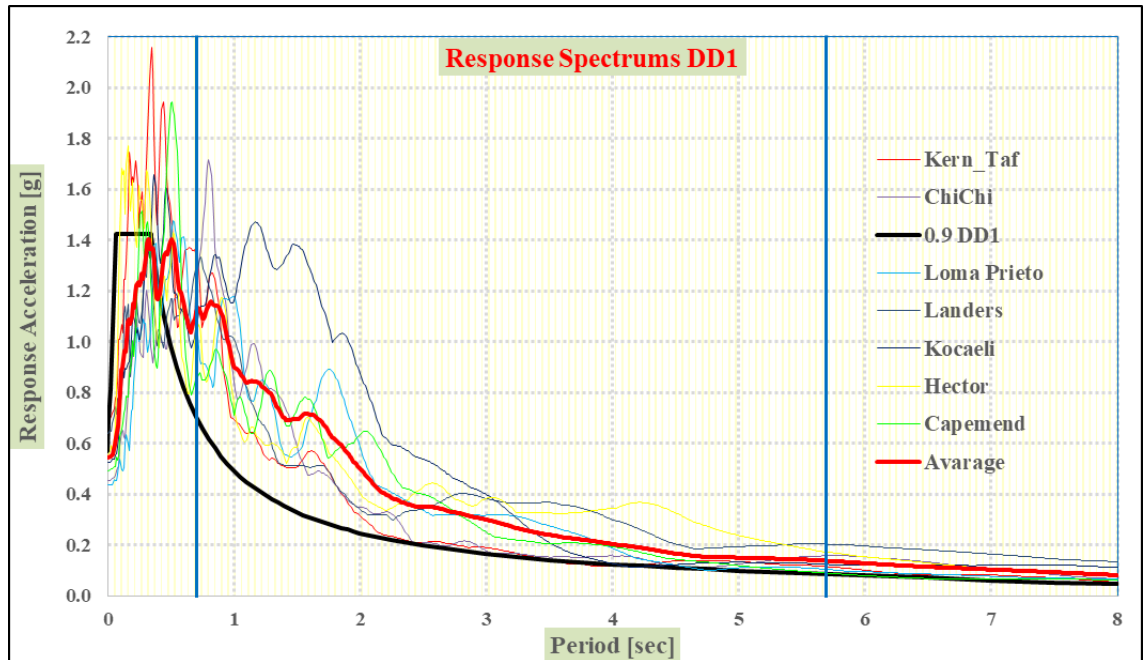
A7.2 RSN3747_CAPEMEND_CRW270 Response Spectrums



A7.3 RSN3747_CAPEMEND_CRW360 Time Series



A8. Avarage of DD1 Ground Motion Level Response Spectrums



It can be seen in the figure below that the ratio of the mean of the resultant spectra between the 0.2 Tp and 1.5 Tp periods to the amplitudes of the design spectrum in the same period interval is equal to or greater than 1.3. The scaling of both horizontal components was done with the same scale coefficients.(TBEC-2020 -2.5.2.2)



ÖZGEÇMİŞ